



universität
wien

MASTERARBEIT / MASTER'S THESIS

Titel der Masterarbeit / Title of the Master's Thesis

„Seismic hazard analysis of the territory of Slovakia
using zoneless approach“

verfasst von / submitted by

Barbara Badová, Bc.

angestrebter akademischer Grad / in partial fulfilment of the requirements for the degree of
Master of Science (MSc)

Wien, 2016 / Vienna 2016

Studienkennzahl lt. Studienblatt /
degree programme code as it appears on
the student record sheet:

A 066 680

Studienrichtung lt. Studienblatt /
degree programme as it appears on
the student record sheet:

Joint-Masterstudium Physics of the Earth (Geophysics)

Betreut von / Supervisor:

RNDr. Róbert Kysel, PhD.

Acknowledgment

I would like to express my gratitude to my supervisor RNDr. Róbert Kysel, PhD., for his guidance, help and support. Furthermore I would like to thank Doc. RNDr. Sebastián Ševčík, CSc. for his help with all programming related problems and RNDr. František Šipka (EQUIS, s.r.o) for providing Figure 3.1. Most importantly, I would like to thank my family for their support during my whole study at university.

Table of content

INTRODUCTION	7
1 STATE OF THE ART	9
1.1 Seismic hazard and seismic risk.....	9
1.2 Ground motion characteristics	9
1.3 Methods of seismic hazard analysis	13
1.3.1 Deterministic seismic hazard analysis.....	13
1.3.2 Probabilistic seismic hazard analysis	15
1.4 Mathematical theory of probabilistic approaches in SHA	19
1.4.1 Parametric and non-parametric methods for PDF estimation	19
1.4.2 Mathematical description of Cornell-McGuire approach.....	26
1.4.3 Mathematical description of zoneless approach.....	31
1.5 Applications of zoneless approach	34
2 OBJECTIVES OF MASTER'S THESIS	38
3 RESULTS.....	39
3.1 Earthquake catalogue for the territory of Slovakia	39
3.2 Bandwidth functions	41
3.3 Effective return periods	44
3.4 Kernel functions	45
3.5 Ground motion prediction equations.....	49
3.6 Sensitivity study on bandwidth parameters.....	51
3.6.1 Seismic activity rate	51
3.6.2 Seismic hazard curves	57
3.6.3 Seismic hazard maps	63
3.7 Sensitivity study on kernel functions	72
3.7.1 Seismic activity rate	72

3.7.2	Seismic hazard curves.....	74
3.7.3	Seismic hazard maps.....	77
3.8	Sensitivity study on effective detection periods	78
3.8.1	Seismic activity rate.....	79
3.8.2	Seismic hazard curves.....	81
3.8.3	Seismic hazard maps.....	83
3.9	Comparison with classical Cornell-McGuire approach	86
3.9.1	Seismic hazard curves.....	86
3.9.2	Seismic hazard maps.....	88
CONCLUSION.....		91
References.....		93
APPENDIX I – ABSTRACT (ENGLISH).....		97
APPENDIX II – ABSTRACT (GERMAN)		99

INTRODUCTION

Earthquake is an interesting natural phenomenon that is capable of causing significant material losses and also losses of life. Examples of such catastrophic events are for example Haiti ($M_w = 7.0$, January 12, 2010) or Tohoku-Oki earthquake in Japan ($M_w = 9.0$, March 3, 2011). The effects of an earthquake depend not only on the size of an earthquake, but also on so-called site effects, i.e. localized amplification or prolongation of duration of seismic motion due to local geological structure. Taking into account also site effects, even relatively weak earthquake can cause significant damage. Therefore has seismic hazard analysis for the whole country or for some specific area a major importance not only for countries with high seismic activity, like USA or Japan, but also for countries with moderate or low seismic activity, like Slovakia.

Seismologist still cannot predict the time, location and size of future earthquakes and it still remains questionable whether such prediction is possible. The aim of the seismic hazard analysis is therefore not to predict future earthquakes, but to predict their effects at the site.

This master's thesis is devoted to the probabilistic seismic hazard analysis of the territory of the Slovakia using zoneless approach proposed by Gordon Woo (1996).

The first chapter introduces to the problematics of the seismic hazard analysis. Basic terms of the seismic hazard analysis and basic ground motion characteristics are defined in sections 1.1 and 1.2. In section 1.3 are briefly described approaches to the seismic hazard analysis, namely deterministic approach, probabilistic approach following methodology proposed by Cornell (1968) and McGuire (1976) and probabilistic approach following methodology proposed by Woo (1996). Mathematical theory of both probabilistic approaches described in this thesis is presented in section 1.4. Section 1.5 is devoted to the brief overview of recent papers, in which zoneless approach was used to probabilistic seismic hazard analysis.

The second chapter presents the objectives of the master's thesis.

The third chapter contains the results of the master's thesis. Earthquake catalogue SLOVEC (2011) used in this thesis is briefly described in 3.1. Sections 3.2 to 3.5 describe the calculation and the selection of individual input parameters. Sensitivity tests to the individual input parameters are presented in sections 3.6 to 3.8. Comparison with the

results of the PSHA calculations following Cornell-McGuire methodology obtained by Kysel (2014) is presented in section 3.9.

1 STATE OF THE ART

1.1 Seismic hazard and seismic risk

There is a significant difference between seismic hazard and seismic risk. Unfortunately, these two terms are used interchangeably in public discussion. The following definitions of basic terms are adapted from Reiter (1990) and McGuire (2004).

Seismic hazard describes the potential for dangerous, earthquake-related natural phenomena such as ground motion, fault rupture, tsunami or soil liquefaction. These phenomena could result in adverse consequences to society such as the destruction of buildings or the loss of life. However, the potential itself does not mean that the damage will actually occur.

Seismic hazard analysis quantifies levels of ground motion parameters at a site. The output of a seismic hazard analysis could be a map which shows levels of ground shaking in various parts of the country that have an equal chance of being exceeded.

Seismic risk is the probability that some humans will incur loss or that their built environment will be damaged due to the seismic hazard. These probabilities usually represent a level of loss or damage that is equalled or exceeded over some time period.

Seismic risk analysis quantifies the loss or damage at a site or in a region, e.g. a monetary loss, the number of casualties, the cost to repair a facility as a percentage of replacement cost.

1.2 Ground motion characteristics

According to Kramer (1996) a strong ground motion is the primary interest of earthquake engineers. Evaluation of the earthquake effects at a particular site requires quantitative ways of describing a strong ground motion. Fortunately, it is not necessary to reproduce each time history exactly to describe the ground motion adequately for engineering purposes. It is necessary, however, to identify a set of ground motion parameters that reflect three significant characteristics of earthquake motion: (1) the *amplitude*, (2) *frequency content*, (3) *duration* of the motion. A number of different ground motion parameters have been proposed; some describe only one of these characteristics, while others may reflect two or three (*Table 1.1*). Due to the complexity of earthquake ground

motion it is impossible to identify a single ground motion parameter that accurately describes all important ground motion characteristics.

Ground motion parameter	Ground motion characteristic		
	Amplitude	Frequency content	Duration
Peak ground acceleration, PGA	×		
Peak ground velocity, PGV	×		
Strong ground motion duration, T_d			×
Root mean square acceleration, a_{rms}	×	×	
Arias intensity, I_a	×	×	×
Cumulative absolute velocity, CAV	×	×	×

Table 1.1 - Ground motion characteristics that are reflected in various ground motion parameters. Adapted from Kramer (1996).

Ground motion parameters listed in *Table 1.1* have following meaning:

Peak ground acceleration (PGA) for a given component of motion (horizontal/vertical) is defined as the largest (absolute) value of acceleration obtained from the accelerogram of that component:

$$PGA(x) = \text{Max}_t [a(x, t)], \quad (1.1)$$

where $a(x, t)$ is acceleration recorded on site x at time t .

Ground motions with high peak accelerations are usually (but not always) more destructive than motions with lower peak accelerations. Although PGA is a very useful and commonly used ground motion parameter, it provides no information on the frequency content of the motion.

Peak ground velocity (PGV) for a given component of motion (horizontal/vertical) is defined as the largest (absolute) value of velocity obtained from the velocigram of that component:

$$PGV(x) = \underset{t}{Max} [v(x, t)], \quad (1.2)$$

where $v(x, t)$ is velocity recorded on site x at time t .

Fourier spectra (Fourier amplitude spectrum, Fourier phase spectrum) expresses the frequency content of a ground motion. The Fourier amplitude spectrum of a ground motion shows how the amplitude of the ground motion is distributed with respect to frequency (or period).

Strong ground motion duration is evaluated by several different approaches (Kramer 1996, IAEA 2010):

- The *bracketed duration* is defined as the time the first and last exceedances of a threshold acceleration (usually 0.05g).
- The time interval between the onset of ground motion and the time at which the acceleration has declined to 5% of its peak value.
- The time interval between the points at which 5% and 95% of the total energy has been recorded.

Root mean square (rms) acceleration is a single parameter that includes the effects of the amplitude and frequency content of a strong ground motion record, defined as

$$a_{rms}(x) = \sqrt{\frac{0.9}{T_d(x)} \int_0^{T_d} a^2(x, t) dt}, \quad (1.3)$$

where $T_d(x)$ is strong ground motion duration and $a(x, t)$ is acceleration recorded on site x at time t . Because the integral contains the strong motion duration, the value of rms acceleration can be very sensitive to the method used to define it.

Arias intensity is a parameter closely related to the rms acceleration and defined as

$$I_A = \frac{\pi}{2g} \int_0^{\infty} a^2(x, t) dt, \quad (1.4)$$

where g is gravitational acceleration and $a(x, t)$ is acceleration recorded on site x at time t . The Arias intensity has units of velocity and is usually expressed in meters per second. Since the definition obtains the integration over the entire duration rather than over the duration of strong motion, its value is independent of the method used to define the duration of strong ground motion.

Cumulative absolute velocity (CAV) is the area under the absolute accelerogram:

$$CAV(x) = \int_0^{t_{total}} |a(t)| dt, \quad (1.5)$$

where $|a(t)|$ is the absolute value of the acceleration time history and t_{total} is the total duration of the ground motion.

Apart from previously mentioned ground motion parameters, another important and useful tool for characterization of strong ground motion are response spectra.

Response spectra are types of spectra extensively used in earthquake engineering practice. The response spectrum describes the maximum response of a single-degree-of-freedom system (SDOF) to a particular input motion as a function of the natural frequency (or natural period) and damping ratio of the SDOF system. Response spectra reflect strong ground motion characteristics indirectly since they are influenced by the response of the SDOF structure. They also represent simplified interaction of the building structure and the ground motion.

There are different types of response spectra:

- relative displacement response spectrum (spectral displacement),
- relative velocity response spectrum (spectral velocity),
- relative acceleration response spectrum,
- absolute displacement response spectrum,
- absolute velocity response spectrum,
- absolute acceleration response spectrum (spectral acceleration),
- pseudo relative velocity response spectrum,
- pseudo absolute acceleration response spectrum.

The most used type of response spectra in seismic hazard analysis is pseudo absolute acceleration response spectrum $PSA(x)$ which is given by relation

$$PSA(x) = \omega^2 SD(x), \quad (1.6)$$

where $SD(x)$ is spectral displacement at site x and ω is ground motion frequency.

Choice of the respective ground motion characteristic for the purposes of seismic hazard analysis depends on the nature of seismic data, on the type of the building structure and on the objectives of seismic hazard analysis.

1.3 Methods of seismic hazard analysis

In this section, we describe two basic approaches to the seismic hazard analysis:

- deterministic seismic hazard analysis (DSHA),
- probabilistic seismic hazard analysis (PSHA).

1.3.1 Deterministic seismic hazard analysis

DSHA make use of discrete, single-valued events or models to arrive at the description of earthquake hazard and according to Reiter (1990) can be described as a four-step process (*Figure 1.1*):

1. Identification of earthquake sources

Using compiled seismological and geological databases, seismic source zones are identified and allocated. The configuration of individual sources could be points, lines, areas and volumes. Source characterization includes definition of each source's geometry (the source zone) and earthquake potential.

2. Selection of controlling earthquake

For each source zone, its earthquake potential is defined in terms of maximum earthquake. This could be earthquake, which is reasonably expected, maximum credible earthquake or some other type of earthquake description. Earthquake magnitude (usually moment magnitude M_w) or epicentral intensity are used to define the earthquake size. For each source zone, the distance (usually closest) to the site is determined. The controlling

earthquake is going to be one of the postulated earthquakes, whose ground motion or other quantity being estimated will dominate the effects of all other earthquakes considered.

3. Determination of earthquake effects

In this step, ground motion prediction equations (GMPEs) are used for chosen ground motion parameters. GMPEs are empirical or stochastic relations which represent the ground motion as a function of magnitude, distance and other relevant parameters (e.g. style of faulting, hanging wall effects and local site conditions). In the past, GMPEs were also called attenuation relationships.

General criteria for the selection of GMPE for seismic hazard analysis were published by Cotton et al. (2006) and updated by Bommer et al. (2010). Selected GMPEs should be current and well established at the time of the study, they should be consistent with the types of earthquake and the attenuation characteristics of the region of interest, they should match as closely as possible the tectonic environment of the region of interest and they should make use of local ground motion data where available. Caution should be put in comparing selected GMPEs with recorded ground motions from locally recorded earthquakes.

4. Determination of the seismic hazard at the site

The seismic hazard at the site in terms of ground motion parameter is obtained for a controlling earthquake and a given GMPE (with respect to its aleatory uncertainty).

Advantage of DSHA is its relative simplicity. According to Kramer (1996) when applied to structures for which failure could have catastrophic consequences, such as nuclear power plants or large dams, DSHA provides a straightforward framework for evaluation of worst-case ground motions. However, it provides no information on the likelihood of occurrence of the controlling earthquake, the likelihood of occurring where it is assumed to occur or the level of ground motion that might be expected during a time period (such as the lifetime of a particular facility). It is not always possible to determine the worst-case scenario, for example to determine maximum credible earthquake (MCE) and its distance from the site.

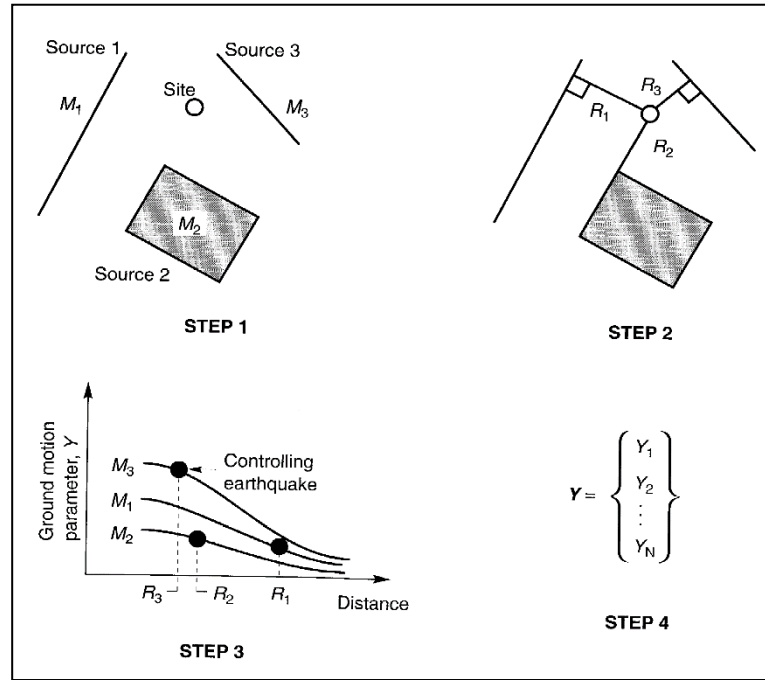


Figure 1.1 – Basic steps of deterministic seismic hazard analysis. Reproduced from Kramer (1996).

1.3.2 Probabilistic seismic hazard analysis

In PSHA hazard descriptions are not restricted to scenario-like statements, they incorporate the effects of all the earthquakes of all magnitudes from all distances that are capable of affecting ground motion parameters at the site. In PSHA, statistical and probabilistic methods are used to compute the rate of exceeding a given level of ground motion parameters during a particular time period. In this subsection we describe two basic probabilistic approaches – classical (Cornell-McGuire) approach and zoneless approach.

1.3.2.1 Classical (Cornell-McGuire) approach

This methodology was developed by Allin Cornell and Luis Esteva in the 1960s (e.g. Cornell 1968; Esteva 1967). In the 1970s, Robin McGuire developed software for seismic hazard computation (McGuire 1976). More about the early history of PSHA can be found in McGuire (2008).

The classical approach is preferred in most PSHA studies. Analogously to the DSHA, it can be described as a four-step process (*Figure 1.2*):

1. Identification of seismic source zones

Generally similar to DSHA, seismic source zones are identified using compiled geological and seismological databases. Unlike in DSHA, seismic activity is considered to be spatially homogenous (implying that earthquakes are equally likely to occur at any point within the source zone) and stationary for a given seismic source zone.

2. Definition of recurrence relation for each source zone

This step is fundamentally different from DSHA. Instead of picking one controlling earthquake, for each source zone recurrence relation (magnitude-frequency relation) and maximum potential magnitude are determined. A recurrence relation indicates the average rate of an earthquake of a given size occurring anywhere inside the source zone during specific period of time, usually one year. Before parameters of recurrence relation are calculated, it is necessary to process earthquake catalogue – it is necessary to choose one type of magnitude and determine its value for each event in the catalogue (homogenization), to identify foreshocks, main shocks and aftershocks (declustering), estimate completeness of the catalogue, estimate the quality of the data obtained by magnitude conversions.

3. Determination of earthquake effects

Similar to the DSHA, GMPEs are used for chosen ground motion parameter, except that in PSHA, the range of considered earthquake sizes requires a family of ground motion curves (each curve is related to different magnitude - distance pair).

4. Determination of the seismic hazard at the site

Last step is fundamentally different from DSHA. The result of PSHA is a seismic hazard curve, which represents the frequency of exceeding different levels of computed ground motion parameter at the site during a specific time (usually one year).

After PSHA calculations are completed, it is often useful to do the deaggregation of the results – a statistical decomposition of the results to show how earthquakes of certain magnitudes from certain distances contribute to the final hazard at the site.

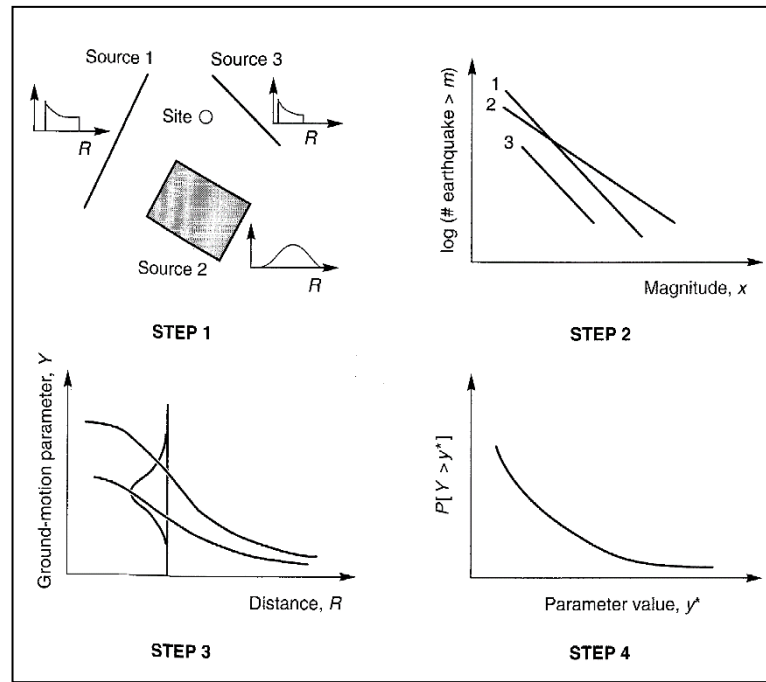


Figure 1.2 – Basic steps of probabilistic seismic hazard analysis.
Reproduced from Kramer (1996).

One of the possible outputs of PSHA is a uniform hazard spectrum (UHS), which is a design response spectrum widely used for structural and geotechnical analysis. To construct UHS, PSHA calculations need to be performed for spectral accelerations at a chosen range of periods. Then, a target rate of exceedance is chosen, and for each period the spectral acceleration amplitude corresponding to that rate is identified. Obtained spectral acceleration amplitudes are then plotted versus their periods. This spectrum is called a uniform hazard spectrum because every spectral ordinate has an equal rate of being exceeded. For more illustrative example see e.g. Baker (2008).

1.3.2.2 Zoneless approach

For many regions, where the association between seismicity and geology is complex, the definition of the source zones is often difficult and to some extent is a matter of expert judgement. It is also known, that the seismicity is not homogeneous within a source zone, but it is only approximation for computational purposes. Therefore, zoneless approach to probabilistic seismic hazard analysis has been developed by Woo (1996). It can also be described as a four-step process:

1. Coverage of the region with a rectangular grid

First step of zoneless approach is significantly different from DSHA and Cornell-McGuire approach. Instead of identification of the seismic source zones, the region over which seismic hazard is being evaluated is covered by a rectangular grid with nodes located at regular intervals. The node spacing depends on desired resolution – if higher resolution is needed, then the node spacing should be denser.

2. Determination of the seismic activity rate

Seismic activity rate represents the expected annual number of events of magnitude m occurring at location \vec{x} . Seismic activity rate is determined by three parameters – kernel function, the effective return period and the bandwidth function. Seismic activity rate is calculated at each grid node as a kernel sum over all events in the catalogue, in desired magnitude range, and contribution of each event is inversely weighted by its effective return period. The bandwidth function is designed to reflect spatial clustering of catalogued earthquakes.

3. Determination of earthquake effects

Similar to DSHA and Cornell-McGuire approach, once seismic activity rate is determined, GMPE are used for chosen ground motion parameter.

4. Determination of the seismic hazard at the site

Similar to Cornell-McGuire approach, when the seismic activity rate is estimated and attenuation model is taken into account through GMPE, seismic hazard curve can be obtained.

Zoneless approach proposed by Woo (1996) is sometimes also called smoothing approach, because in this procedure earthquake epicentres are smoothed according to their fractal distribution in space. Apart from this alternative approach, also another smoothing approach was proposed by Frankel (1995). This approach is still based on zonation but Gaussian function is used to smooth a values from Gutenberg-Richter recurrence relation (1.20) for each zone. However, many authors refer to this approach as a zoneless approach, what we consider to be incorrect.

1.4 Mathematical theory of probabilistic approaches in SHA

1.4.1 Parametric and non-parametric methods for PDF estimation

The probability density function (PDF) $f(x)$ is a fundamental concept in statistics. It is defined as non-negative integrable function with following properties

$$\int_{-\infty}^{\infty} f(x)dx = 1, \quad (1.7)$$

$$F(x) = \int_{-\infty}^x f(t)dt, \quad (1.8)$$

$$F(b) - F(a) = \int_a^b f(x)dx, \quad (1.9)$$

$$P(a < X \leq b) = \int_a^b f(x)dx, \quad (1.10)$$

where $F(x)$ is cumulative distribution function of random variable X defined as $F(x) = P(X \leq x)$. It follows from equations (1.7) – (1.10) that $f(x)$ gives a natural description of the distribution of random quantity X and allows to find probability that X fall in the interval (a, b) , therefore knowing $f(x)$ is often very convenient.

In practice, we are often dealing with a problem that we have a set of observed data points assumed to be a sample from an unknown probability density function. Despite the fact, that the real probability density function is unknown, it is possible to estimate probability density function from the observed data set. There are many methods how to estimate a density function from a given data set, but in general they can be divided into two groups – parametric and non-parametric.

Parametric methods to density estimation are based on the assumption that the observed data set are drawn from one of a known parametric family of distributions and our task is to find parameters of this distribution. For example, let's assume that the observed data set is a sample from normal Gaussian distribution. General form of the probability density function

$$f(x) = \frac{1}{\sigma\sqrt{2\pi}} e^{-\frac{(x-\mu)^2}{2\sigma^2}} \quad (1.11)$$

is known, but specific values of mean μ and variance σ^2 are unknown and need to be estimated.

On the other hand, in ***non-parametric methods*** less rigid assumptions are to be made about the distribution of the observed data. It is assumed that the distribution has a probability density function $f(x)$, but the data are allowed to speak for themselves and the estimate of $f(x)$ is found with use of the observed data set, without assumption that $f(x)$ fall in a given parametric family. The most commonly used non-parametric estimation methods are histogram and kernel estimator. We will use the symbol \hat{f} to denote density estimator currently considered.

1.4.1.1 Histograms

Histogram is known mainly as a graphical representation of the distribution of numerical data. It is considered to be the oldest and most widely used density estimator. To construct the histogram, two parameters have to be chosen – an origin x_0 and a bin width h . Then we can define the bins of the histogram to be the intervals $[x_0 + mh, x_0 + (m+1)h]$ for positive and negative integers m . The intervals have to be non-overlapping, chosen closed on one side and open on the other. Considering that we are given a sample of n real observations X_1, \dots, X_n the histogram is then defined by

$$\hat{f}(x) = \frac{1}{nh} (\text{no. of } X_i \text{ in the same bin as } x). \quad (1.12)$$

The histogram can be generalized by allowing the bin widths to vary. Formally, suppose that we have any dissection of the real line into bins, then the estimate will be defined by

$$\hat{f}(x) = \frac{1}{n} \times \frac{(\text{no. of } X_i \text{ in the same bin as } x)}{(\text{width of bin containing } x)}. \quad (1.13)$$

The choice of bin width primarily controls the amount of smoothing inherent in the procedure and the choice of origin can have quite an effect on the histogram too. For demonstration, let's use the data set adapted from Silverman (1986) - observations of the eruptions of Old Faithful geyser in Yellowstone National Park in USA, reproduced in *Table 1.2*. *Figure 1.3* shows two histograms constructed with the same bin width but different origins.

As we mentioned before, histogram is really powerful tool for graphical representation of the distribution of numerical data. However, when density estimates are needed as intermediate components of other methods, it is necessary to use method more sophisticated than histogram itself. Strong disadvantage of histogram is its discontinuity, especially if derivatives of the estimate are required. Other problems arise if histograms are used for graphical representation of bivariate or trivariate data. In such case, the estimate depends not only on the choice of an origin but also on the choice of the coordinate directions of the grid of cells.

4.37	3.87	4.00	4.03	3.50	4.08	2.25
4.70	1.73	4.93	1.73	4.62	3.43	4.25
1.68	3.92	3.68	3.10	4.03	1.77	4.08
1.75	3.20	1.85	4.62	1.97	4.50	3.92
4.35	2.33	3.83	1.88	4.60	1.80	4.73
1.77	4.57	1.85	3.52	4.00	3.70	3.72
4.25	3.58	3.80	3.77	3.75	2.50	4.50
4.10	3.70	3.80	3.43	4.00	2.27	4.40
4.05	4.25	3.33	2.00	4.33	2.93	4.58
1.90	3.58	3.73	3.73	1.82	4.63	3.50
4.00	3.67	1.67	4.60	1.67	4.00	1.80
4.42	1.90	4.63	2.93	3.50	1.97	4.28
1.83	4.13	1.83	4.65	4.20	3.93	4.33
1.83	4.53	2.03	4.18	4.43	4.07	4.13
3.95	4.10	2.72	4.58	1.90	4.50	1.95
4.83	4.12					

Table 1.2 – Eruption lengths (in minutes) of 107 eruptions of Old Faithful geyser. Reproduced from Silverman (1986).

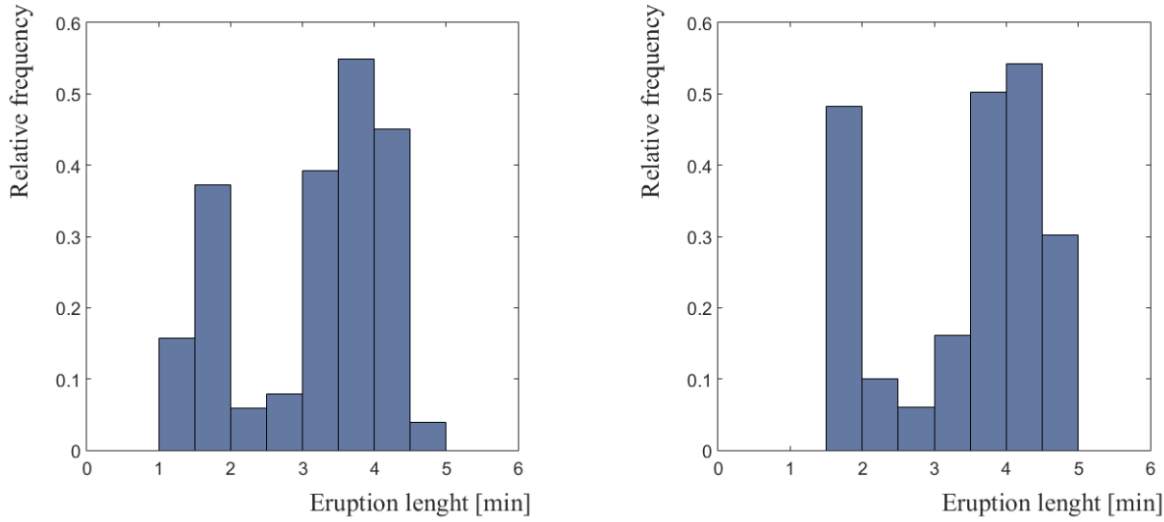


Figure 1.3 – Histogram of eruption lengths of Old Faithful geyser. Reproduced from Silverman (1986).

1.4.1.2 The naive estimator

For the random variable X with density f from the definition of a probability density function we can write

$$f(x) = \lim_{h \rightarrow 0} \frac{1}{2h} P(x-h < X < x+h). \quad (1.14)$$

For any given h , we can estimate probability $P(x-h < X < x+h)$ as a ratio of the sample falling in the interval $(x-h < X < x+h)$ and sample of n real observations. Thus a natural estimator \hat{f} of the density is given by

$$\hat{f}(x) = \frac{1}{2hn} [\text{no. of } X_i \text{ falling in } (x-h, x+h)] \quad (1.15)$$

and we shall call this the naive estimator.

We can also define the estimator using weight function w defined as

$$w(x) = \begin{cases} \frac{1}{2} & \text{if } |x| < 1 \\ 0 & \text{otherwise.} \end{cases} \quad (1.16)$$

Then the estimator can be written in the form

$$\hat{f}(x) = \frac{1}{n} \sum_{i=1}^n \frac{1}{h} w\left(\frac{x - X_i}{h}\right). \quad (1.17)$$

It follows from (1.16) and (1.17) that the estimate is constructed as a sum of boxes with width $2h$ and height $(2hn)^{-1}$ and each of these boxes is placed on one observation. We can see, that there is strong connection between naive estimator and histogram – naive estimator is practically histogram, where every point is the centre of a sampling interval. Then we do not have to choose the bin positions, but we still have to choose bin width h , which controls the amount of smoothing in the procedure.

Using the naive estimator as a density estimate might not be completely satisfactory solution, because \hat{f} is not continuous function, it has jumps at the points $X_i \pm h$ and has zero derivative everywhere else. To overcome these, we have to generalize the naive estimator.

1.4.1.3 The kernel estimator

Another non-parametric method for density estimation of random data set is the kernel estimator. The kernel estimator is defined by

$$f(x) = \frac{1}{nh} \sum_{i=1}^n K\left(\frac{x - X_i}{h}\right), \quad (1.18)$$

where $K(x - X_i / h)$ is kernel function (also known as kernel) and h is the window width, also called the smoothing parameter or bandwidth. Kernel function, like probability density function, is non-negative integrable function which satisfies the condition (1.7).

According to the equation (1.18), the kernel estimator is closely related to histogram and even more closely to the naive estimator. The kernel estimator can be considered as a generalization of the naive estimator which was created by replacing the weight function w by the kernel function K . Just as the naive estimator can be considered as a sum of boxes placed at the observations, the kernel estimator is a sum of bumps placed at the observations. Shape of these bumps is given by the kernel function K and their width is determined by the bandwidth h .

An example is given in *Figure 1.4*. To construct this estimate, we used sample of six numbers $\{13; 14; 15; 25; 29; 32\}$, which is really a small sample for any real density estimation, but it is enough to demonstrate some important properties of kernel function. We placed normal Gaussian kernel at each observation and construct the estimate by adding them up. We estimated density for three different values of bandwidth - $h \in \{1; 4; 8\}$ and *Figure 1.4* shows the effect of varying the window width. If h is chosen too small [*Figure 1.4 B*], the estimate of density is given by a sum of Dirac delta functions. On the other hand, if h becomes larger [*Figure 1.4 C*], all details are obscured.

The choice of the kernel function K and its shape does not affect the estimate as much as the choice of the bandwidth h . An example is shown in *Figure 1.5*. We constructed kernel estimates for data set from *Table 1.2* using two different kernel functions K - normal kernel [*Figure 1.5 A*] and box kernel [*Figure 1.5 B*] and we can see, that the shape of these density estimates is not so much different. Although the shape of these estimates looks quite similar, these functions have different properties and these properties correspond to properties of the kernel function K , which we used. It means that if we want, for example, our estimate to be continuous function with continuous derivative, we need to use kernel function K with these properties.

The kernel estimator is one of the most commonly used estimators but it also has its disadvantages. Problems arise when it is applied to data from long-tailed distribution and it is mainly because the bandwidth is constant across the entire sample. In the tails of the estimate spurious noise can appear and if we smooth the estimate sufficiently to overcome this, essential details in the main part can be obscured.

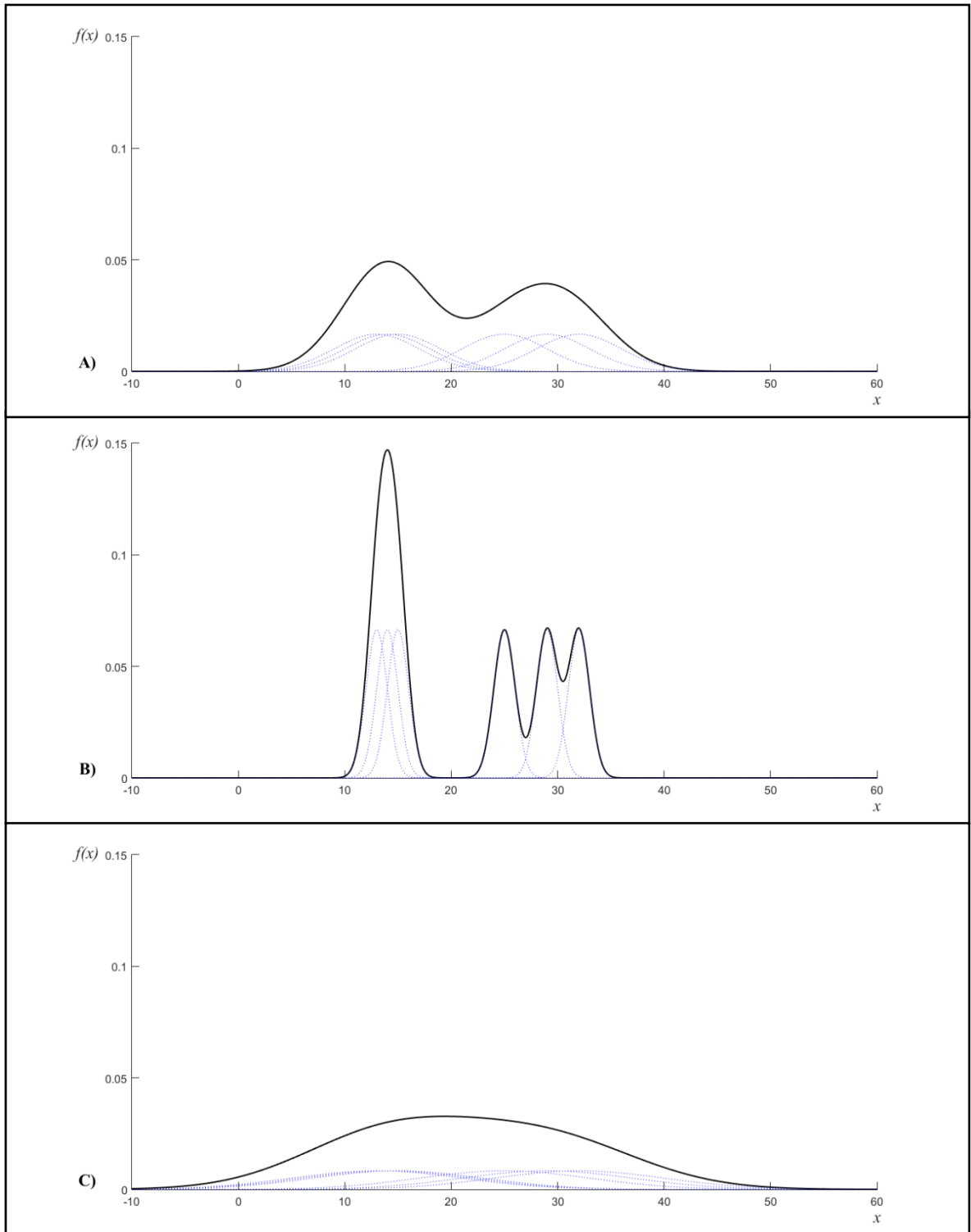


Figure 1.4 - Kernel density estimation for sample $\{13; 14; 15; 25; 29; 32\}$ using normal kernel with bandwidth **A)** 4; **B)** 1; **C)** 8. Adapted from Silverman (1986).

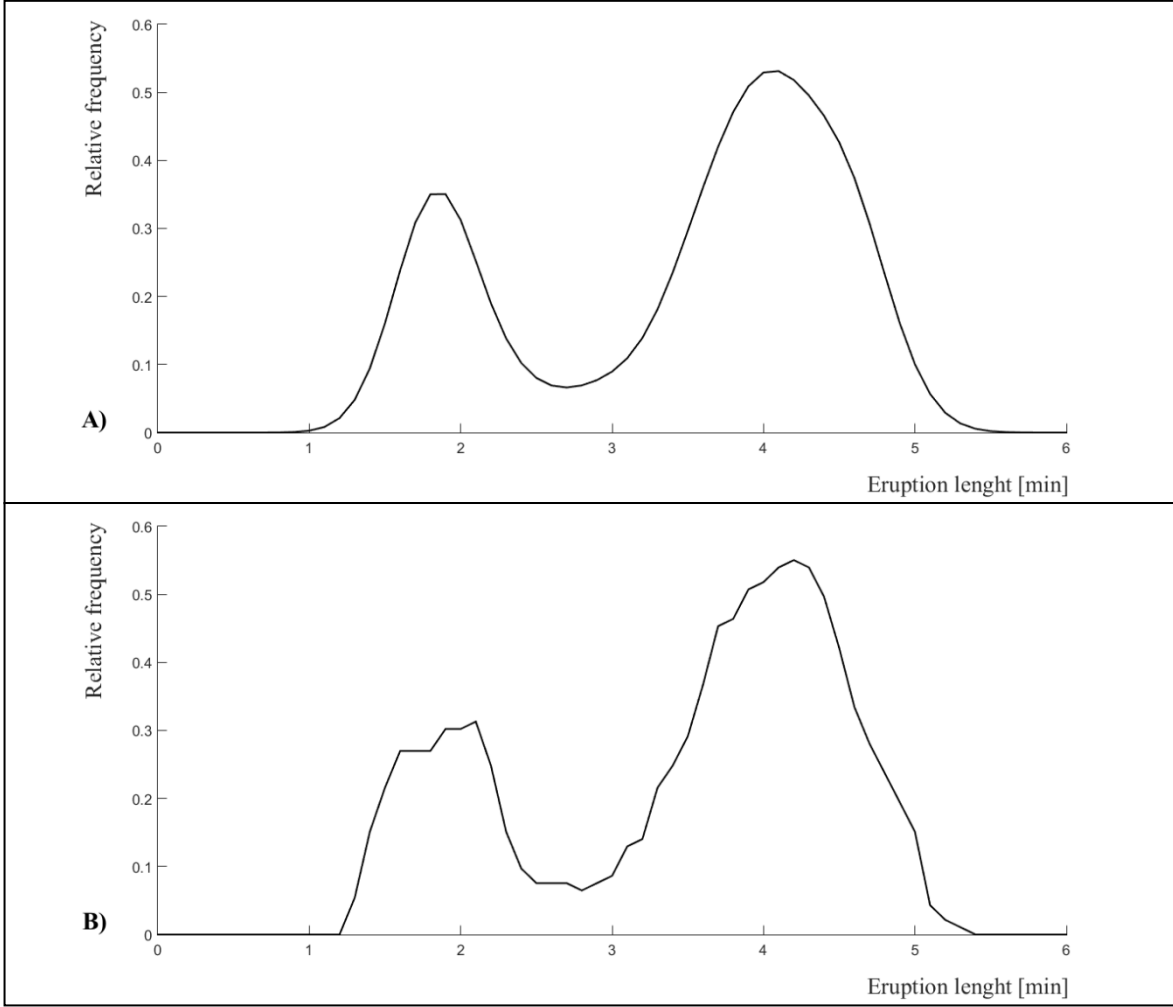


Figure 1.5 - Kernel estimate for Old Faithful geyser data using **A)** normal kernel **B)** box kernel with bandwidth $h = 0.25$. Adapted from Silverman (1986).

1.4.2 Mathematical description of Cornell-McGuire approach

In Cornell-McGuire approach, the annual rate of exceedance $N[C > c]$ (frequency of the ground motion parameter C exceeding a particular value c) is given by relation

$$N[C > c] = \sum_{j=1}^J \lambda_j^{\min} \int_{M_j^{\min}}^{M_j^{\max}} \int_0^{R^{\max}} f_j^R(r) f_j^M(m) P[C > c | m, r] dm dr. \quad (1.19)$$

Individual components in the seismic hazard integral (1.19) have following meanings:

J number of seismic source zones

M^{\min} *minimum (computational) magnitude*

Minimum (computational) magnitude is chosen usually at a value at which contribution to damage on buildings will occur. Its value should be selected in consultation with the seismic designer and/or the fragility analyst.

M_j^{\max} *maximum potential magnitude for seismic source j*

Maximum potential magnitude represents the strongest earthquake, which may occur in seismic source j . Due to the short period of observations, maximum potential magnitude for seismic source j is not chosen as a maximum observed magnitude, but it should be chosen as a maximum observed magnitude plus some additional increment (e.g. 0.3, 0.5, 1.0).

If sufficient seismological and geological data about the seismotectonic structure of the region are available, maximum potential magnitude can be obtained from the fault parameters (e.g. surface rupture length, subsurface rupture length, rupture area, maximum and average displacement per event) using empirical relations. Well-known and preferably used relations are Wells and Coppersmith (1994) and Leonard (2010).

Another possible approach how to determine maximum potential earthquake is based on statistical analysis of recurrence relations for earthquakes related to seismogenic structure (e.g. Kijko 2004) or statistical analysis of historical data and seismotectonic regional characteristics by the comparison with similar (analogous) seismotectonic regions for which sufficient historical data are available (e.g. Johnson et al. 1994).

R^{\max} *maximum (computational) distance of seismic sources*

$f_j^R(r)$ *probability density function for distance between seismic source j and the site*

This component is the result of the seismotectonic model of the region and it is affected by the allocation of the source zones, geometry of the source zones, and relative position of the source zone to the site.

$f_j^M(m)$ *probability density function for magnitude for seismic source j*

This component is determined from the recurrence (magnitude-frequency) relation. The most famous one is Gutenberg-Richter recurrence law (Gutenberg and Richter 1944) in form

$$\log(N) = a - bm, \quad (1.20)$$

where N is cumulative rate of earthquakes with magnitude greater than or equal to m , a and b are constants. It follows from relation (1.20) that the parameter a represents annual number of earthquakes with magnitude greater than or equal to zero. Parameter (the b value) indicates the relative ratio of small and large magnitudes for a given seismic source. For intraplate seismotectonic regions, typical b values are approximately equal to 1. As the b value increases, the number of larger magnitude earthquakes decreases compared to those of smaller magnitudes.

Relation (1.20) can be also written in form

$$N(m) = \alpha e^{-\beta m}, \quad (1.21)$$

where

$$\alpha = 10^a, \quad \beta = b \ln 10. \quad (1.22)$$

For the seismic source j , range of magnitudes m is given by interval

$$M_{\min} \leq m \leq M_j^{\max}. \quad (1.23)$$

The upper bound of the interval is determined by maximum potential magnitude M_j^{\max} .

The lower bound of the interval M_{\min} is different from minimum magnitude M^{\min} and it depends on the quality of the catalogue, especially on its spatial and temporal completeness that is closely related to the detection efficiency of the network of seismic stations.

For thus bounded magnitude interval can be from relation (1.21) derived doubly truncated Gutenberg-Richter recurrence law

$$N(m) = \alpha^{\min} \left[1 - \frac{1 - e^{-\beta(m - M_{\min})}}{1 - e^{-\beta(M_j^{\max} - M_{\min})}} \right], \quad (1.24)$$

where α^{\min} is the rate of earthquakes with magnitude m from interval $M_{\min} \leq m \leq M_j^{\max}$. It can be shown, that corresponding probability density function for magnitude for the seismic source j is given by relation

$$f_j^M(m) = \beta \frac{e^{-\beta(m-M_{\min})}}{1 - e^{-\beta(M_j^{\max}-M_{\min})}}. \quad (1.25)$$

λ_j^{\min} *rate of occurrence of earthquakes greater than M^{\min} from the source j*

It follows from relation (1.24) that

$$\alpha^{\min} = \lambda_j^{\min}. \quad (1.26)$$

$P[C > c | m, r]$ *conditional probability of exceeding a particular value c of a ground motion parameter C for a given magnitude m and distance r*

This conditional probability can be determined using GMPE. GMPE usually have the form

$$\ln C = g(m, r, s_i) + \varepsilon, \quad (1.27)$$

where $g(m, r, s_i)$ is a mathematical function, that denote the dependence of the ground motion parameter C on magnitude m , source-to-site distance r and the set of other relevant parameters s_i (e.g. style of faulting, hanging wall effects and local site conditions). ε is a random variable corresponding to the uncertainty of the particular GMPE. We assume that ε has normal (Gaussian) distribution, given by relation (1.11), with mean $\mu = 0$ and standard deviation σ .

If we use relation (1.27), we can rewrite the inequality $C > c$ as follows

$$\begin{aligned} C &> c \\ \ln C &> \ln c \\ g(m, r) + \varepsilon &> \ln c \\ \varepsilon &> \ln c - g(m, r) \end{aligned} \quad (1.28)$$

and thus the probability $P[C > c | m, r]$ can be rewritten as

$$P[C > c | m, r] = P[\varepsilon > \ln c - g(m, r) | m, r]. \quad (1.29)$$

Since ε is given by relation (1.11) with mean $\mu = 0$ and standard deviation σ , we get

$$\begin{aligned} P[C > c | m, r] &= P[\varepsilon > \ln c - g(m, r) | m, r] \\ &= \int_{\ln c - g(m, r)}^{\infty} \frac{1}{\sigma\sqrt{2\pi}} \exp\left(-\frac{\varepsilon^2}{2\sigma^2}\right) \\ &= 1 - \int_{-\infty}^{\ln c - g(m, r)} \frac{1}{\sigma\sqrt{2\pi}} \exp\left(-\frac{\varepsilon^2}{2\sigma^2}\right) \\ &= 1 - \Phi\left(\frac{1}{\sigma}[\ln c - g(m, r)]\right), \end{aligned} \quad (1.30)$$

where Φ is the standard normal cumulative distribution function. The conditional probability $P[C > c | m, r]$ of exceeding a particular value c of a ground motion parameter C for a given magnitude m and distance r is thus given by relation

$$P[C > c | m, r] = 1 - \Phi\left(\frac{1}{\sigma}[\ln c - g(m, r)]\right). \quad (1.31)$$

Graphical illustration of relation (1.31) is shown in *Figure 1.6*.

Reciprocal value of the annual rate of exceedance $N[C > c]$ is called return period RP and is given by relation

$$RP = \frac{1}{N[C > c]}. \quad (1.32)$$

Return period can also be expressed as

$$RP = -\frac{T}{\ln(1 - P[C > c])}, \quad (1.33)$$

where $P[C > c]$ is probability of the ground motion parameter C exceeding a particular value c during the period T .

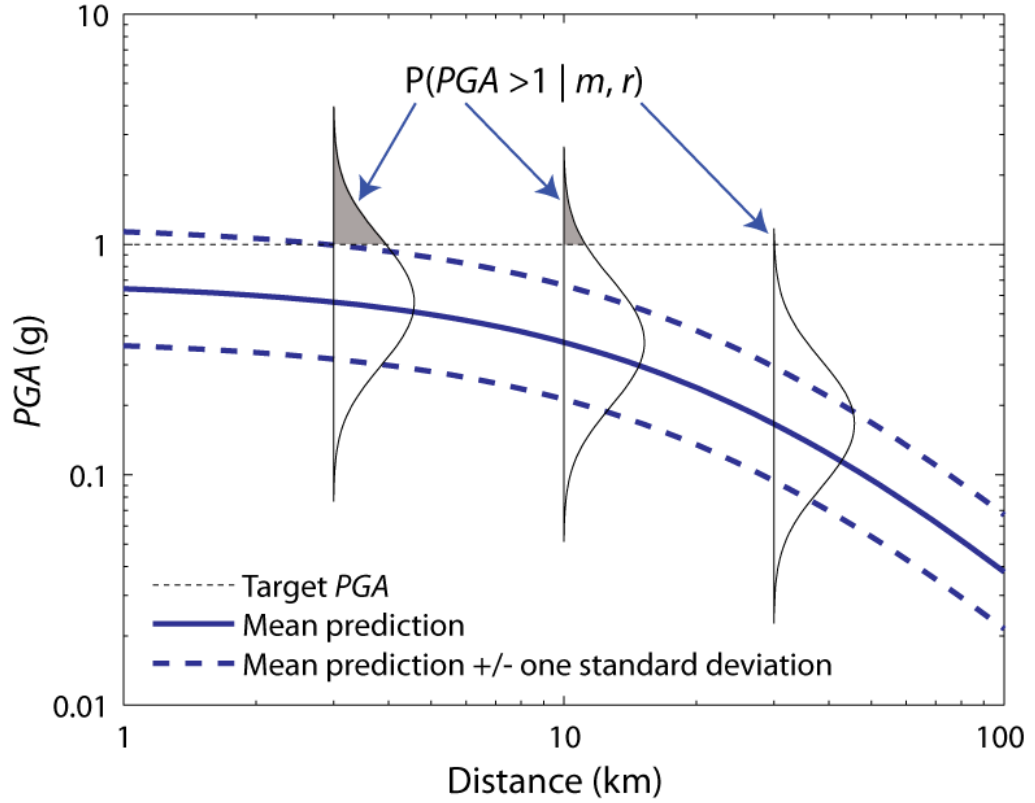


Figure 1.6 – Graphical illustration of conditional probability $P[C > c | m, r]$ from relation (1.19). GMPE by Cornell et al. (1979) is depicted for $m = 6.5$ at several source-to-site distances. Grey part represents the searched conditional probability of exceeding the selected value $PGA > 1$ for a given pair of magnitude m and distance r . Reproduced from Baker (2008).

1.4.3 Mathematical description of zoneless approach

In zoneless approach, the annual rate of exceedance $N[C > c]$ (frequency of the ground motion parameter C exceeding a particular value c) is given by relation

$$N[C > c] = \int_{\Omega} \int_{M^{\min}}^{M^{\max}} \lambda(m, \vec{x}) P[C > c | m, \vec{x}] dm dx. \quad (1.34)$$

If we compare relation (1.34) to relation (1.19), we can see that in relation (1.34) there is no summation over all seismic source zones, since in zoneless approach seismic source zones are not allocated. Probability density functions $f_j^R(r)$, $f_j^M(m)$ are omitted and the rate of occurrence λ_j^{\min} is replaced by the seismic activity rate $\lambda(m, \vec{x})$. Individual components in relation (1.34) have following meanings:

Ω *computational area covered by a rectangular grid*

M^{\min} *minimum (computational) magnitude*

Minimum (computational) magnitude has the same meaning as in the classical approach and is chosen usually at a value at which contribution to damage on buildings will occur.

M^{\max} *maximum considered magnitude*

Maximum considered magnitude M^{\max} is different from maximum potential magnitude M_j^{\max} in Cornell-McGuire approach. In zoneless approach, maximum considered magnitude is chosen as maximum recorded magnitude, without an additional value.

$P[C > c | m, \vec{x}]$ *conditional probability of exceeding a particular value c of a ground motion parameter C for a given magnitude m at a point \vec{x}*

This conditional probability has the same meaning as in the classical approach and is given by relation (1.31).

$\lambda(m, \vec{x})$ *seismic activity rate for events of magnitude m at point \vec{x}*

Seismic activity rate represents expected annual number of events of magnitude m occurring at location \vec{x} . It is given by relation

$$\lambda(m, \vec{x}) = \sum_{i=1}^N \frac{K(m, \vec{x} - \vec{x}_i)}{T(\vec{x}_i)}, \quad (1.35)$$

where N is the number of earthquakes in the catalogue, \vec{x}_i is epicentre of earthquake i in the catalogue, $K(m, \vec{x} - \vec{x}_i)$ is kernel function and $T(\vec{x}_i)$ is the effective return period of earthquake i , which is a measure of the detection probability of that earthquake in the past.

According to relation (1.35), the seismic activity rate is obtained as a summation of kernel functions placed on each event of the catalogue and the contribution of each event is inversely weighted by the effective return period of that event.

Various forms of kernel functions can be chosen. One example is kernel function suggested by Woo (1996), which is an anisotropic modification of the isotropic kernel function suggested by Vere-Jones (1992), expressed as

$$K(m, \vec{x} - \vec{x}_i) = \frac{n-1}{\pi h^2(m)} \frac{1 + \delta \cos^2 \phi}{1 + (\delta/2)} \left(1 + \frac{r^2}{h^2(m)} \right)^{-n}, \quad (1.36)$$

where r is the distance between location \vec{x} and the epicentre of earthquake \vec{x}_i .

The parameter n in relation (1.36) is called kernel fractal scaling index. It scales the fall off of the kernel function and according to Vere-Jones (1992), recommended values are between 1.5 and 2.0, thus corresponding to a cubic or quadratic decay of the kernel function with epicentral distance.

Parameters δ and ϕ both represent anisotropy. The parameter δ is the degree of anisotropy – a value of 0 indicates isotropy, on the other hand a value of 100 indicates significant anisotropy. The parameter ϕ is the angle of anisotropy – it is the angle subtended at \vec{x} between the intersection of the fault plane with the Earth's surface and the epicentral location. Its values are between 0 and 2π . These parameters of anisotropy allow to shape kernel function to reflect a degree of correlation with faults and fault systems.

Function $h(m)$ is the bandwidth function. The bandwidth function is designed to reflect the degree of spatial clustering of catalogued earthquakes in a given magnitude range, because it is often observed that smaller events are spatially clustered, whereas the larger less frequent earthquakes are spatially more disperse. Woo (1996) suggested exponential representation of the bandwidth function expressed as

$$h(m) = c e^{(dm)}, \quad (1.37)$$

where c and d are regionally specific constants, that depend on the spatial distribution of catalogued earthquakes. Evaluation of parameters c and d consists of following steps:

- Events are sorted in groups according to their magnitude (magnitude bins).
- For each event, the distance to the nearest epicentre within the same magnitude bin is determined.
- All minimum distances determined for the same magnitude bin are averaged and the mean nearest distance for each magnitude bin is calculated.
- Through a least-square fit between the magnitude m the mean nearest distance h , parameters c and d are obtained.

Lower values of $h(m)$ for certain magnitudes implies that these events are highly clustered, while higher values of $h(m)$ implies less clustering. According to Molina et al. (2001), the bandwidth function $h(m)$ has a decisive influence on the kernel function, its evaluation is therefore one of the most important steps in zoneless approach.

1.5 Applications of zoneless approach

Kernel density estimation was first applied to seismic hazard analysis by Gordon Woo (Woo 1996). The aim of this paper was to propose an alternative procedure for area source modelling that avoids seismic source zonation and an assumption of uniform seismicity within a zone. Seismic activity rate $\lambda(m, \vec{x})$ was proposed by relation (1.35) and apart from Vere-Jones (1992) kernel function given by relation (1.36) also alternative finite-range kernel function $K(m, \vec{x} - \vec{x}_i)$ was proposed in form

$$\begin{aligned} K(m, \vec{x} - \vec{x}_i) &= [D/2\pi h(m)] [h(m)/r]^{2-D} \quad \text{for } r \leq h(m), \\ &= 0 \quad \text{for } r > h(m), \end{aligned} \tag{1.38}$$

where D is fractal dimension of epicentres and was chosen 1.5 in this paper.

One example presented in Woo (1996) where zoneless approach might be useful is Great Britain. Great Britain is an example of an intraplate region with modest seismicity, where because of observed significant magnitude-dependent variations (smaller events are significantly clustered, whereas larger are more regularly spaced) and regional anomalies in b -values no scientifically based zonation is commonly accepted.

A comparison of zoneless approach and classical Cornell-McGuire approach was done by Molina et al. (2001) using four different data sets – two synthetic catalogues, a temporarily short earthquake catalogue from Norway with records from 1657 to 1995, and a temporarily long earthquake catalogue from Spain with records from 1300 to 1998.

Firstly, synthetic catalogue with pseudo random epicentre distribution was generated based on doubly truncated Gutenberg-Richter relation containing 165 earthquakes with magnitudes ranging from 4.0 to 6.2. In this case, seismic hazard curves were computed for four different sites. Hazard curves computed by using zoneless approach better reflect source-to-site distance than Cornell-McGuire approach and therefore provide a more

realistic result in this case. This can be explained by the fact, that the generated earthquake distribution did not satisfy the requirement of a homogenous seismicity within a zone.

Second synthetic catalogue was generated to simulate fault behaviour – it reflects activity along a 380 km long and 30 km wide structure, with higher activity rate per unit area than in the previous case. Hazard curves were also computed for four different sites, but in this case, classical approach yields higher values of annual exceedance probability.

For Southern Norway, hazard was evaluated at three sites and for each site one classical computation and three zoneless computations (one with real data and two with additional background seismicity) were conducted. For two sites, all three results obtained by zoneless procedure are much lower than results obtained by classical approach and for the third, low activity site, results from all four computations were quite similar. The observed difference may be caused by the extrapolation of the recurrence relation up to $M^{\max} = 7.0$, whereas data for Norway are insufficient to evaluate the recurrence relation for magnitudes greater than 5.5.

The same procedure as for the Norwegian catalogue was followed for Spanish catalogue. Hazard was evaluated at three sites and for each site three zoneless computations were conducted, which were compared to results obtained by classical approach by Molina (1998). Obtained results showed the same features as previous ones, annual exceedance probability computed by both procedures differs for sites with higher seismic activity, but is quite similar for the site with lower seismic activity.

In this study, also sensitivity of the results to the bandwidth function, fractal scaling index and anisotropy parameter δ was tested and it was shown, that the bandwidth function has the most significant impact on the results.

Beauval et al. (2006) also compared the results obtained by zoneless and classical approach for two profiles in France – first chosen profile was along the meridian crossing first the West Pyrenees, then the Aquitaine Basin and Brittany, the second profile was transversal crossing first the Alps, then the Limagne zone and Brittany. For both profiles three return periods – 475, 10 000 and 100 000 years, were considered. Obtained results were consistent with results from Molina et al. (2001) – for regions with high seismic activity, zoneless approach yields much lower results than classical approach but results were quite similar for low activity regions.

Also the impact of the choice of the kernel function was evaluated in this study and apart from Vere-Jones kernel function also $1/r$ kernel function truncated at 100 km was used. It was shown, that the choice of the kernel function has small impact on hazard in moderate and low seismicity regions, but has an important impact on hazard values in very low seismicity regions, especially for long return periods.

In this study, both methods were also compared through deaggregation studies for the site in the Alps and the site in the Rhine Basin. For both sites, the distributions of contributions according to the distance are rather similar, but the distributions of contributions according to the magnitude differ significantly.

Apart from kernel density estimation introduced in subsection 1.4.1.3 also adaptive kernel density estimation (Silverman, 1986) was used for seismic hazard analysis of South India (Ramanna and Dodagoudar 2011). It was found that in regions with very high seismic activity, the adaptive kernel technique yielded higher values than kernel technique and on the other hand, in regions with very low seismic activity, results obtained with adaptive kernel technique were lower than results obtained with kernel technique.

For four sites also the effect of varying bandwidth parameter was studied for both adaptive and fixed kernel technique – for each site uniform hazard spectra was evaluated using c and d values evaluated from the whole earthquake catalogue and using local c and d values evaluated only events lying in an influence area of 300 km radius around a particular site. For all four sites higher values of peak spectral acceleration were obtained when using local c and d values.

Both kernel techniques mentioned above and results obtained by these zoneless approaches were later compared to classical Cornell-McGuire approach for Chennai City by Ramanna and Dodagoudar (2012), where influence area of 300 km radius around Chennai City was considered. Since Chennai City lies in a low to moderate seismic region, results obtained by all three procedures were comparable. However, for a lower return periods, classical approach yielded higher values of peak spectral acceleration.

Further evaluation of seismic hazard using zoneless approach was done by Crespo et al. (2014) for the Iberian Peninsula. Obtained results, computed for return periods of 475 and 2475 years, were compared with previous studies for this region. Good consistency was achieved with different recent studies at a regional scale, for example Benito et al. (2010) study for Andalusia, small differences may be partially explained from the consideration of

different soil types. For two regions – south-east of Spain and the Pyrenean region, consistency was only achieved with studies that followed an alternative PSHA approach (Peláez-Montilla and López-Casado, 2002) or incorporated kernel approach as a branch of a logic tree (Secanell et al., 2008). Results obtained for these two regions were significantly higher than results obtained by classical approach, which suggest that the spatial gradient of the activity rate in these areas is high and smaller zonation would be needed.

As already mentioned before, in some studies zoneless approach was incorporated in the PSHA together with classical approach as branches of a logic tree. For example Bozzoni et al. (2011) in the PSHA calculations for the Eastern Caribbean Islands assigned a weight of 0.65 to classical Cornell-McGuire approach and a weight of 0.35 to zoneless approach, Salazar et al. (2013) in the PSHA calculations for Jamaica assigned to both approaches the same weight of 0.5 and Corigliano et al. (2014) in the PSHA calculation for Chile assigned a weight of 0.7 to classical Cornell-McGuire approach and a weight of 0.3 to zoneless approach.

2 OBJECTIVES OF MASTER'S THESIS

The main objective of the Master's Thesis is to assess the applicability of zoneless approach for the probabilistic seismic hazard assessment of the territory of Slovakia.

To achieve the main objective of the Master's Thesis, following partial steps were done:

1. Determination of the bandwidth function parameters.
2. Calculation of the effective return periods.
3. Computation of the seismic activity rate using alternatively finite and infinite kernel function.
4. Analyses of sensitivity of the seismic hazard curves in PGA and seismic hazard map for 475 yr return period to
 - a. bandwidth parameters
 - b. kernel functions
 - c. effective return periods
5. Comparison of the seismic hazard for the territory of Slovakia obtained by the zoneless approach with the results from the classical Cornell-McGuire approach.

3 RESULTS

3.1 Earthquake catalogue for the territory of Slovakia

In this thesis we used earthquake catalogue SLOVEC (2011). This catalogue has been compiled using data from the following sources:

- previous version of the Slovak national earthquake catalogue (Labák 1998),
- CENEC catalogue (Grünthal et al. 2009),
- the earthquake catalogue of the local networks of seismic stations situated around nuclear power plants Jaslovské Bohunice and Mochovce (Progseis 2010),
- the earthquake databases of Geophysical Institute, Slovak Academy of Sciences, containing data on macroseismically observed and/or instrumentally recorded earthquakes for the territory of Slovakia and its vicinity for the period from 1998 to 2009.

Catalogue SLOVEC (2011) was also used for PSHA of Slovakia following classical Cornell-McGuire procedure, presented in subsection 1.3.2.1, by Kysel (2014). The numbers of foreshocks, main shocks and aftershocks included in this catalogue are listed in *Table 3.1*.

FORESHOCKS	MAIN SHOCKS	AFTERSHOCKS	TOTAL
149	993	506	1 648

Table 3.1 – The numbers of earthquakes in catalogue SLOVEC (2011) by category.

Minimum computational magnitude used for hazard assessment of the territory of Slovakia using zoneless approach was $M_w = 4.5$. A modified version of the computer code KERGRID developed by Woo (2001a) was used for calculations. Depths which were assigned to individual events in SLOVEC (2011) catalogue were not included in our calculations and each event was assumed to have hypocentre at the surface, because applied computer code KERGRID (Woo 2001a) does not include hypocentral depths. Since in zoneless method no assumptions about the earthquake distribution are made, also the dependent events were retained and computations were done for both clustered and

declustered catalogue. The numbers of foreshocks, main shocks and aftershocks included in the SLOVEC (2011) catalogue used for zoneless PSHA calculations are listed in *Table 3.2* and shown in *Figure 3.1* together with zonation proposed by Hók et al. (2016).

FORESHOCKS	MAIN SHOCKS	AFTERSHOCKS	TOTAL
1	75	7	83

Table 3.2 – The numbers of earthquakes in catalogue SLOVEC (2011) with magnitudes equal or greater than $M_w = 4.5$ by category.

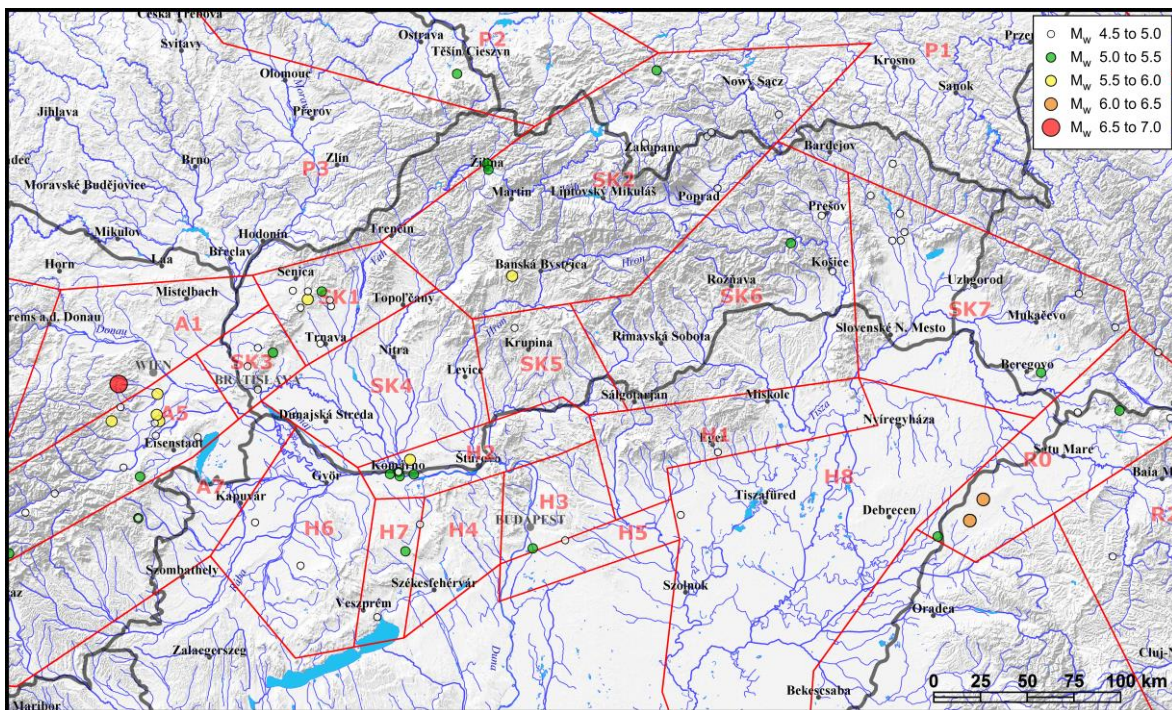


Figure 3.1 – Map of earthquake epicentres included in catalogue SLOVEC (2011) with magnitudes equal or greater than $M_w = 4.5$.

3.2 Bandwidth functions

To estimate parameters of the bandwidth function $h(m)$, individual events were sorted into magnitude bins as listed in *Table 3.3*. For calculation of the bandwidth function parameters, we followed procedure described in subsection 1.4.3 and we determined the bandwidth function parameters in four different ways.

First we wanted to find out, how is the estimate of bandwidth function parameters and the bandwidth function itself influenced by the choice of the threshold magnitude used in calculation of the bandwidth function parameters, since it was not mentioned in studies that used zoneless approach, whether threshold magnitude used for calculation of the bandwidth function parameters should correspond to the minimum computational magnitude used for hazard assessment. Therefore we calculate bandwidth function parameters using two threshold magnitudes - $M_w = 2.5$ and $M_w = 4.5$.

For both threshold magnitudes we again considered two alternatives for calculation of the bandwidth function parameters, which arise from *Table 3.3*. As can be seen, last two magnitude bins contain only two events, so their distance would also represent the mean nearest distance for particular magnitude bin. It is a natural question, whether such obtained mean nearest distance can be considered, since no statistical averaging is done in that case. Therefore we decided to calculate the bandwidth function parameters for both threshold magnitudes in two ways – first last two bins were considered separately (marked as S) and then they were merged and the mean nearest distance was calculated from four events instead of two (marked as M).

Calculations of the bandwidth function parameters were done for both clustered and declustered catalogue. Obtained values of bandwidth function parameters are listed in *Table 3.4* and obtained bandwidth functions are shown in *Figure 3.2*. We can see, that bandwidth function parameters obtained for separate last two magnitude bins have higher uncertainties when compared to bandwidth function parameters obtained for merged last two magnitude bins.

		Number of earthquakes in catalogue	
<i>Magnitude bin</i>	<i>Bin centre</i>	<i>Clustered</i>	<i>Declustered</i>
2.50 – 2.99	2.75	552	239
3.00 – 3.49	3.25	211	109
3.50 – 3.99	3.75	130	92
4.00 – 4.49	4.25	73	63
4.50 – 4.99	4.75	46	39
5.00 – 5.49	5.25	21	20
5.50 – 5.99	5.75	12	12
6.00 – 6.49	6.25	2	2
6.50 – 6.99	6.75	2	2

Table 3.3 – Magnitude bins used for calculation of the bandwidth function parameters.

Bandwidth function $h(m) = c e^{(dm)}$				
<i>Catalogue</i>	<i>Clustered</i>		<i>Declustered</i>	
Parameter	<i>c</i>	<i>d</i>	<i>c</i>	<i>d</i>
S/2.5	0.399	1.077	0.433	1.065
S/4.5	0.474	1.051	0.496	1.044
M/2.5	0.114	1.079	0.225	0.972
M/4.5	0.076	1.143	0.114	1.080

Table 3.4 – Calculated bandwidth function parameters.

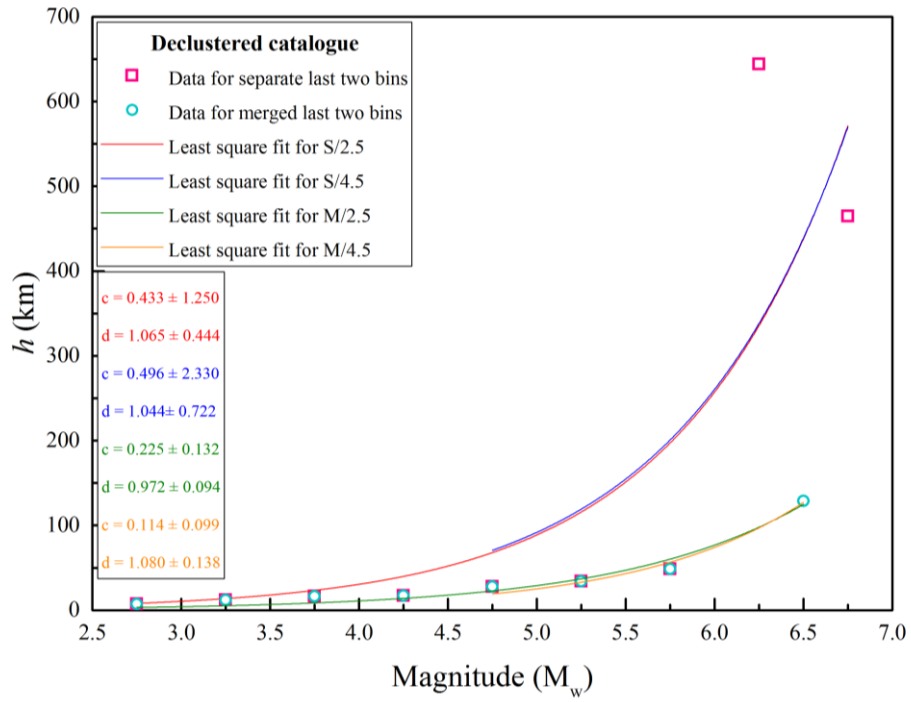
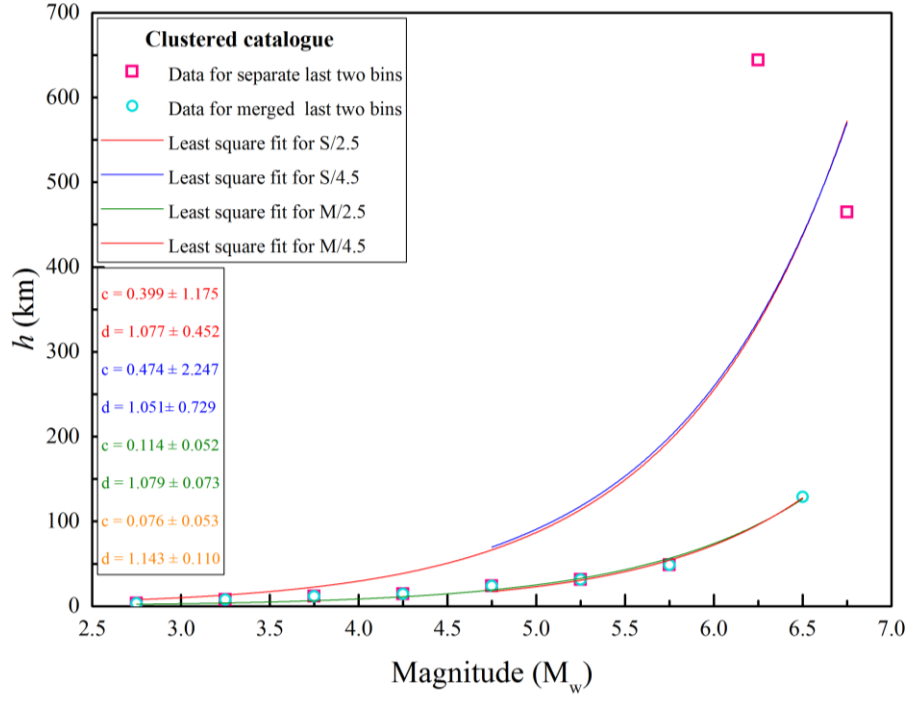


Figure 3.2 – Depiction of bandwidth functions for **A)** clustered **B)** declustered catalogue.

3.3 Effective return periods

For activity rate computation and hazard assessment also effective return period $T(x_i)$ need to be assigned to each event in the catalogue. In this thesis effective return period has been considered correspondent to the completeness period for a given magnitude bin. The completeness of the catalogue was determined by displaying the cumulative number of events for given magnitude bin with respect to the time (*Figure 3.3*). The most recent linear segment indicates a stable seismic activity, i.e. lower bound of the completeness time interval. Magnitude bins listed in *Table 3.3* for magnitudes equal or greater than $M_w = 4.5$ were also used for completeness period determination. Obtained completeness periods, which are the same for both clustered and declustered catalogue, are listed in *Table 3.5*.

MAGNITUDE BIN	COMPLETENESS TIME INTERVAL	EFFECTIVE RETURN PERIOD
4.50 – 4.99	1810 - 2009	199
5.00 – 5.49	1785 - 2009	224
5.50 – 5.99	1443 - 2009	566
6.00 – 6.49	1200 - 2009	809
6.50 – 6.99	1200 - 2009	809

Table 3.5 – Time completeness of the catalogue SLOVEC (2011) for magnitudes equal or greater than $M_w = 4.5$.

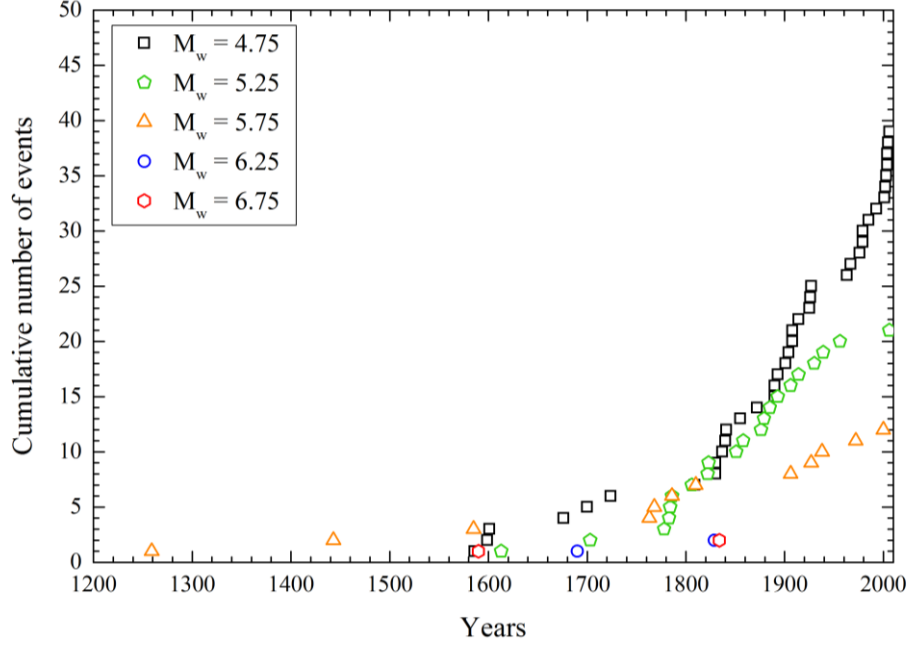


Figure 3.3 – Graphical representation of the time completeness of the catalogue SLOVEC (2011).

3.4 Kernel functions

In order to evaluate the impact of the choice of the kernel function $K(m, \vec{x} - \vec{x}_i)$ on the hazard results, we used three kernel functions in this study. First one was infinite kernel function K_1 given by relation (1.36) with fractal scaling index $n = 1.5$, but anisotropy was not considered, thus the second fraction, which represent anisotropy, was omitted. Second and third one were finite kernel functions proposed by Woo (2001b) in the manual of the KERGRID code given by relation

$$\begin{aligned}
 K(m, \vec{x} - \vec{x}_i) &= \frac{1}{2\pi(R_{\max} - 0.5R_{\min})} \frac{1}{R_{\min}} \quad \text{if } R < R_{\min}, \\
 &= \frac{1}{2\pi(R_{\max} - 0.5R_{\min})} \frac{1}{R} \quad \text{if } R_{\min} \leq R < R_{\max}, \\
 &= 0 \quad \text{if } R_{\max} \leq R.
 \end{aligned} \tag{3.1}$$

We considered two alternatives of the finite kernel function:

- K_2 with $R_{\min} = 10$ km and $R_{\max} = 50$ km,

- K_3 with $R_{\min} = 15$ km and $R_{\max} = 100$ km.

If we compare relation (3.1) with relation (1.36), we can see that finite kernel function is no longer magnitude dependent. If also for finite kernel function anisotropy is wanted, which was not the case in this thesis, relation (3.1) needs to be multiplied with second fraction in relation (1.36).

In order to evaluate how is the shape of the kernel function influenced by the computed bandwidth function, we plotted kernel function for each pair of bandwidth function parameters listed in *Table 3.4* for magnitude $m = 5$ (*Figure 3.4*). We can see that shape of the kernel function is strongly influenced by whether were last two magnitude bins merged or separated.

Since the kernel function is also magnitude dependent, we also wanted to show how the shape of the kernel function is affected by the magnitude. In this case, we considered only two alternatives of computed bandwidth function parameters – when last two magnitude bins were merged and separate for the threshold magnitude $M_w = 4.5$ for clustered catalogue. Results are shown in *Figure 3.5*.

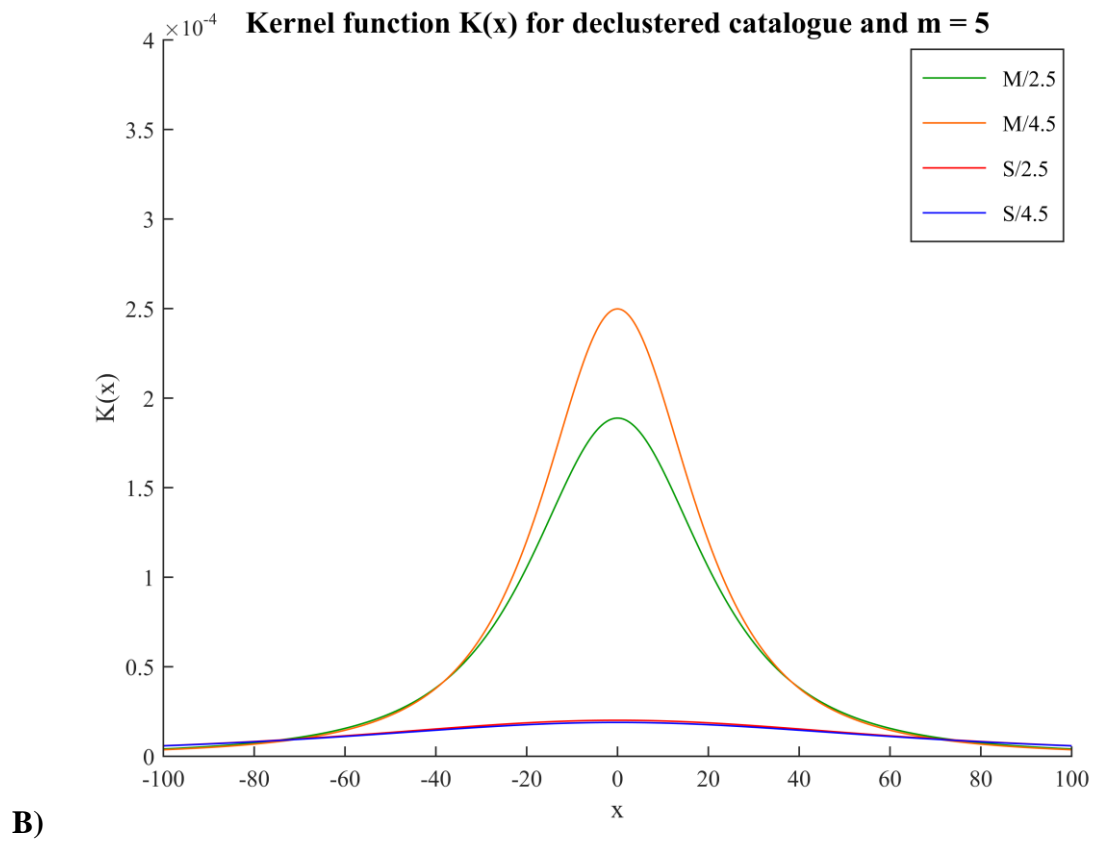
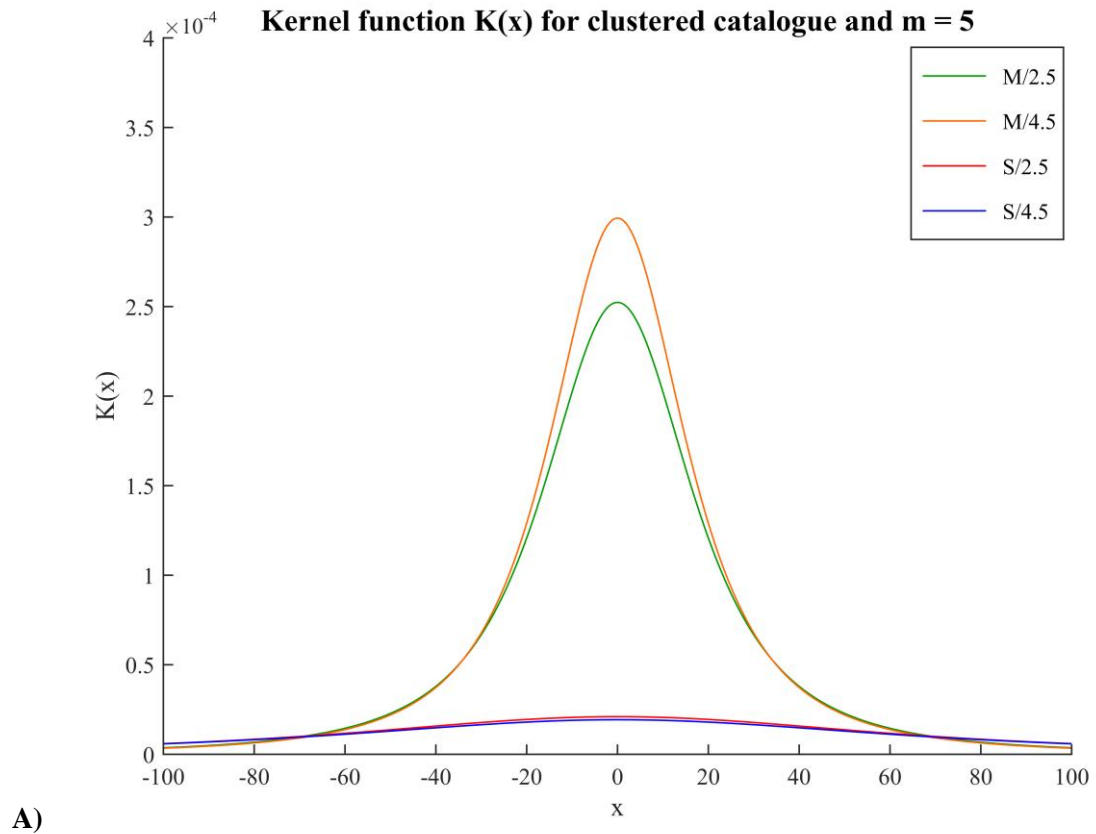
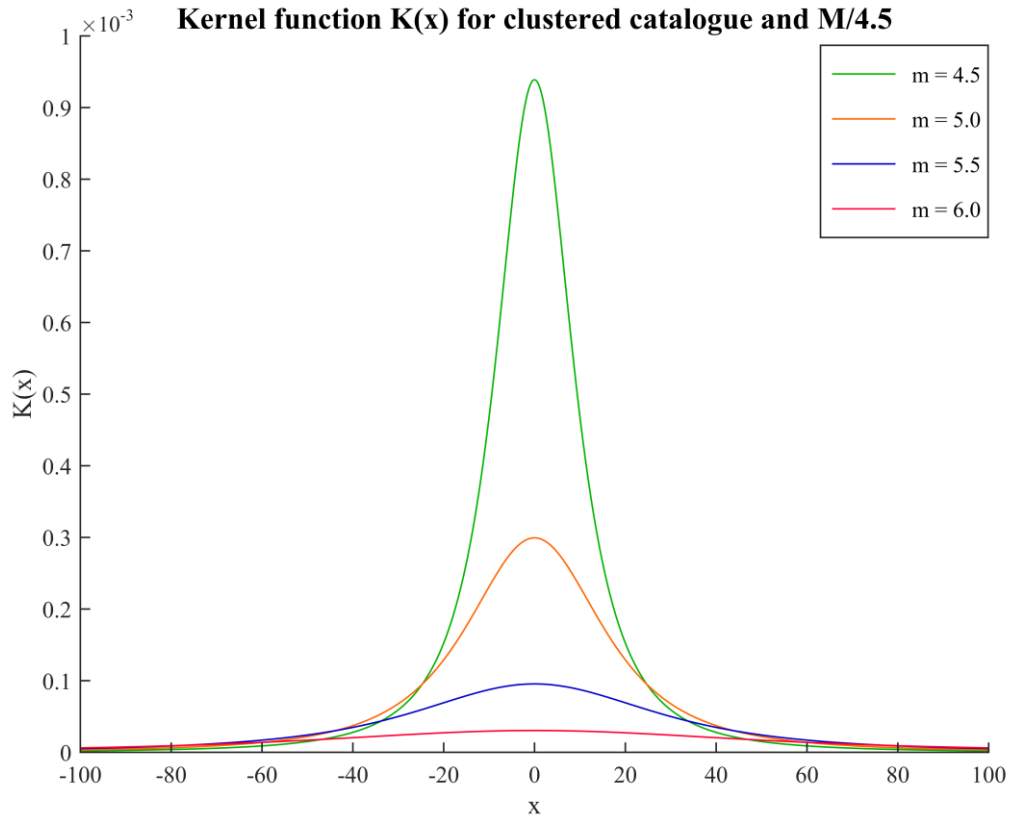
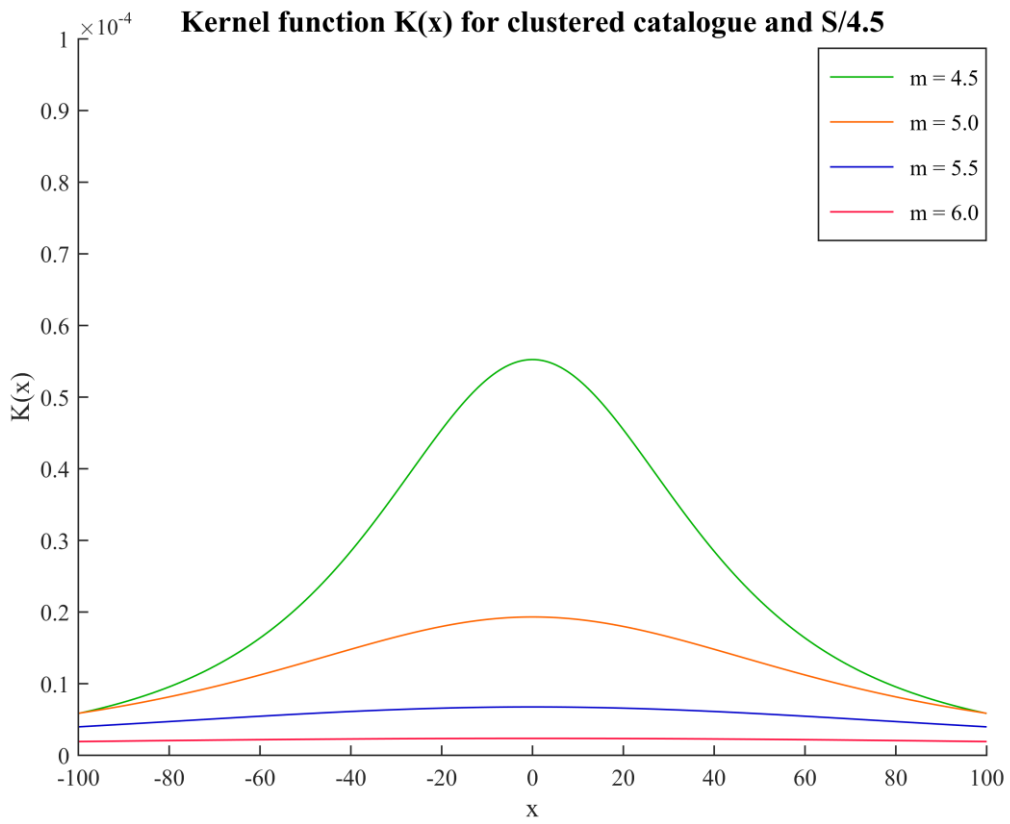


Figure 3.4 – Kernel function changes with respect to the bandwidth function parameters for **A)** clustered **B)** declustered catalogue.



A)



B)

Figure 3.5 – Kernel function changes with respect to the magnitude for M/4.5 and A) clustered B) declustered catalogue.

3.5 Ground motion prediction equations

For the territory of Slovakia, GMPEs derived from local accelerogram records are not available due to a lack of strong motion data. Therefore GMPEs for other regions with similar macroseismic intensity attenuation as has been found for the territory of Slovakia (Labák et al. 1997) were used in this thesis.

In order to evaluate how is the resulting seismic hazard influenced by a choice of GMPE we used two GMPEs – Akkar and Bommer (2010) and Cauzzi and Faccioli (2008). Both equations were used by Kysel (2014) for PSHA computations following classical approach and they yielded different results. In study Kysel (2014) six GMPEs were used and Akkar and Bommer (2010) was one of those equations, that gave the highest hazard values, on the other hand Cauzzi and Faccioli (2008) was one of those equations that gave the lowest hazard values.

Akkar and Bommer (2010) is given by relation

$$\begin{aligned} \log PGA = & 1.04159 + 0.91333 M_w - 0.08140 M_w^2 \\ & + (-2.92728 + 0.28120 M_w) \log(\sqrt{R^2 + 7.86638^2}) \\ & + 0.08753 S_s + 0.01527 S_A - 0.04189 F_N + 0.08015 F_R + \varepsilon \sigma. \end{aligned} \quad (3.2)$$

Individual components in relation (3.2) have following meanings:

PGA	geometric mean of horizontal components of peak ground acceleration in cm/s^2 (5% damping)
M_w	moment magnitude
R	Joyner-Boore distance
S_x	site term
	<ul style="list-style-type: none"> • $S_s = S_A = 0$ for rock site ($750 \text{ m/s} < v_{s,30}$) • $S_s = 0, S_A = 1$ for stiff soil site ($360 \text{ m/s} < v_{s,30} < 750 \text{ m/s}$) • $S_s = 1, S_A = 0$ for soft soil site ($v_{s,30} < 360 \text{ m/s}$)
F_x	style-of-faulting term

- $F_N = 1, F_R = 0$ for normal faulting
- $F_N = 0, F_R = 1$ for reverse faulting
- $F_N = F_R = 0$ for strike-slip faulting

ε number of standard deviations above/below the mean value of $\log(PGA)$

σ total standard deviation, $\sigma = \sqrt{0.2610^2 + 0.0994^2}$

Cauzzi and Faccioli (2008) is given by relation

$$\begin{aligned} \log PGA = & -1.296 + 0.556 M_w - 1.582 \log R \\ & + 0.220 S_B + 0.304 S_C + 0.332 S_D \\ & - 0.060 E_N + 0.094 E_R - 0.013 E_S + \sigma. \end{aligned} \quad (3.3)$$

Individual components in relation (3.3) have following meanings:

PGA geometric mean of horizontal components of peak ground acceleration in m/s^2 (5% damping)

M_w moment magnitude

R hypocentral distance

S_x site term of the type of the subsoil

- $S_B = S_C = S_D = 0$ for $800 \text{ m/s} \leq v_{s,30}$
ground category A by EUROCODE 8 classification
- $S_B = 1, S_C = S_D = 0$ for $360 \text{ m/s} \leq v_{s,30} < 800 \text{ m/s}$
subsoil category B by EUROCODE 8 classification
- $S_C = 1, S_B = S_D = 0$ for $180 \text{ m/s} \leq v_{s,30} < 360 \text{ m/s}$
subsoil category C by EUROCODE 8 classification
- $S_D = 1, S_B = S_C = 0$ for $v_{s,30} < 180 \text{ m/s}$
subsoil category D by EUROCODE 8 classification

E_x style-of-faulting term

- $E_N = 1, E_R = 0, E_S = 0$ for normal faulting
- $E_N = 0, E_R = 1, E_S = 0$ for reverse faulting

- $E_N = 0, E_R = 0, E_S = 1$ for strike-slip faulting
- σ total standard deviation, $\sigma = 0.344$

In this thesis we considered $v_{s,30} = 800$ m/s, what correspond to rock-like ground. Style-of-faulting terms were in both cases assigned equal weights, i.e. $F_N = F_R = 1/2$, $E_N = E_R = E_S = 1/3$, because the style-of-faulting for the earthquakes in SLOVEC (2011) catalogue is unknown. Since all events were assumed to have hypocentre at the surface, because computer code KERGRID (2001a) does not include hypocentral depths, both the Joyner-Boore and hypocentral distance give the same values.

3.6 Sensitivity study on bandwidth parameters

After the determination of bandwidth function $h(m)$, the effective return period $T(x_i)$ and the kernel function $K(m, \vec{x} - \vec{x}_i)$ the activity rate $\lambda(m, \vec{x})$ and the annual rate of exceedance $N[C > c]$ can be evaluated at each grid node. In this section we calculated seismic activity rate for all pairs of bandwidth function parameters listed in *Table 3.4* in order to determine how the choice of bandwidth function parameters affects the resulting activity rate and the annual rate of exceedance. In this sensitivity study, only infinite kernel was used.

Computational area was chosen the same as in Kysel (2014) for all sensitivity tests.

Parameter	Longitude	Latitude
South West corner position (in °)	16.5	47.4
Width of grid rectangle (in °)	0.1	0.1
Number of grid rectangles	66	27

Table 3.6 – Parameters of the computational area used for zoneless PSHA computations.

3.6.1 Seismic activity rate

Seismic activity rate was calculated according to the relation (1.35) using a modified version of the computer code KERGRID developed by Woo (2001a). Resulting activity

rate for all pairs of bandwidth function parameters listed in *Table 3.4* together with earthquake epicentres are presented in *Figure 3.6-Figure 3.13*.

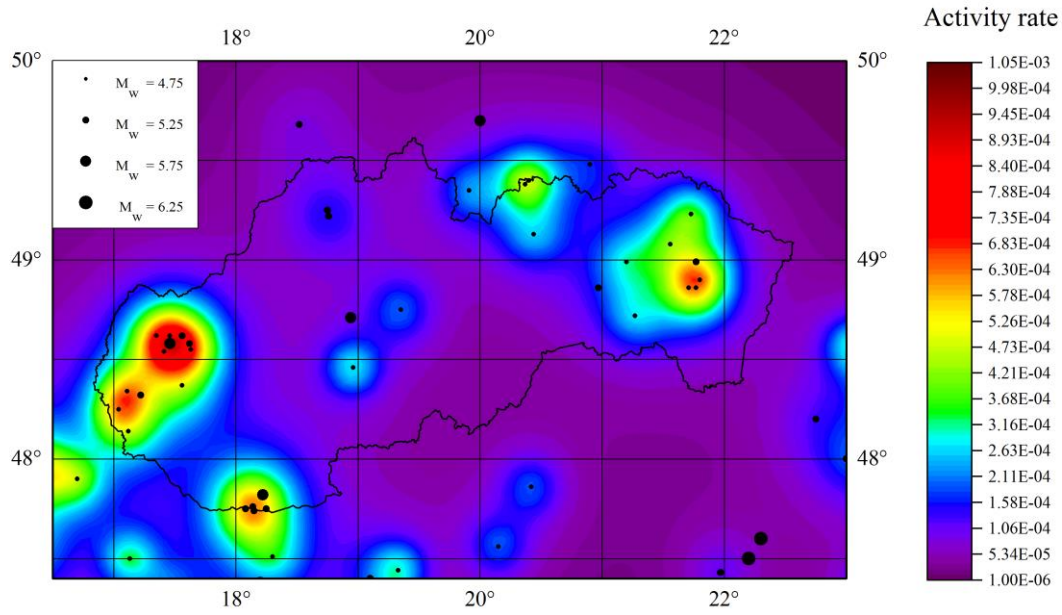


Figure 3.7 – Seismic activity rate for $M/2.5$, clustered catalogue and effective return periods listed in *Table 3.5*.

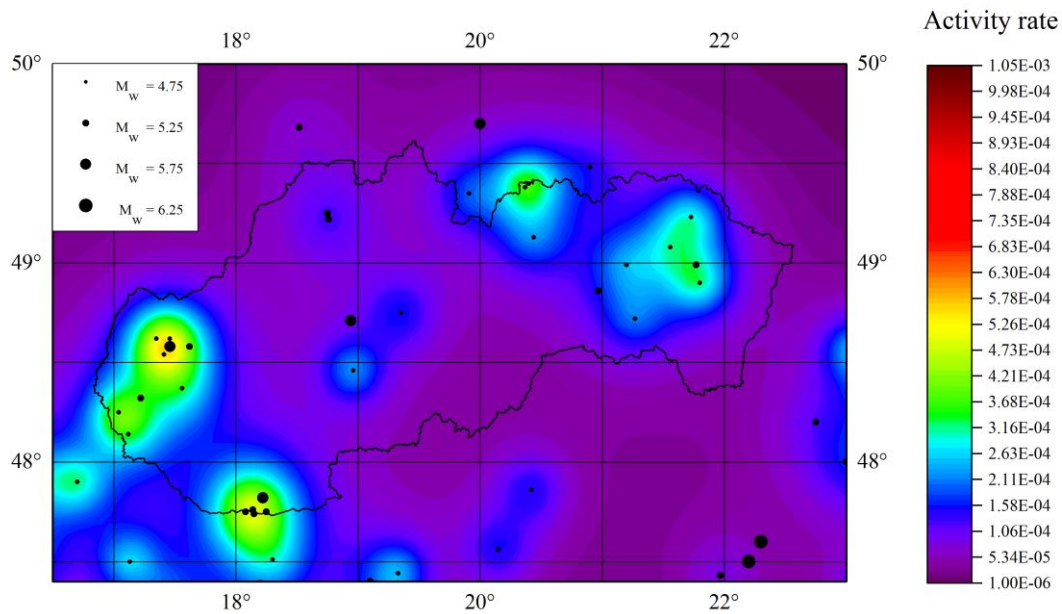


Figure 3.6 – Seismic hazard map for $M/2.5$, declustered catalogue and effective return periods listed in *Table 3.5*.

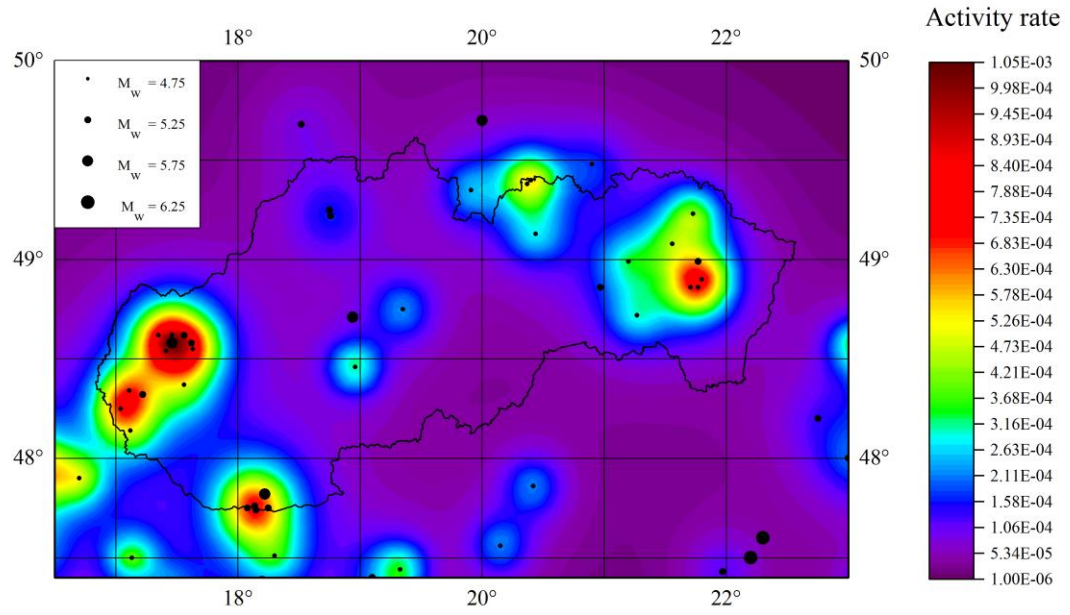


Figure 3.9 – Seismic activity rate for M/4.5, clustered catalogue and effective return periods listed in Table 3.5.

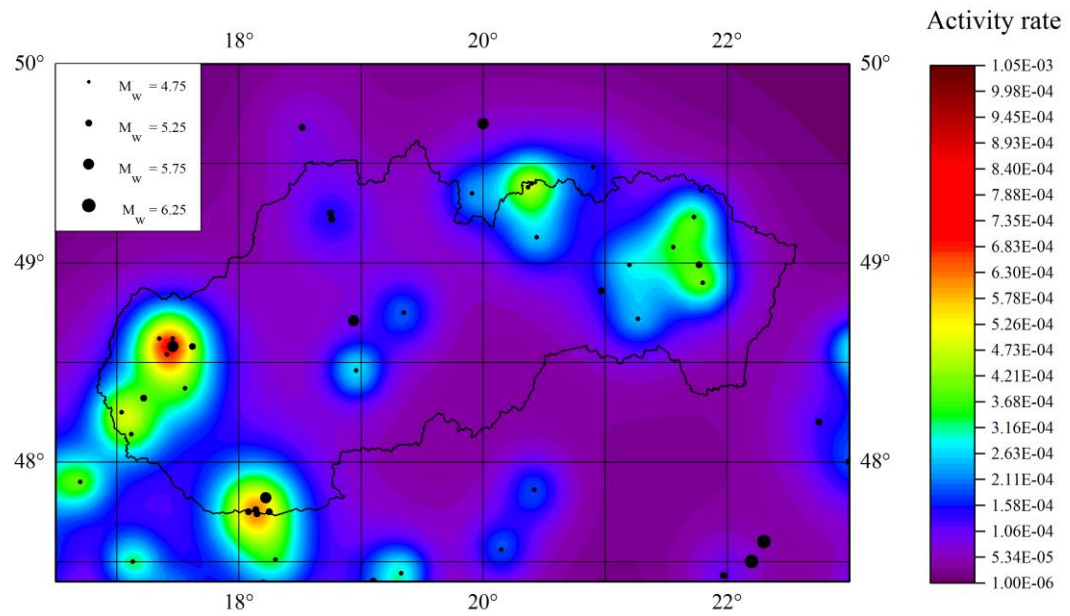


Figure 3.8 – Seismic activity rate for M/4.5, declustered catalogue and effective return periods listed in Table 3.5.

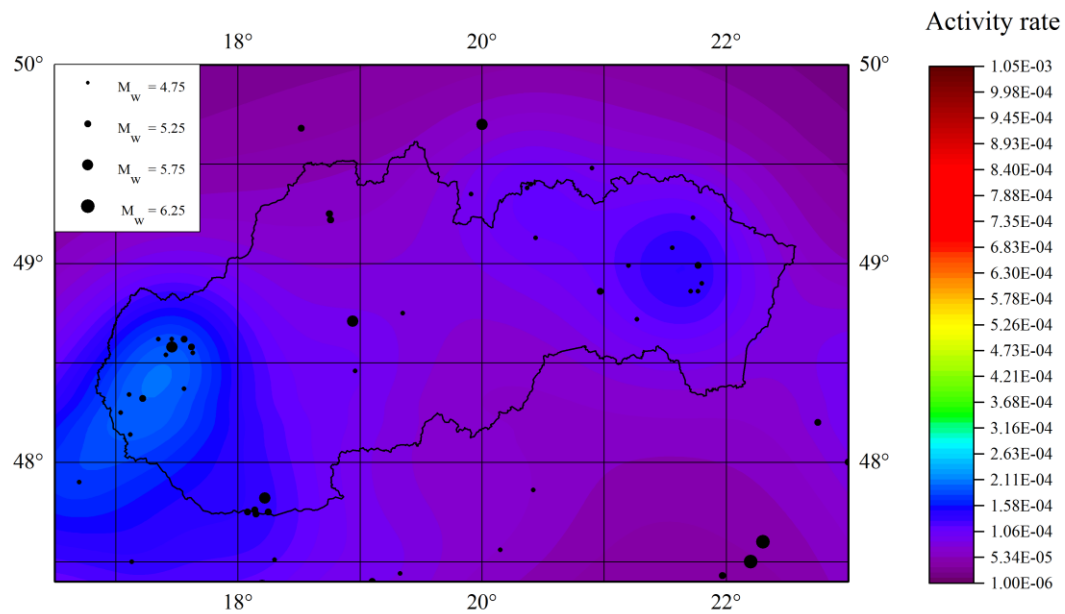


Figure 3.11 – Seismic activity rate for S/2.5, clustered catalogue and effective return periods listed in Table 3.5.

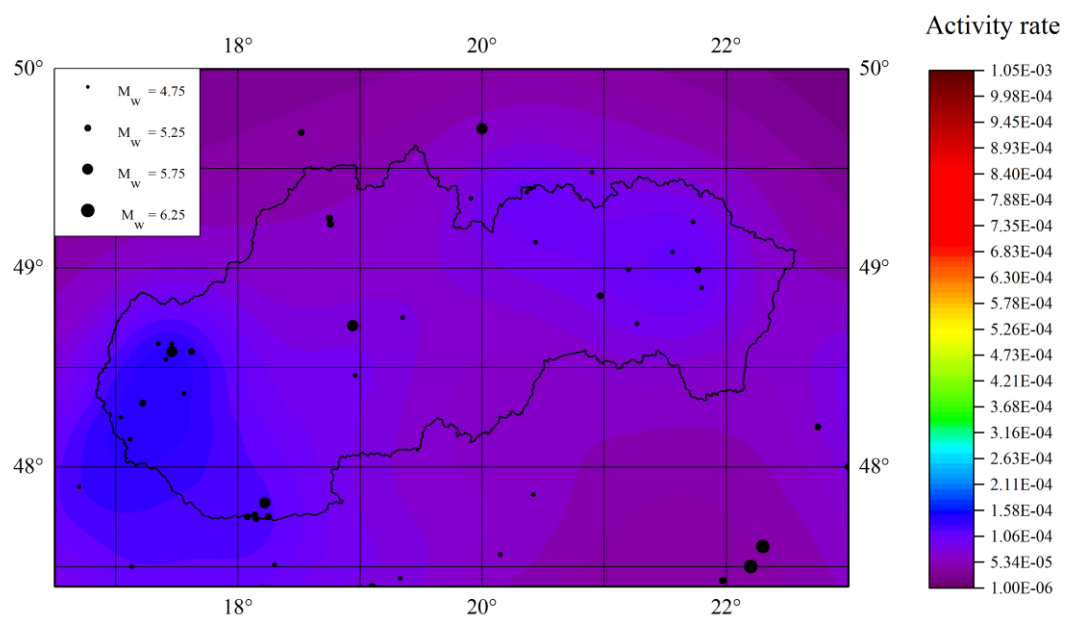


Figure 3.10 – Seismic activity rate for S/2.5, declustered catalogue and effective return periods listed in Table 3.5.

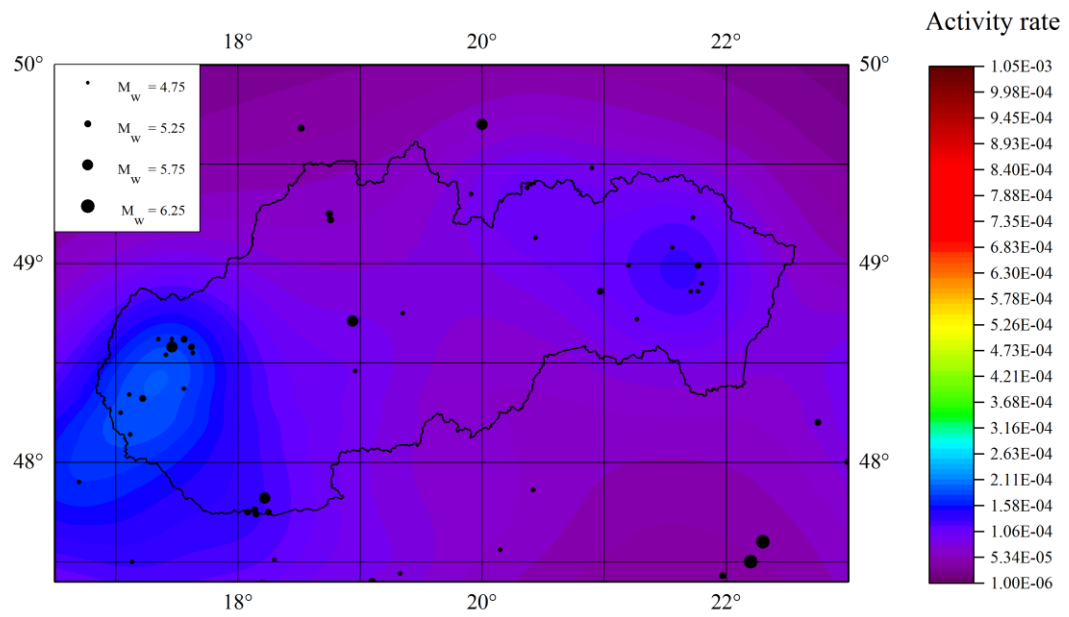


Figure 3.13 – Seismic activity rate for S/4.5, clustered catalogue and effective return periods listed in Table 3.5.

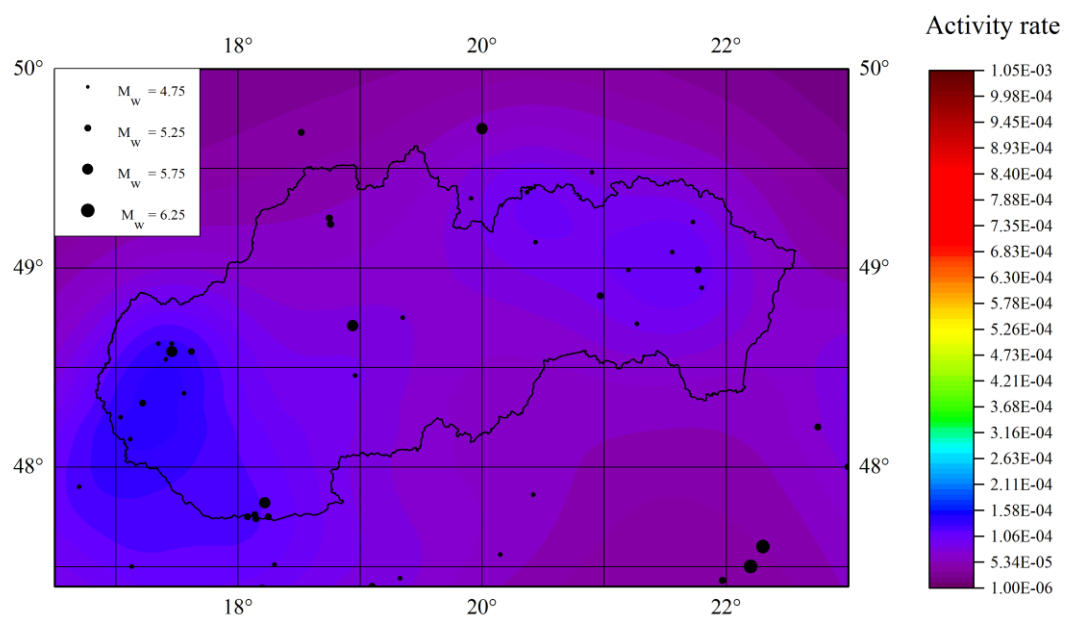


Figure 3.12 – Seismic activity rate for S/4.5, declustered catalogue and effective return periods listed in Table 3.5.

We can see that resulting activity rate is strongly influenced by the choice of the bandwidth function and that results obtained for different bins definitions differs significantly. Activity rate computed for bandwidth function parameters obtained with merged last two magnitude bins is more spatially clustered and has higher values in regions where earthquakes epicenters are localized. Activity rate computed for bandwidth function parameters obtained with separate last two magnitude bins is less spatially clustered, has lower values in the whole computational area and the values in regions where earthquakes epicenters are localized do not differ so much from the regions with no historical seismicity. The difference is caused by the different shape of the kernel functions. As we can see in *Figure 3.4*, kernel functions obtained for separate last two magnitude bins are more widespread with no significant maximum in comparison with kernel function obtained for merged last two bins.

The difference can also be seen between activity rate values obtained from clustered and declustered catalogue. Computations with declustered catalogue yielded lower values, what can be expected, since fewer events were incorporated in computations.

The smallest impact on the resulting activity rate has the choice of the threshold magnitude for computation of the bandwidth function parameters. Small differences can also be seen between *Figure 3.7* and *Figure 3.9*, but we can say that these differences are negligible in comparison with differences caused by different bins definition.

The seismic activity rate reaches the highest values in areas with historical seismicity, as might be expected. But what is interesting and should be noted is that the seismic activity rate reaches higher values in areas where earthquakes with magnitudes around $M_w = 4.5$ were documented while the higher values of the seismic activity rate are not seen in areas where larger earthquakes with magnitudes around $M_w = 6.0$ were documented. One possible reason is the fact that the shape and the maximum of the kernel function K_1 is affected by the magnitude and the values of kernel function K_1 decreases with increasing magnitude. Another possible reason is the effect of the effective return period. Contribution of each event into resulting activity rate is weighted by its effective return period and since events with higher magnitude has longer effective return periods, their contribution to the resulting activity rate is also lower. Both of these parameters will be studied further in this thesis.

3.6.2 Seismic hazard curves

In previous subsection, seismic activity rate was computed for each grid node of the computational area. To obtain seismic hazard curve for one grid node, computed activity rate for each node need to be multiplied with the respective conditional probability given by relation (1.31) and then contributions from individual grid nodes are summed up.

In this subsection we computed seismic hazard curves for four cities in Slovakia with location listed in *Table 3.7*. Two of them, Dobrá Voda and Komárno, lie in a region with higher seismicity, where some of the biggest earthquakes in Slovakia were recorded. Žilina and Banská Bystrica lie in moderate seismicity regions, but in the past, larger earthquakes have also occurred in their vicinity.

In computations of seismic hazard curves we considered all pairs of the bandwidth function parameters listed in *Table 3.4*. In order to evaluate the impact of chosen GMPE on the results we used both Akkar and Bommer (2010) and Cauzzi and Faccioli (2008) GMPEs. Results are shown in *Figure 3.14* and *Figure 3.15*.

CITY	LATITUDE	LONGITUDE
Banská Bystrica	48.7	19.1
Dobrá Voda	48.6	17.5
Komárno	47.8	18.1
Žilina	49.2	18.7

Table 3.7 – Locations of four cities for which seismic hazard curves were computed.

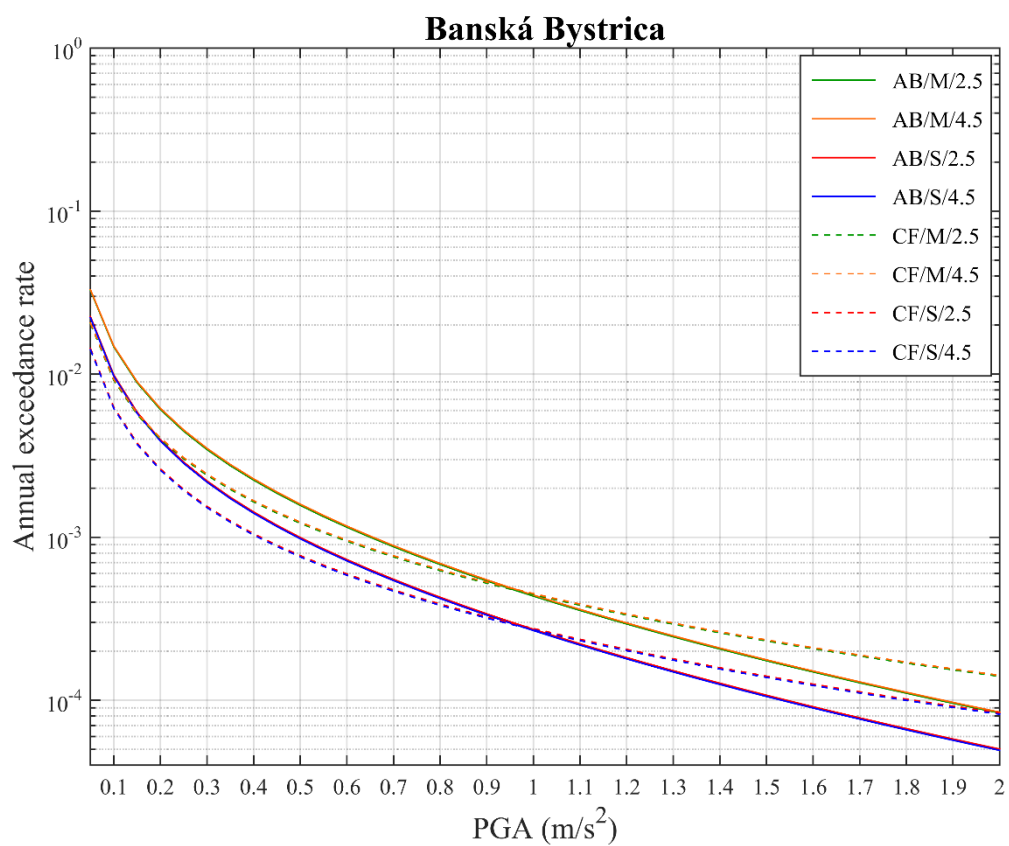
In the figures we can see the same trends as for the activity rate maps. The results are most affected by the choice of bins definition. Values of the annual exceedance rate obtained for bandwidth function parameters calculated with merged last two magnitude bins are for all four cities higher than values obtained for bandwidth function parameters with separate last two magnitude bins.

As already said before, the choice of the threshold magnitude for computation of the bandwidth function parameters does not affect results so much, for example for Banská Bystrica, the annual exceedance rate curves obtained for threshold magnitude $M_w = 2.5$

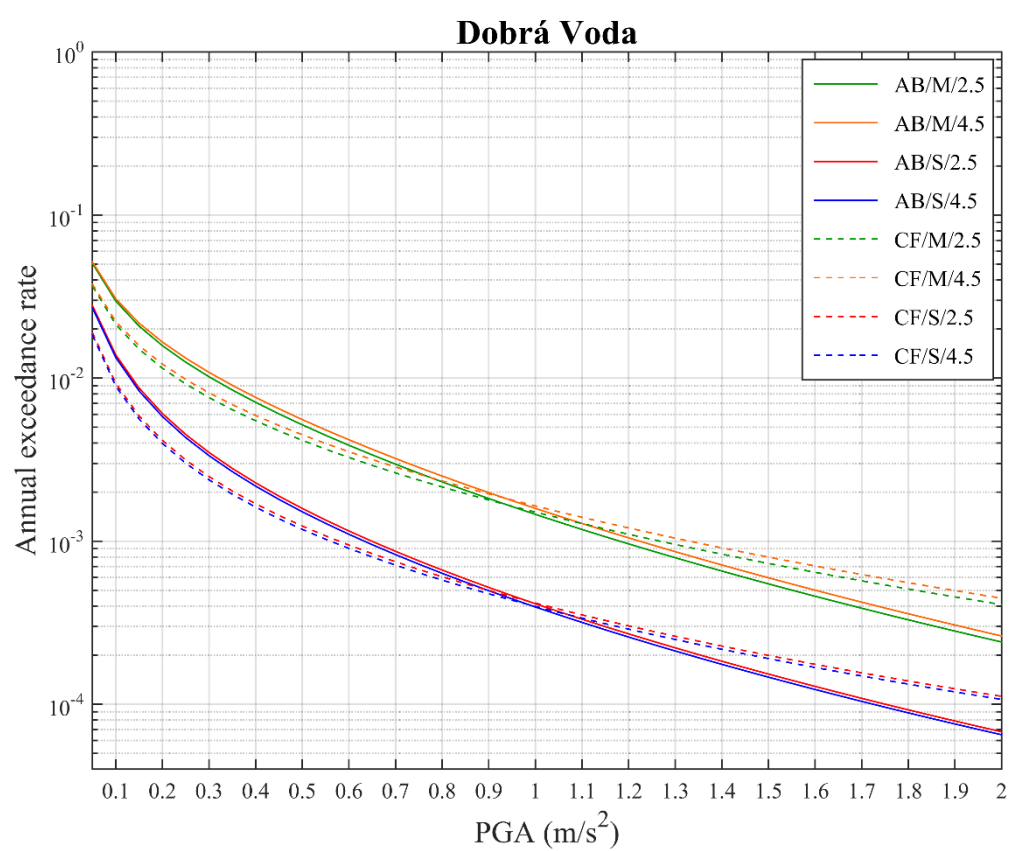
and $M_w = 4.5$ are almost identical. For three other cities computation with threshold magnitude $M_w = 4.5$ yields slightly higher results than with $M_w = 2.5$.

Values of the annual exceedance rate obtained for clustered and declustered catalogue differ the most for Dobrá Voda and the least for Banská Bystrica. This is due to the fact, that most of the foreshocks and aftershocks which were excluded in declustering were located near the location of Dobrá Voda.

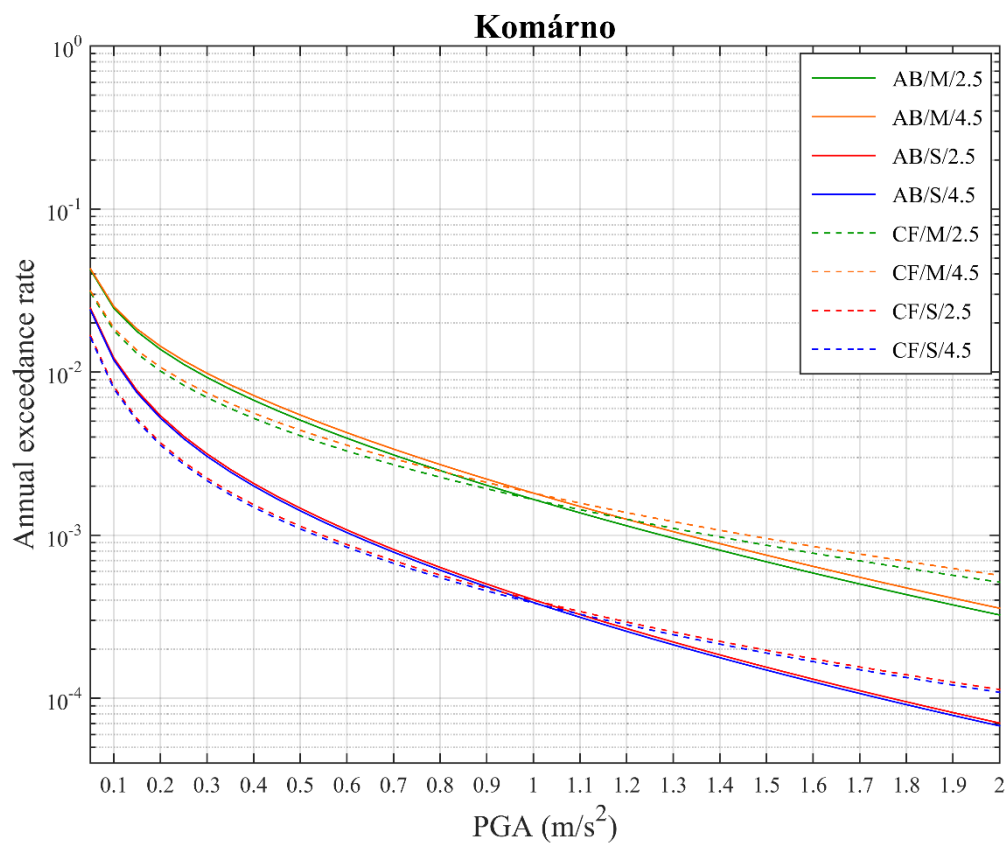
Akkar and Bommer (2010) and Cauzzi and Faccioli (2008) GMPEs were chosen for zoneless PSHA calculations because they yielded different values when used for PSHA calculations following standard Cornell-McGuire procedure (Kysel 2014). We can see, that this no longer holds for zoneless approach and the values of the annual exceedance rate obtained with both GMPEs do not differ so much. For PGA values lower than 1m/s^2 Akkar and Bommer (2010) yields slightly higher values of the annual exceedance rate than Cauzzi and Faccioli (2008), on the contrary for PGA values higher than 1m/s^2 Akkar and Bommer (2010) yields slightly lower values of the annual exceedance rate than Cauzzi and Faccioli (2008) and the curves intersect around PGA equal to 1m/s^2 . Comparison with values of the annual exceedance rate obtained with classical approach will be shown later in section 3.9.



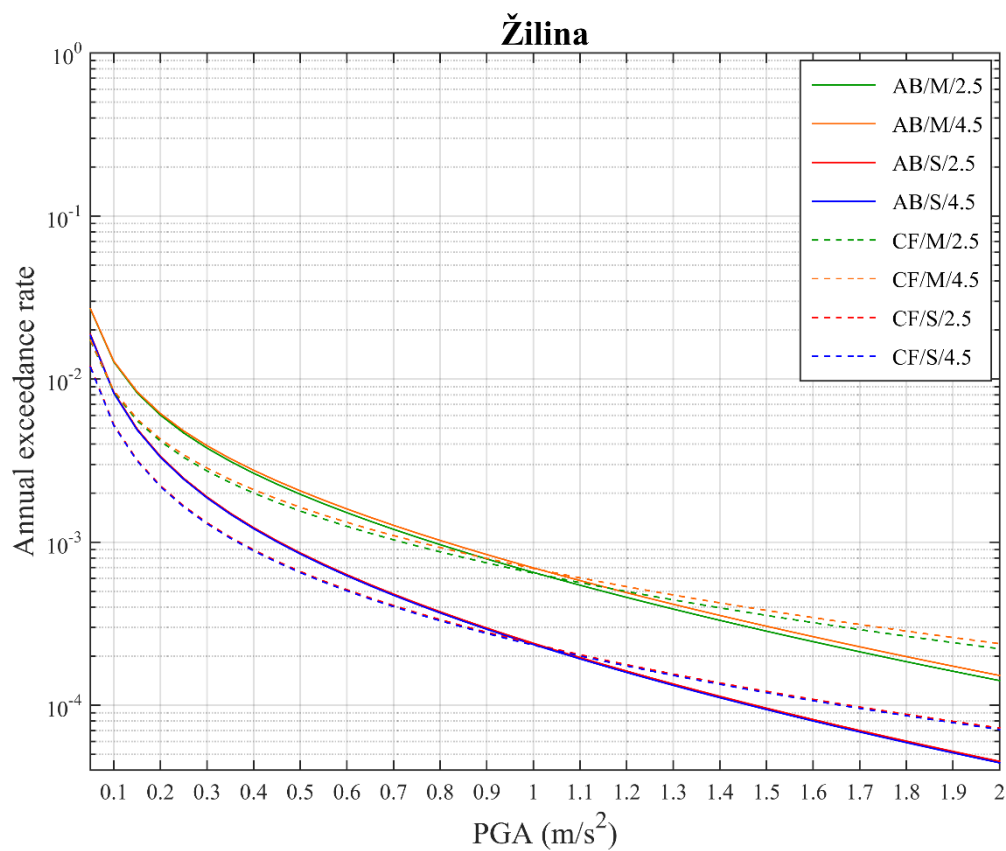
A)



B)

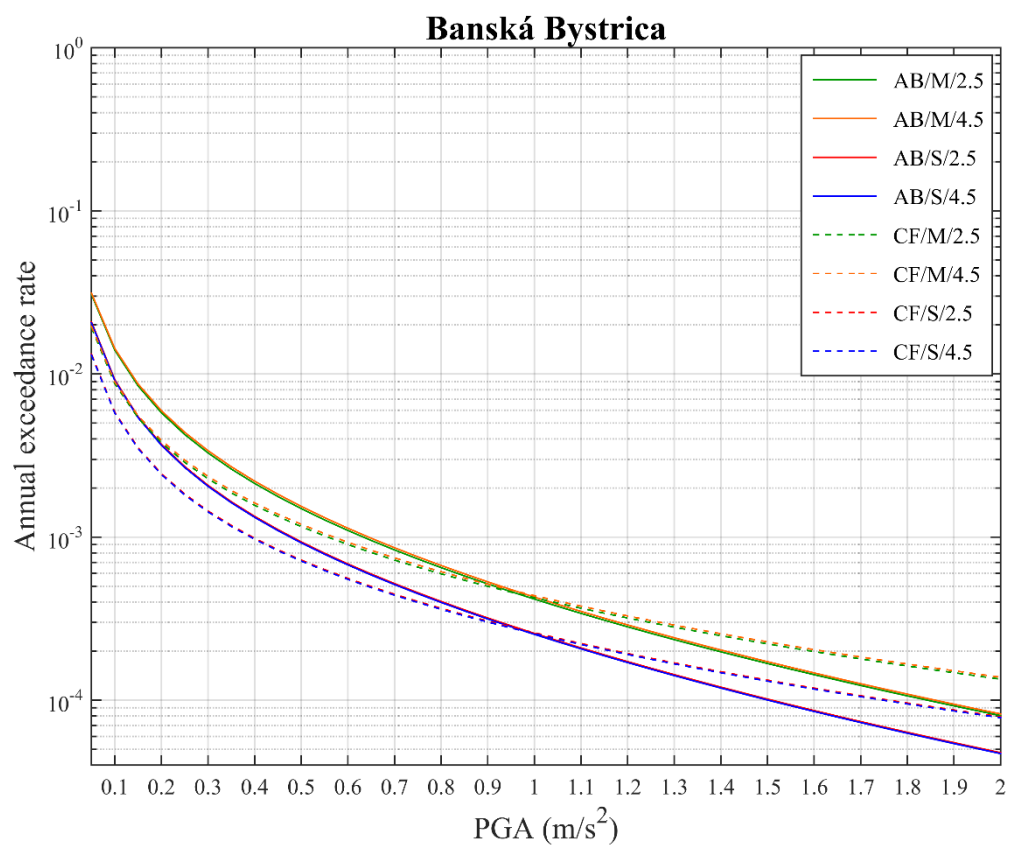


C)

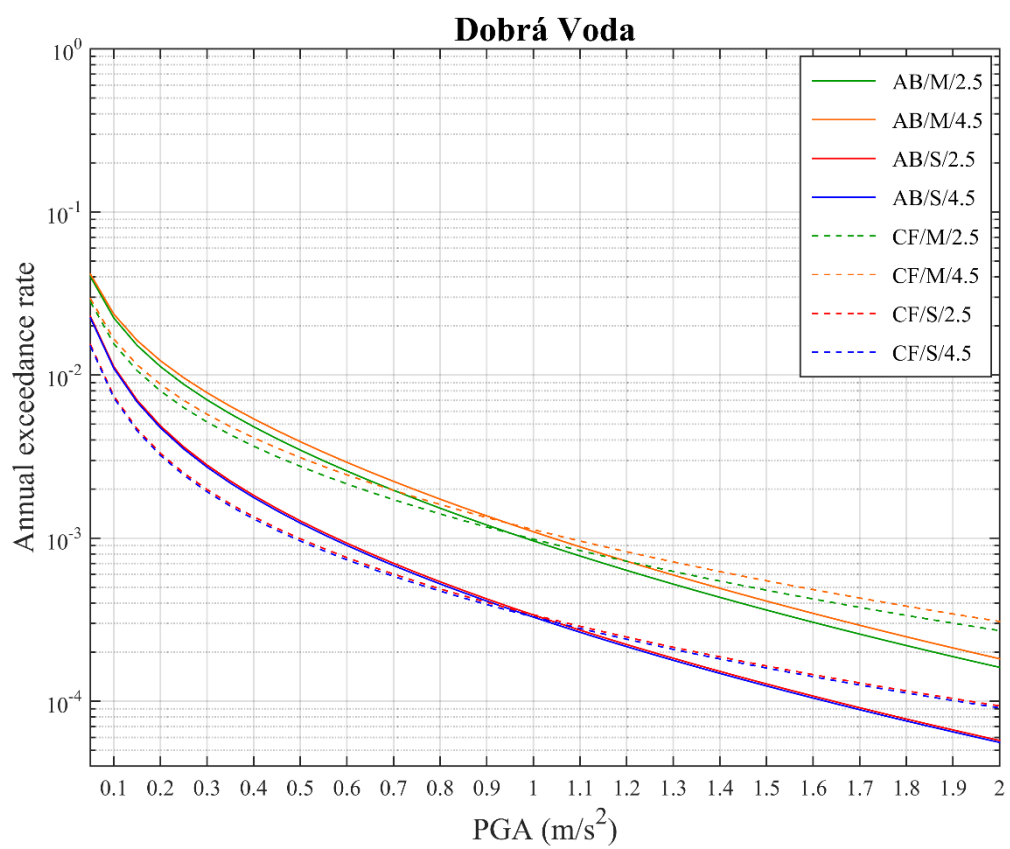


D)

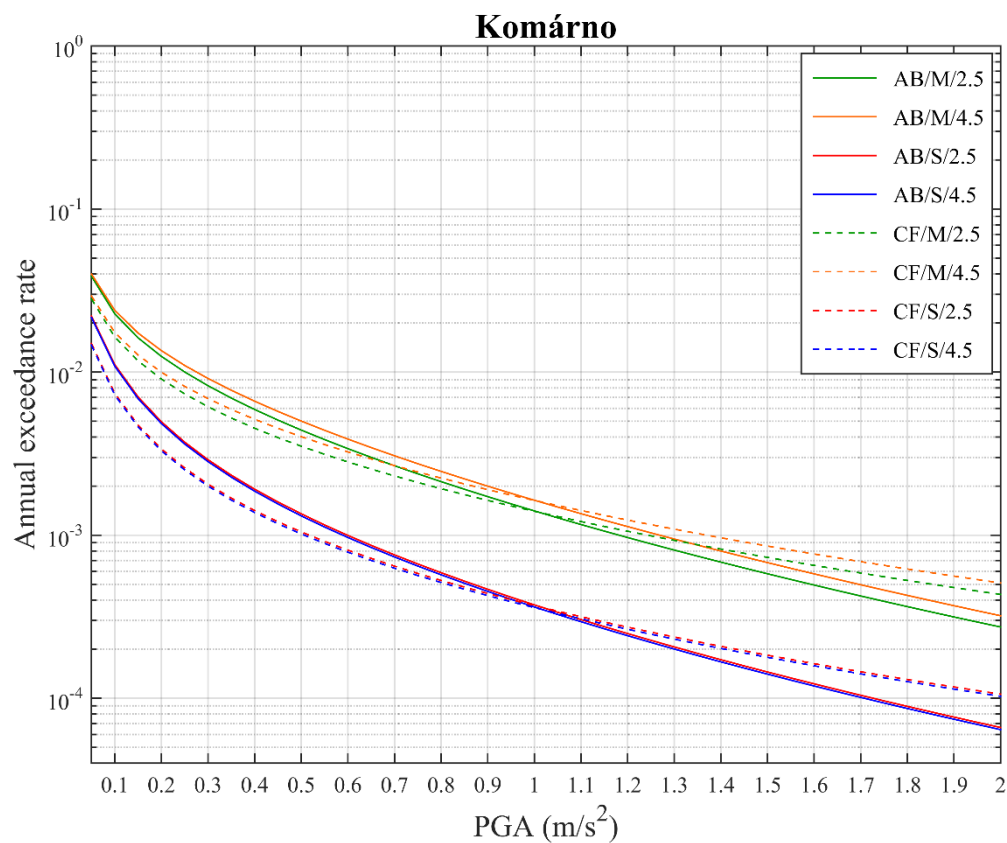
Figure 3.14 A) – D) – Seismic hazard curves for four cities listed in Table 3.7, for different bandwidth functions, clustered catalogue and effective return periods listed in Table 3.5.



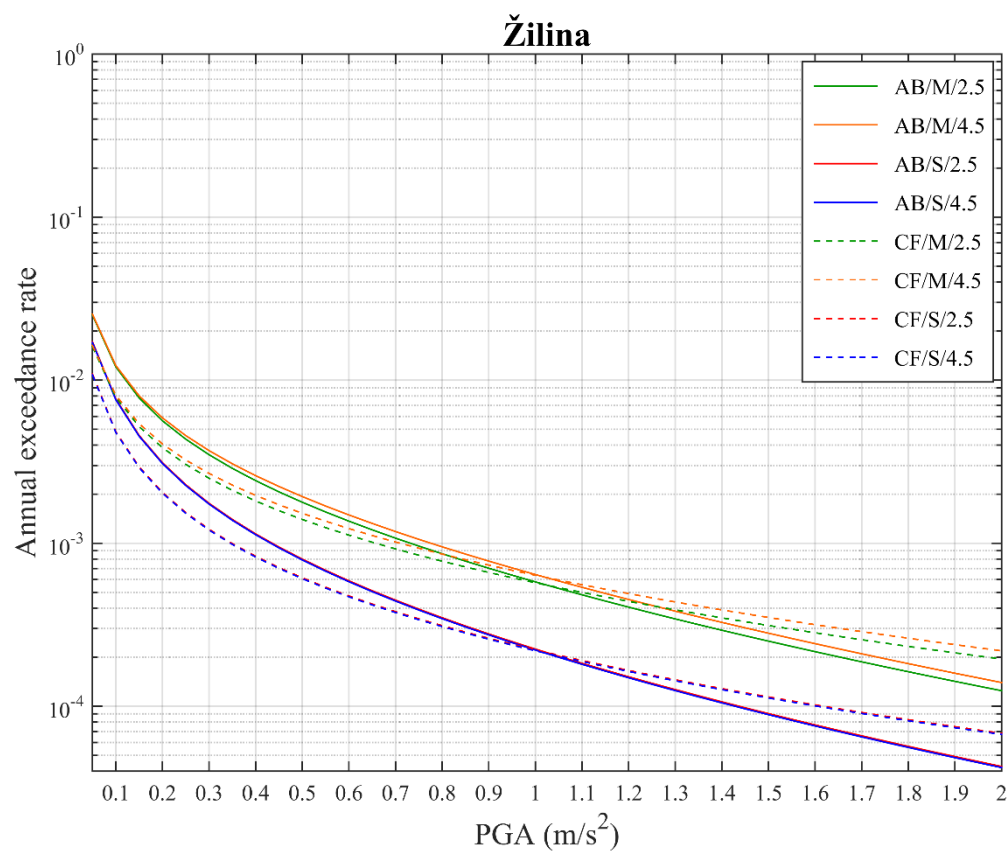
A)



B)



C)



D)

Figure 3.15 A) – D) – Seismic hazard curves for four cities listed in Table 3.7 for different bandwidth functions, declustered catalogue and effective return periods listed in Table 3.5.

3.6.3 Seismic hazard maps

To obtain seismic hazard map, seismic hazard curve need to be computed for every grid node. Then a desired value of the annual exceedance rate is chosen, and for each grid node the peak ground acceleration (or other chosen ground motion parameter) corresponding to that annual rate of exceedance is identified. Obtained values of peak ground acceleration are then plotted with respect to latitude and longitude.

In this thesis we chose the value of annual exceedance rate $N[C > c] = 2.105 \times 10^{-3}$ which according to relations (1.32) and (1.33) corresponds to return period 475 years and to 10% probability of exceedance in 50 years. Seismic hazard maps were plotted for all pairs of bandwidth function parameters listed in and for both GMPEs. Results are shown in *Figure 3.16-Figure 3.31*.

The same trends that can be seen in the activity rate maps can also be seen in the seismic hazard maps. If we compare results obtained with different GMPEs, we can see that Cauzzi and Faccioli (2008) GMPE yield overall lower hazard values for all sets of bandwidth function parameters listed in *Table 3.4*.

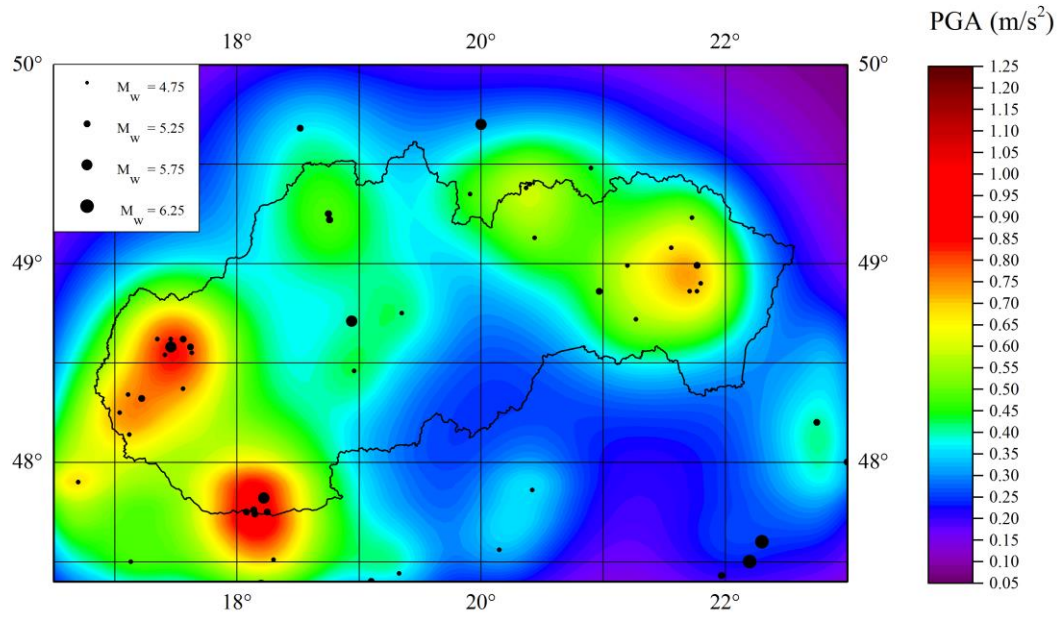


Figure 3.17 – Seismic hazard map for M/2.5, GMPE Akkar and Bommer (2010), clustered catalogue and effective return periods listed in Table 3.5.

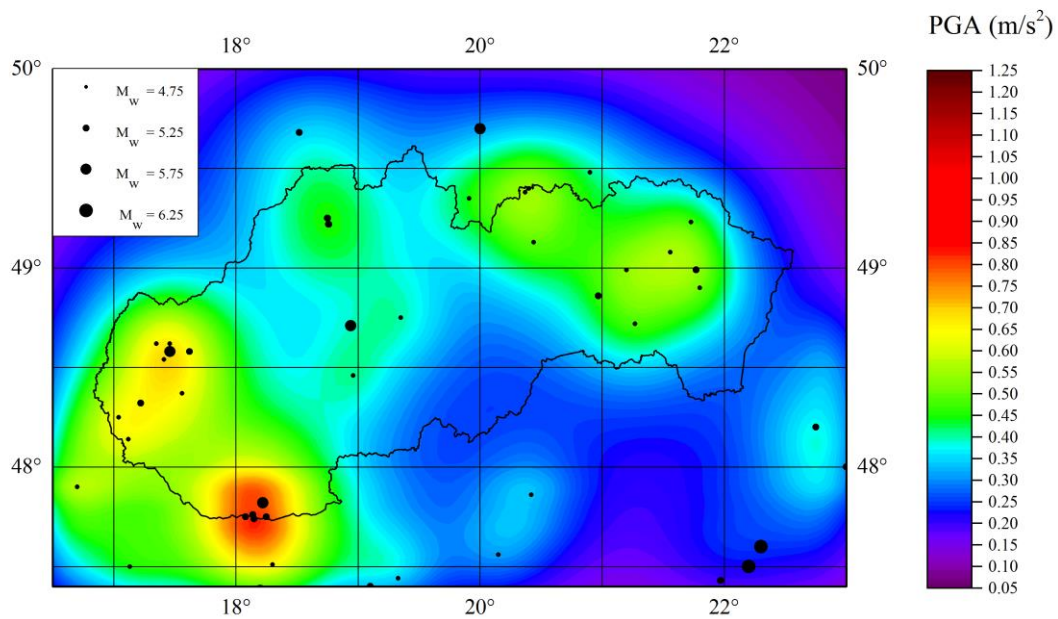


Figure 3.16 – Seismic hazard map for M/2.5, GMPE Akkar and Bommer (2010), declustered catalogue and effective return periods listed in Table 3.5.

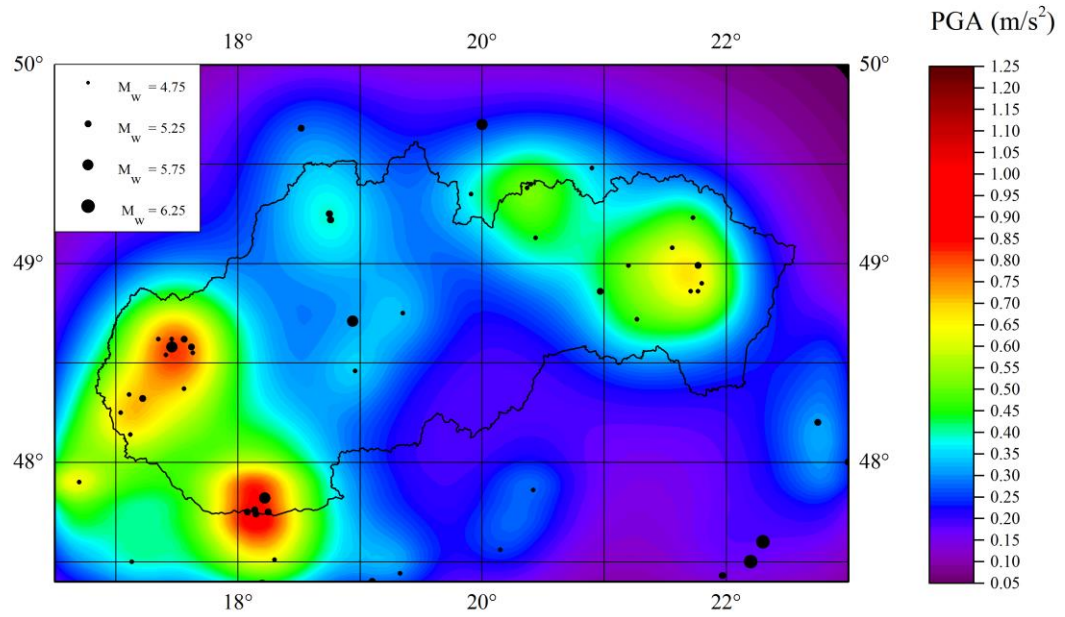


Figure 3.19 – Seismic hazard map for M/2.5, GMPE Cauzzi and Faccioli (2008), clustered catalogue and effective return periods listed in Table 3.5.

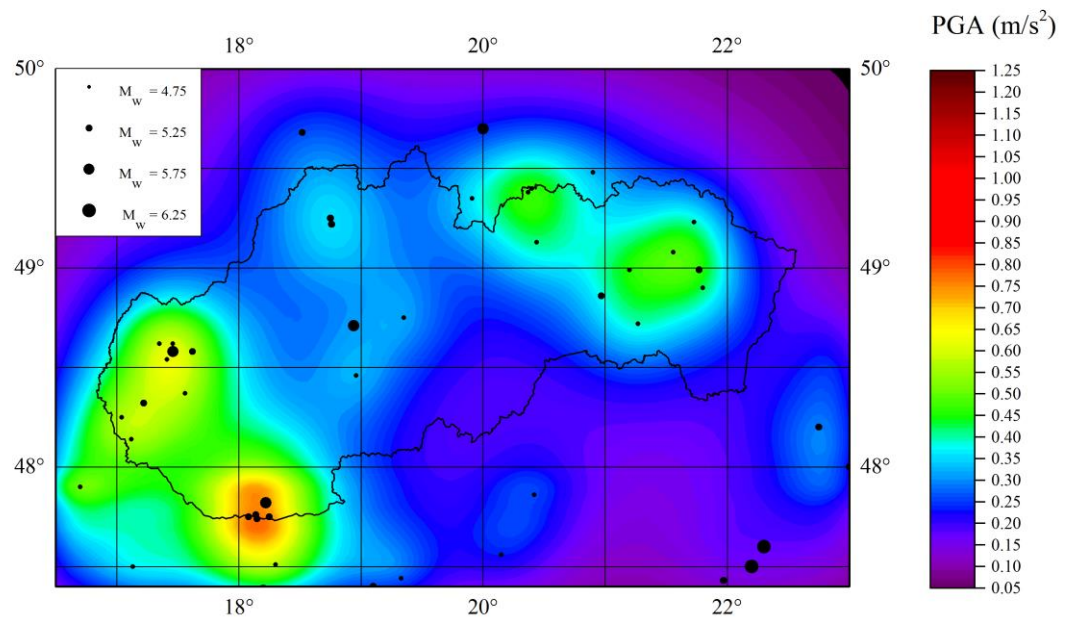


Figure 3.18 – Seismic hazard map for M/2.5, GMPE Cauzzi and Faccioli (2008), declustered catalogue and effective return periods listed in Table 3.5.

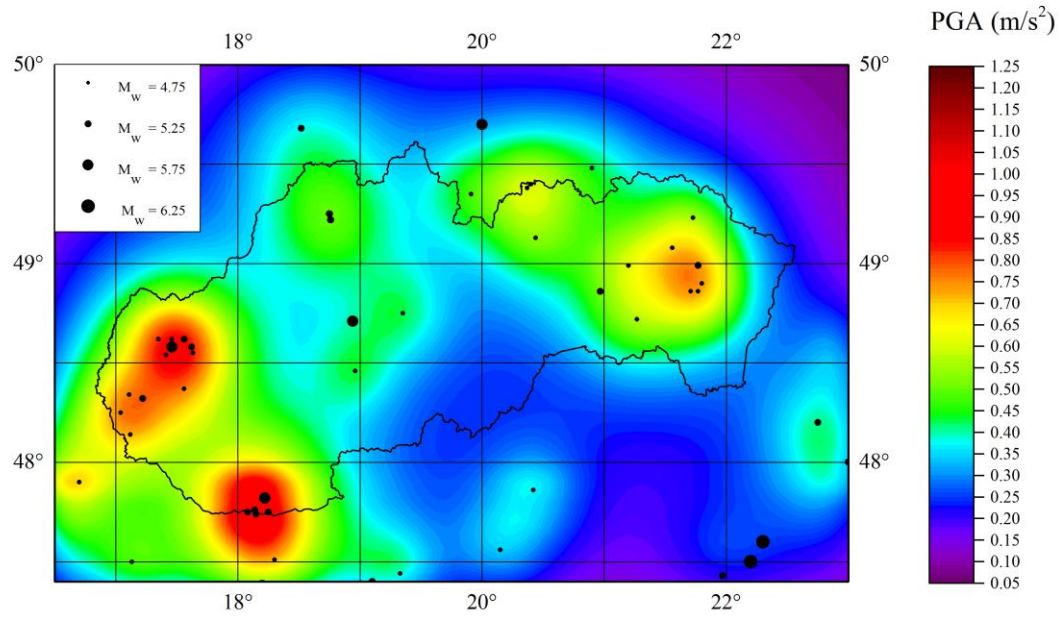


Figure 3.21 – Seismic hazard map for M/4.5, GMPE Akkar and Bommer (2010), clustered catalogue and effective return periods listed in Table 3.5.

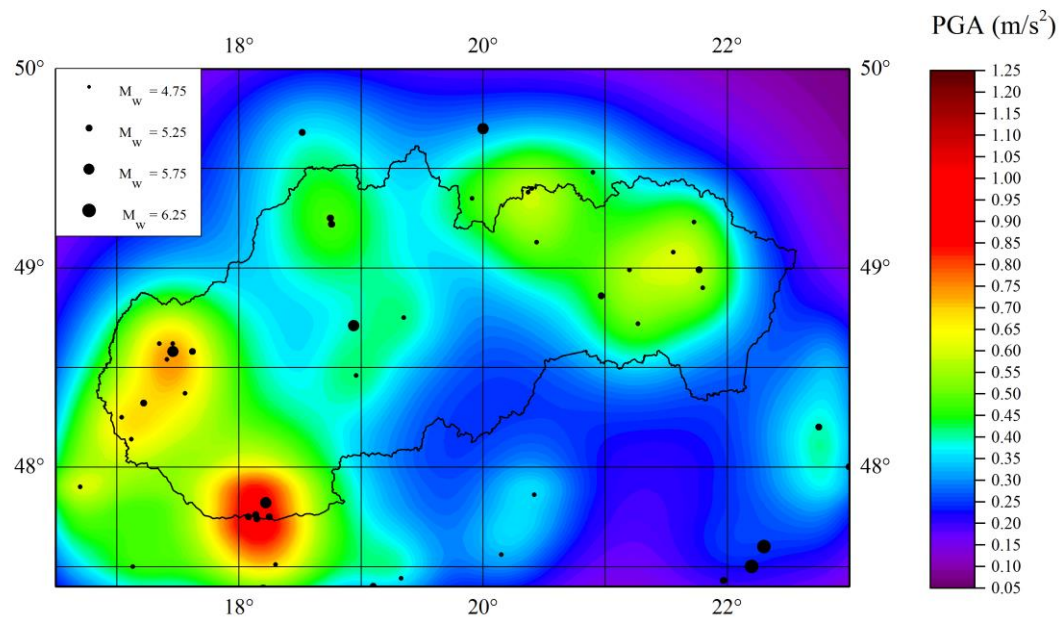


Figure 3.20 – Seismic hazard map for M/4.5, GMPE Akkar and Bommer (2010), declustered catalogue and effective return periods listed in Table 3.5.

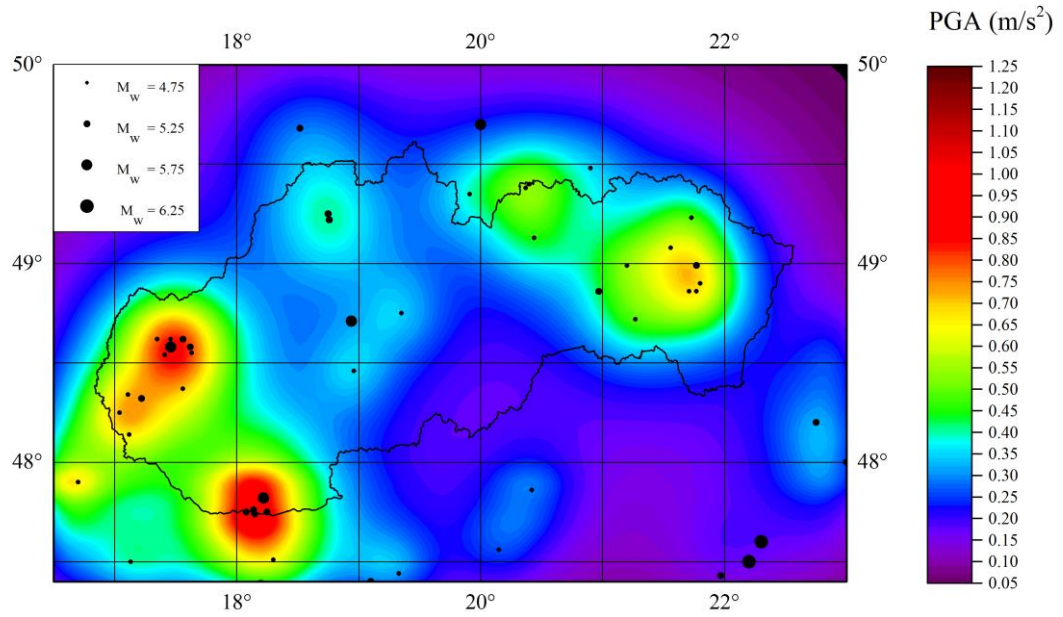


Figure 3.23 – Seismic hazard map for M/4.5, GMPE Cauzzi and Faccioli (2008), clustered catalogue and effective return periods listed in Table 3.5.

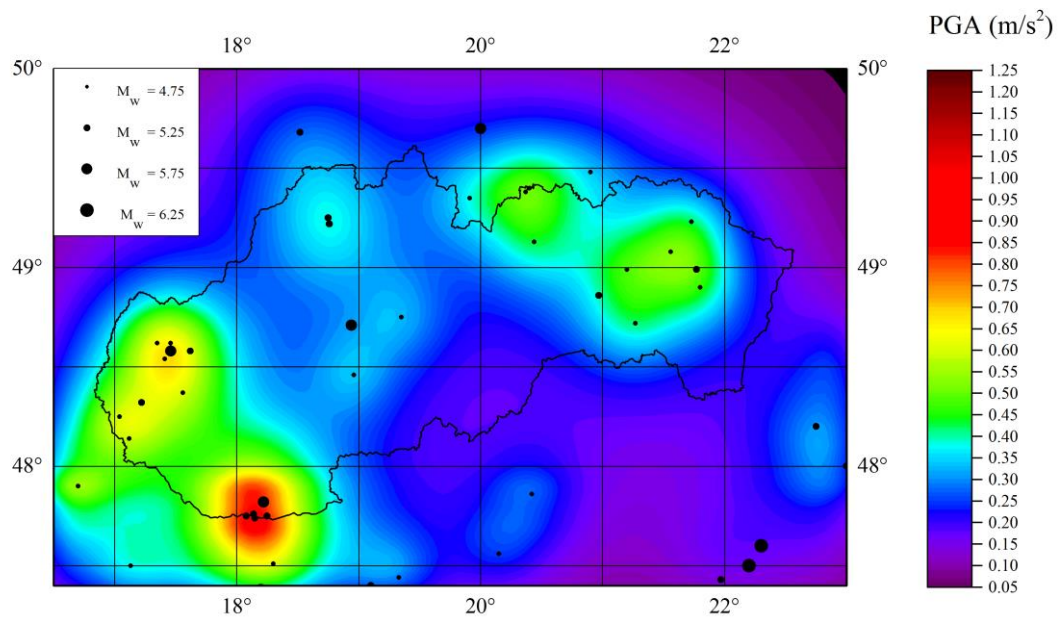


Figure 3.22 – Seismic hazard map for M/4.5, GMPE Cauzzi and Faccioli (2008), declustered catalogue and effective return periods listed in Table 3.5.

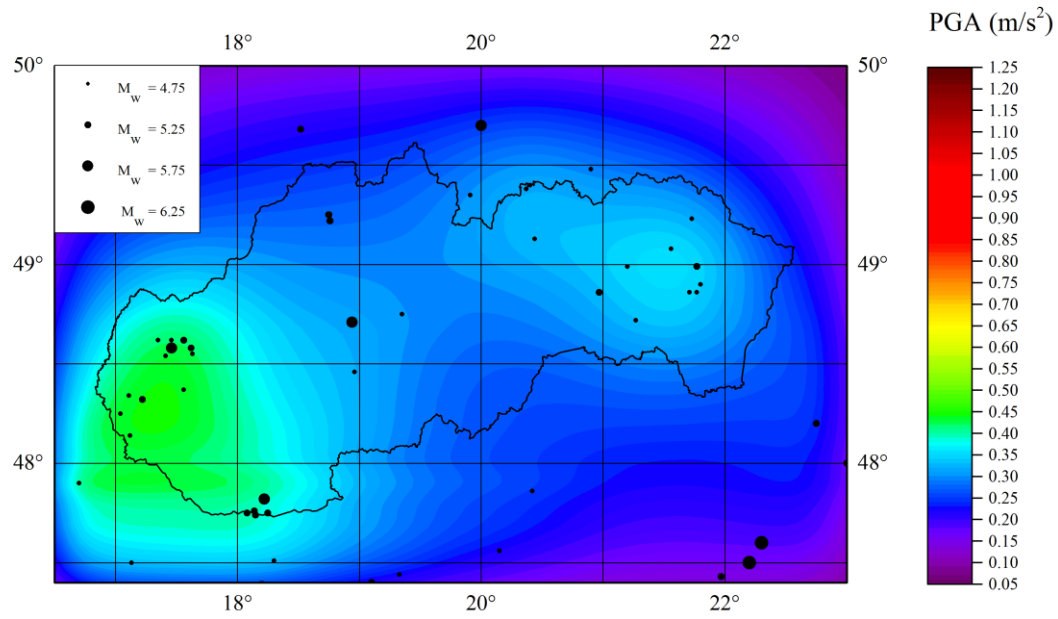


Figure 3.25 – Seismic hazard map for S/2.5, GMPE Akkar and Bommer (2010), clustered catalogue and effective return periods listed in Table 3.5.

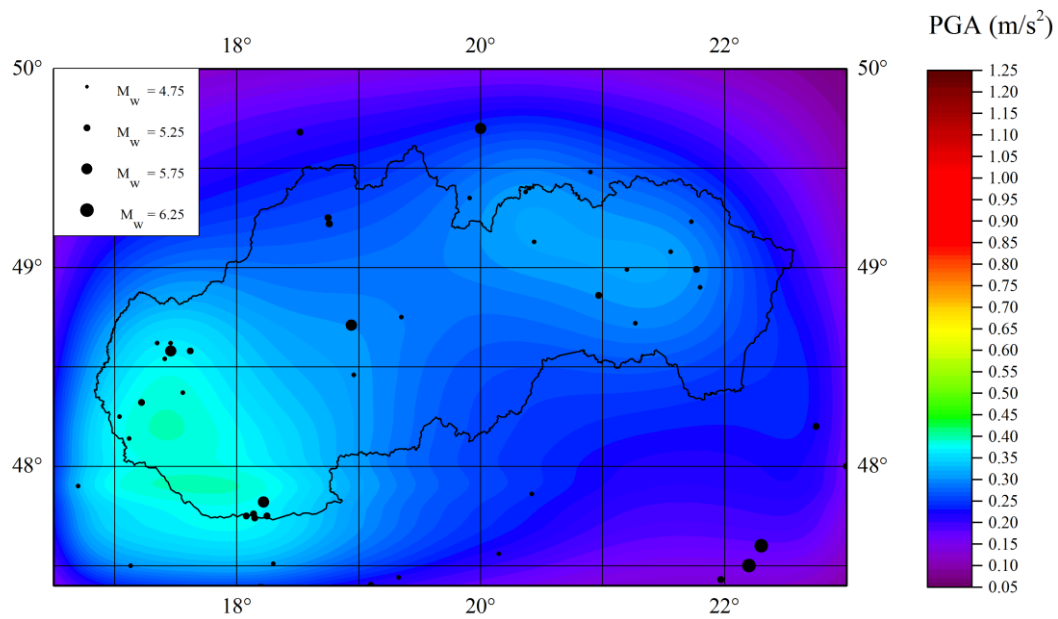


Figure 3.24 – Seismic hazard map for S/2.5, GMPE Akkar and Bommer (2010), declustered catalogue and effective return periods listed in Table 3.5.

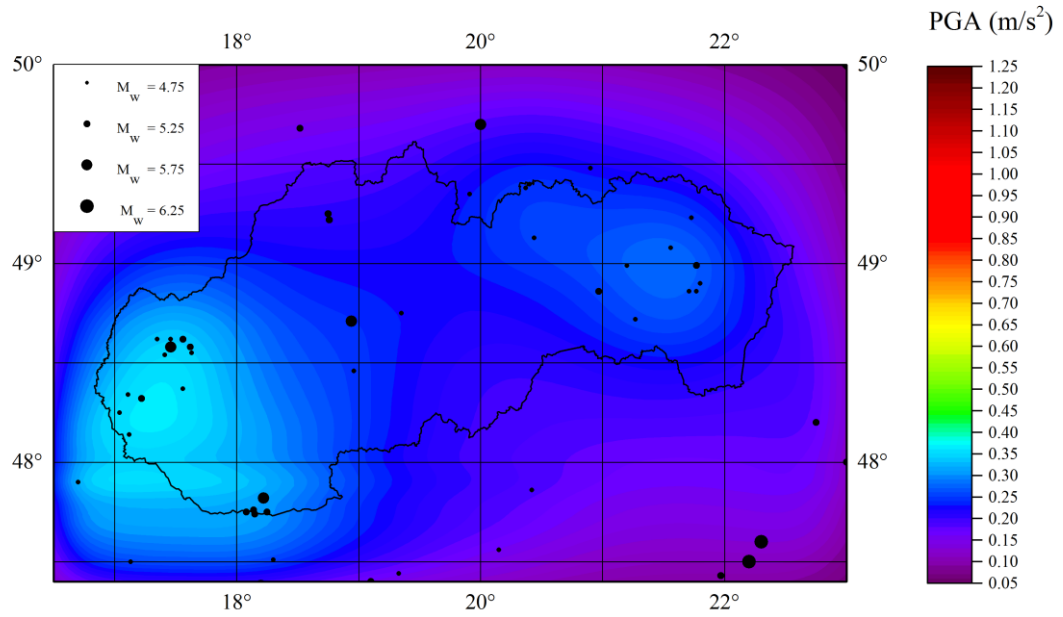


Figure 3.27 – Seismic hazard map for $S/2.5$, GMPE Cauzzi and Faccioli (2008), clustered catalogue and effective return periods listed in Table 3.5.

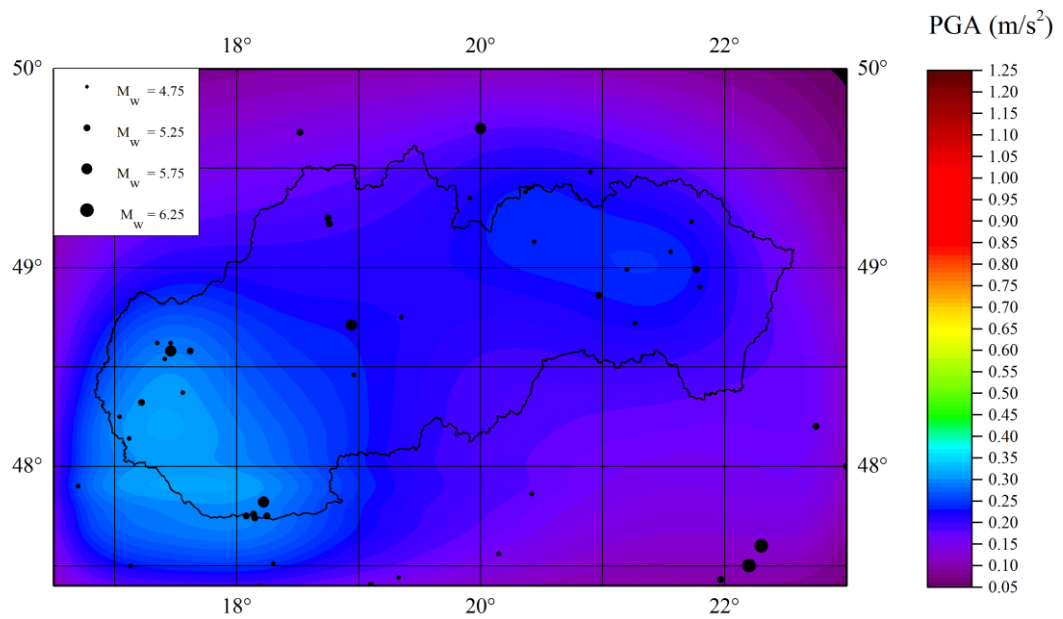


Figure 3.26 – Seismic hazard map for $S/2.5$, GMPE Cauzzi and Faccioli (2008), declustered catalogue and effective return periods listed in Table 3.5.

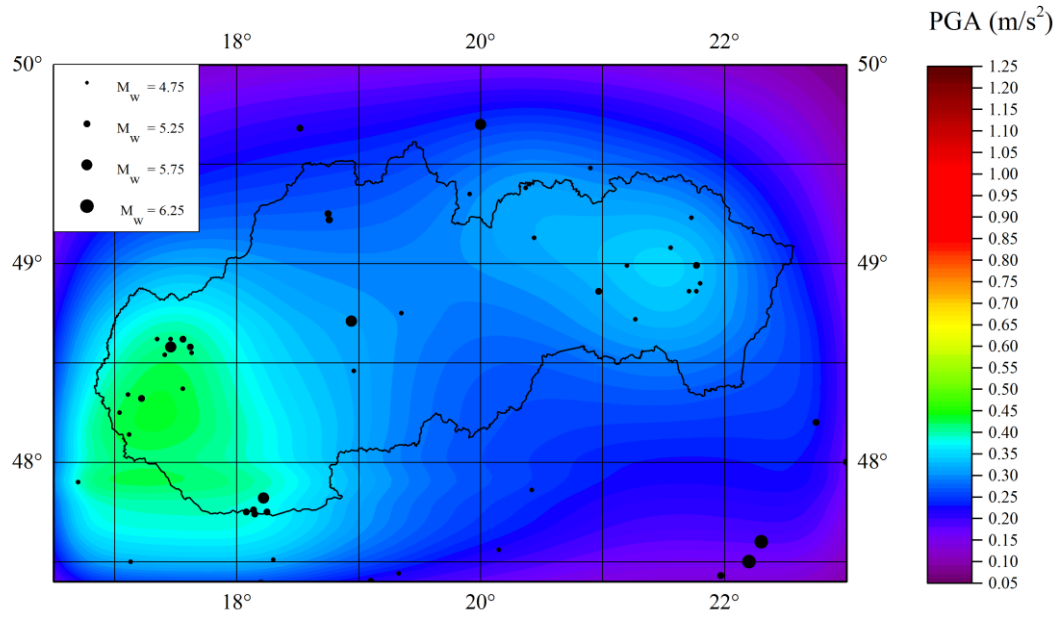


Figure 3.29 – Seismic hazard map for S/4.5, GMPE Akkar and Bommer (2010), clustered catalogue and effective return periods listed in Table 3.5.

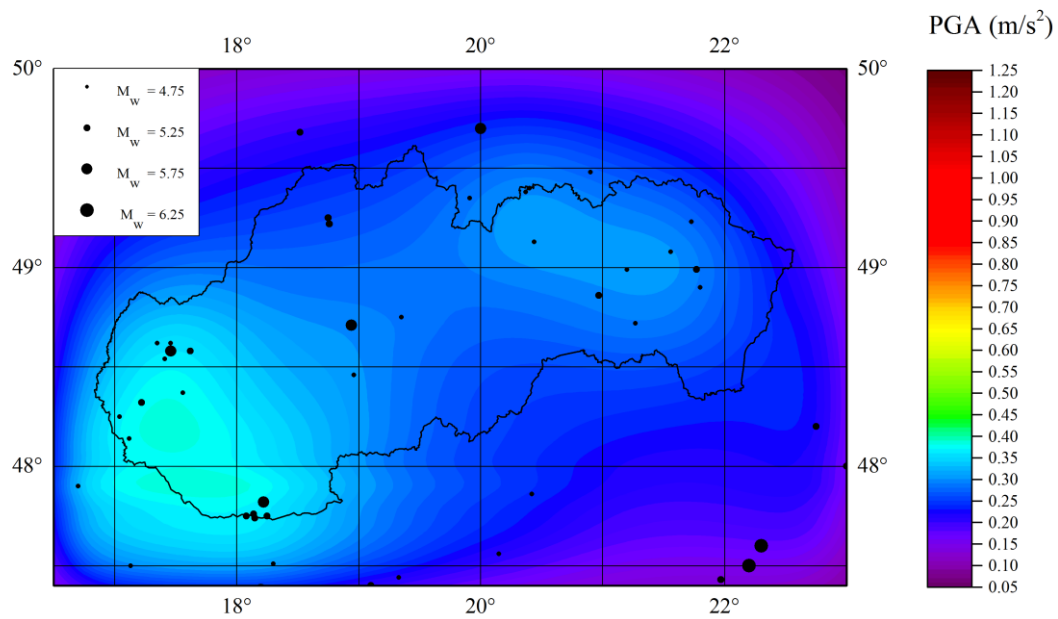


Figure 3.28 – Seismic hazard map for S/4.5, GMPE Akkar and Bommer (2010), declustered catalogue and effective return periods listed in Table 3.5.

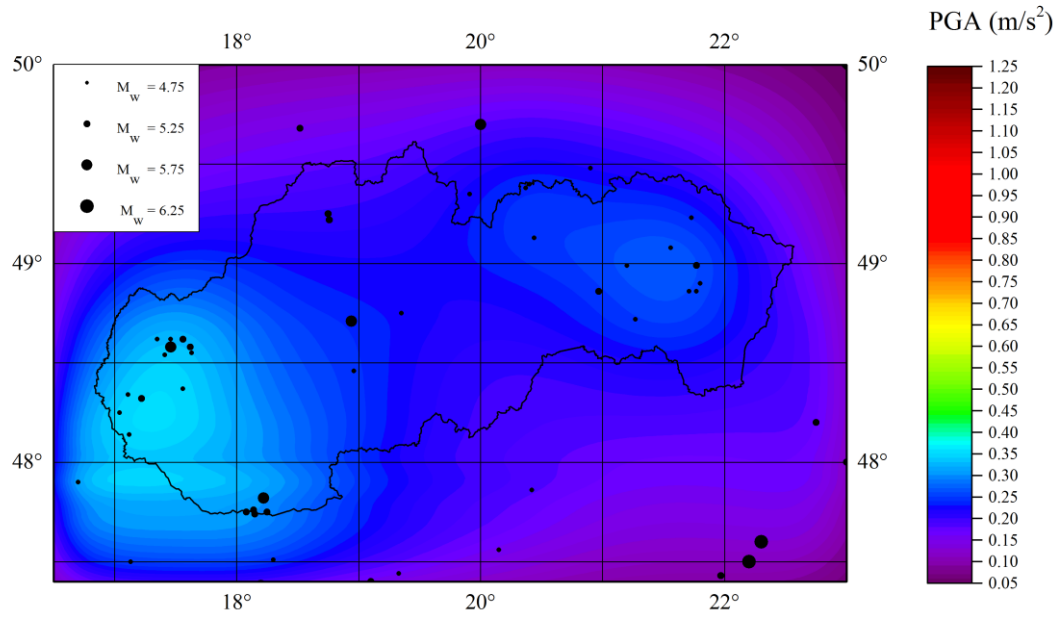


Figure 3.31 – Seismic hazard map for S/4.5, GMPE Cauzzi and Faccioli (2008), clustered catalogue and effective return periods listed in Table 3.5.

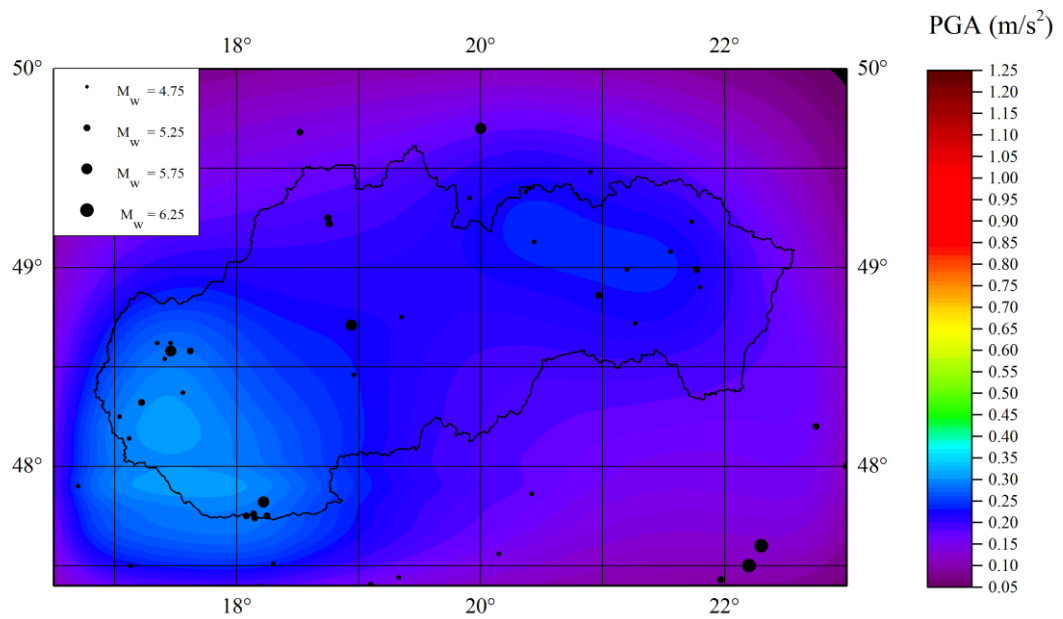


Figure 3.30 – Seismic hazard map for S/4.5, GMPE Cauzzi and Faccioli (2008), declustered catalogue and effective return periods listed in Table 3.5.

3.7 Sensitivity study on kernel functions

In the previous section sensitivity of the resulting seismic activity rate and the annual rate of exceedance was studied and it was shown that the threshold magnitude for the computation of the bandwidth parameters, the use of clustered or declustered catalogue or type of used GMPE do not influence the results so much as the bins definition. Therefore, we decided to use for further computations only clustered earthquake catalogue and GMPE Akkar and Bommer (2010).

3.7.1 Seismic activity rate

Resulting seismic activity rates computed for finite kernel functions K_2 and K_3 defined in section 3.4 are shown in *Figure 3.32* and *Figure 3.33*. Obtained values of the activity rate using kernel function K_2 represent the highest values obtained until now. This is due to the fact that kernel function K_2 is constant in 50 km radius area around the grid node and if we insert respective values of R_{\min} and R_{\max} into relation (3.1) we get a value $C_2 = 3.54 \times 10^{-4}$. This value approximately correspond to the maximum of the kernel function K_1 for the alternative M/4.5 and $m = 5$, which can be seen in *Figure 3.5*. For kernel function K_1 , an earthquake with magnitude $m = 5$ would contribute to the resulting activity rate with this value, weighted by the respective effective return period, only if it was located directly in the grid node and its contribution decreases with distance from the grid node. If we consider kernel function K_2 all the earthquakes with magnitude $m = 5$ in the 50 km radius area around the grid node contribute to the resulting activity rate equally. Contribution of earthquakes with magnitudes greater than $m = 5$ is even smaller when kernel function K_1 is used because kernel function K_1 is magnitude dependent and its values decreases with increasing magnitude, as can be seen in the *Figure 3.5*. To sum up, even though fewer events contribute to the resulting activity rate, it yields higher values, because contributions of individual events are higher.

Lower values of the seismic activity rate were obtained when the kernel function K_3 was used. If we again insert respective values of R_{\min} and R_{\max} into relation (3.1) we get a value $C_3 = 1.15 \times 10^{-4}$. This value approximately correspond to the maximum of the

kernel function K_1 for the alternative $M/4.5$ and $m = 5.5$. This explains why lower values of the activity rate were obtained, because when kernel function K_3 was used, contributions of all lower events were reduced.

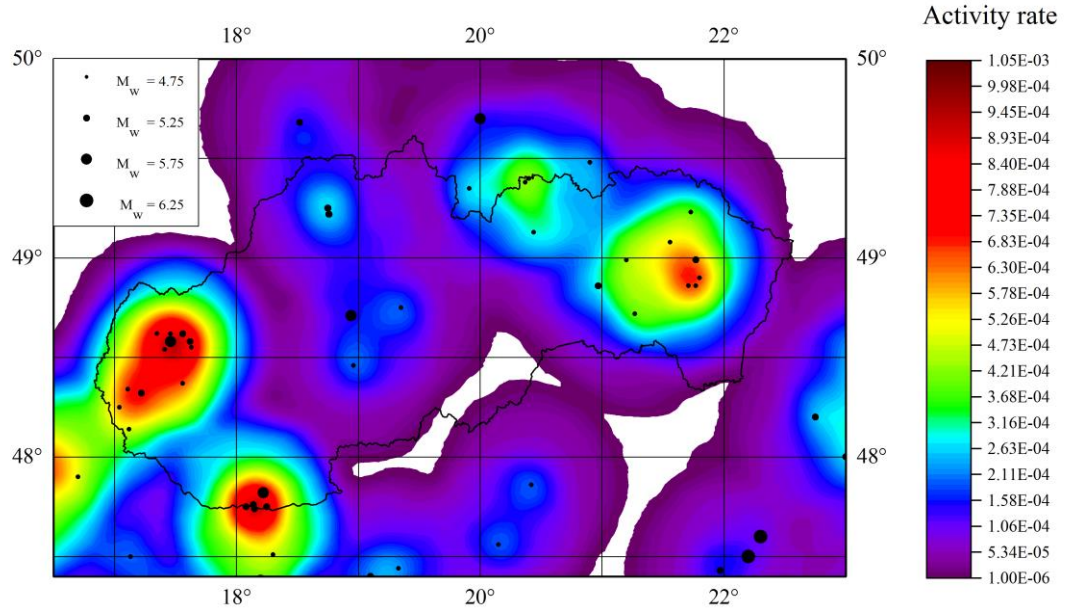


Figure 3.33 – Seismic activity rate for the kernel function K_2 , clustered catalogue and effective return periods listed in Table 3.5.

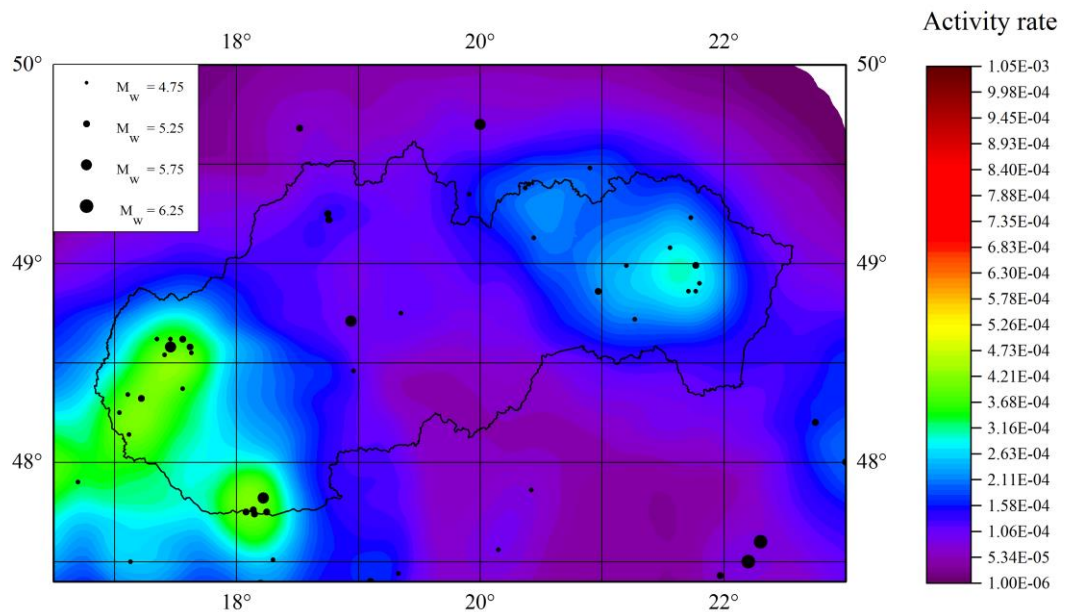


Figure 3.32 – Seismic activity rate for the kernel function K_3 , clustered catalogue and effective return periods listed in Table 3.5.

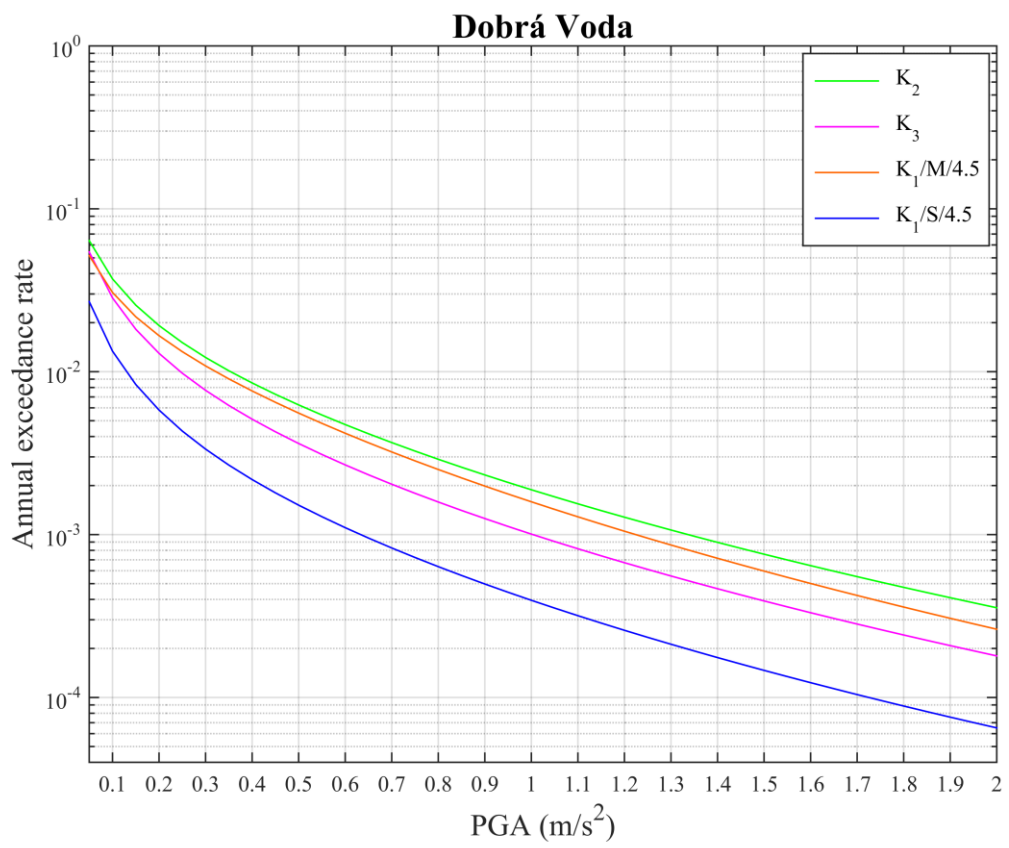
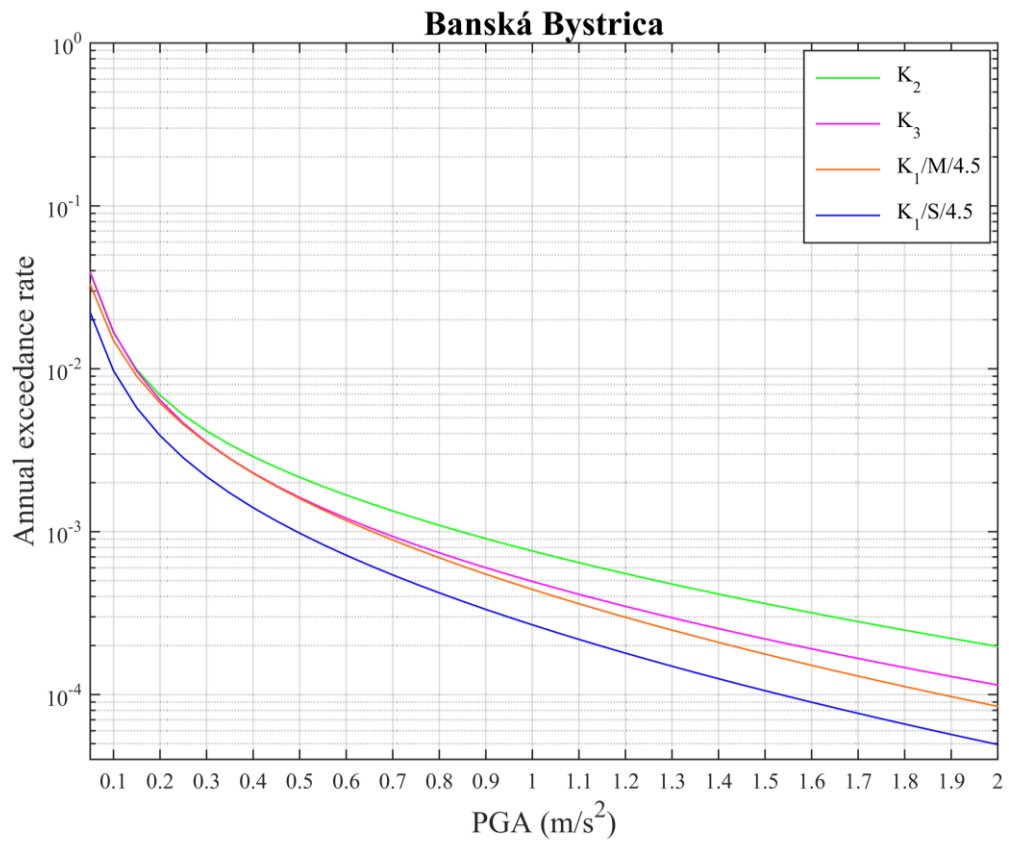
If we compare this results with activity rate maps obtained using infinite kernel function K_1 , we can see that the activity rate reaches higher values in the areas where earthquakes with magnitude around $M_w = 6.0$ occurred in the past.

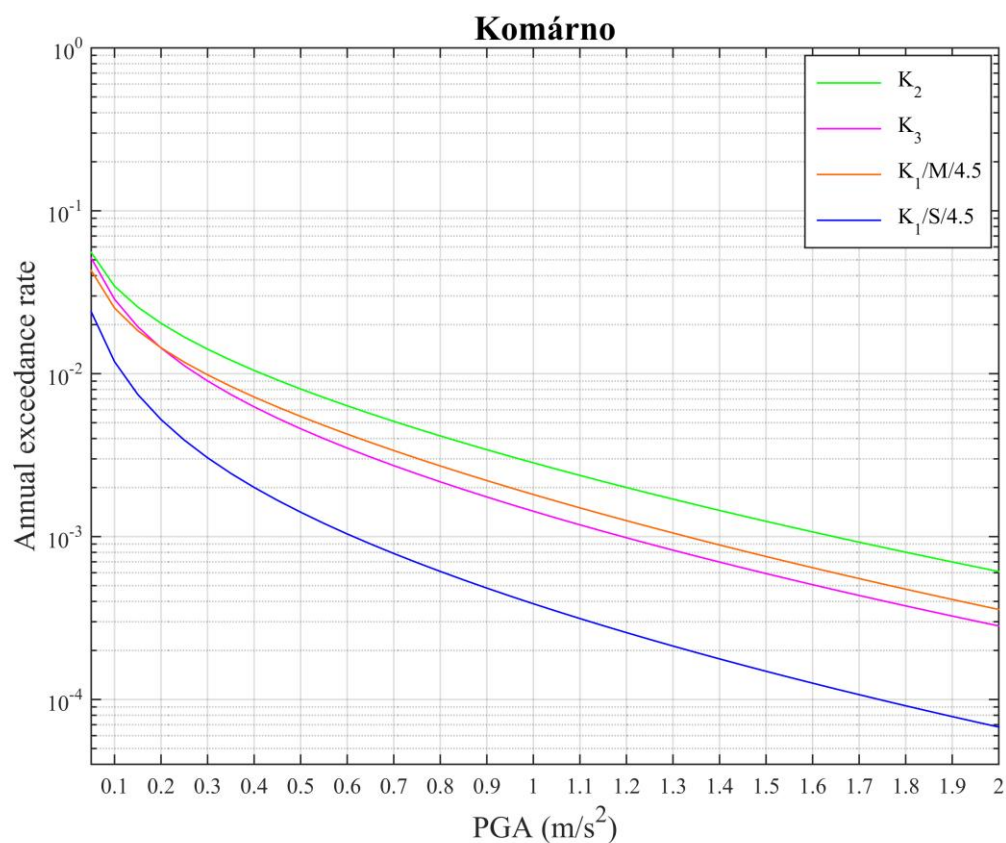
3.7.2 Seismic hazard curves

After the seismic activity rate is computed for the whole computational area, seismic hazard curves for four cities listed in *Table 3.7* can be plotted. In this case, only GMPE Akkar and Bommer (2010) was used.

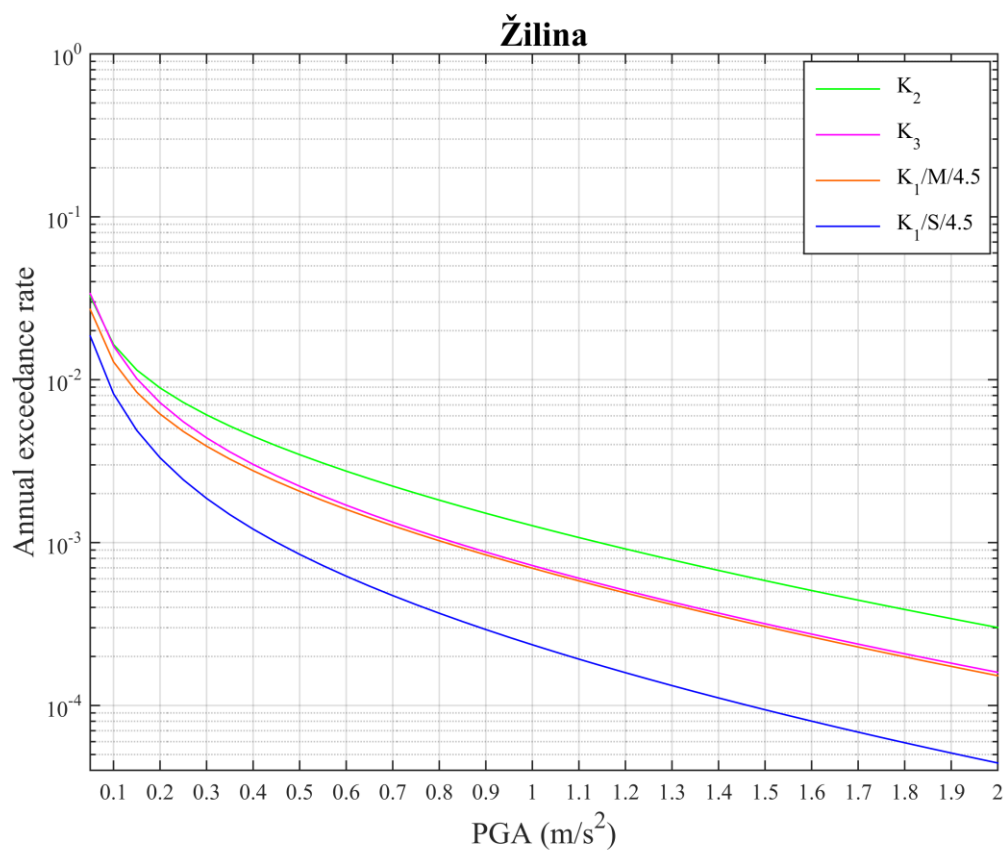
Obtained seismic hazard curves are shown in *Figure 3.34* together with seismic hazard curves computed for alternatives M/4.5 and S/4.5 using kernel function K_1 and GMPE Akkar and Bommer (2010).

For all four cities the highest values of the annual rate of exceedance were obtained when the kernel function K_2 was used. For Dobrá Voda, these values are not so much higher than values obtained using the kernel function K_1 for the alternative M/4.5 in comparison with other cities. This is due to the fact that Dobrá Voda lies in a region with higher seismic activity, where more events even with magnitudes around $M_w = 4.5$ occurred in the past and as already said before, these events contribute more to the resulting activity rate, when kernel function K_1 is used. On the other hand, for three other cities differences between values of the annual exceedance rate obtained when the kernel function K_2 was used and values of the annual exceedance rate obtained when kernel function K_1 for the alternative M/4.5 was used, are higher. This is due to the fact that bigger earthquakes have occurred in their vicinity in the past.





C)



D)

Figure 3.34 A) – D) – Seismic hazard curves for four cities listed in Table 3.7 for different kernel functions, clustered catalogue and effective return periods listed in Table 3.5.

3.7.3 Seismic hazard maps

Obtained seismic hazard maps are shown in *Figure 3.35* and *Figure 3.36*.

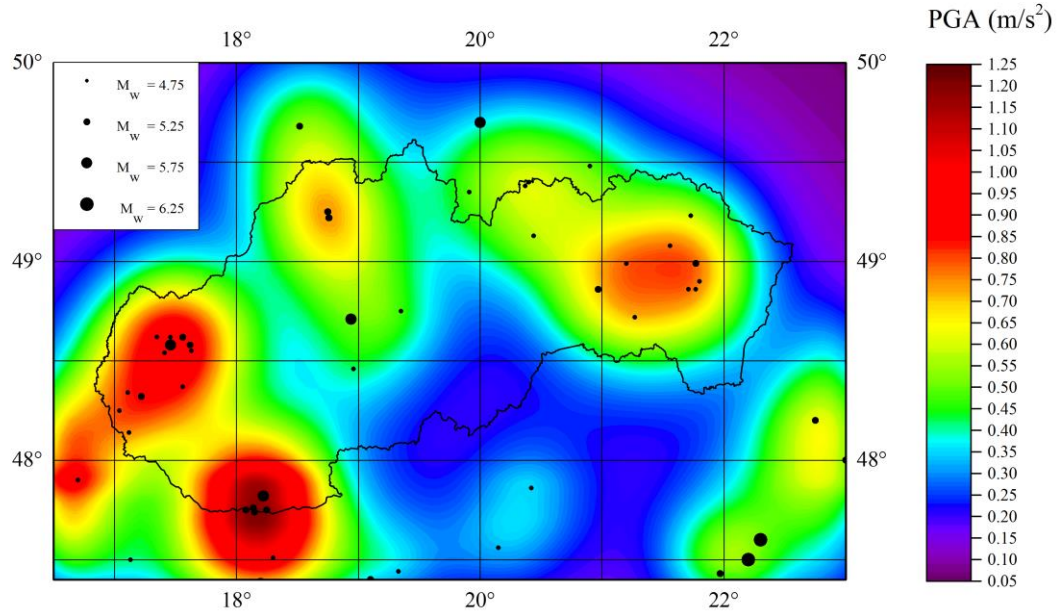


Figure 3.36 – Seismic hazard map for the kernel function K_2 , GMPE Akkar and Bommer (2010), clustered catalogue and effective return periods listed in *Table 3.5*.

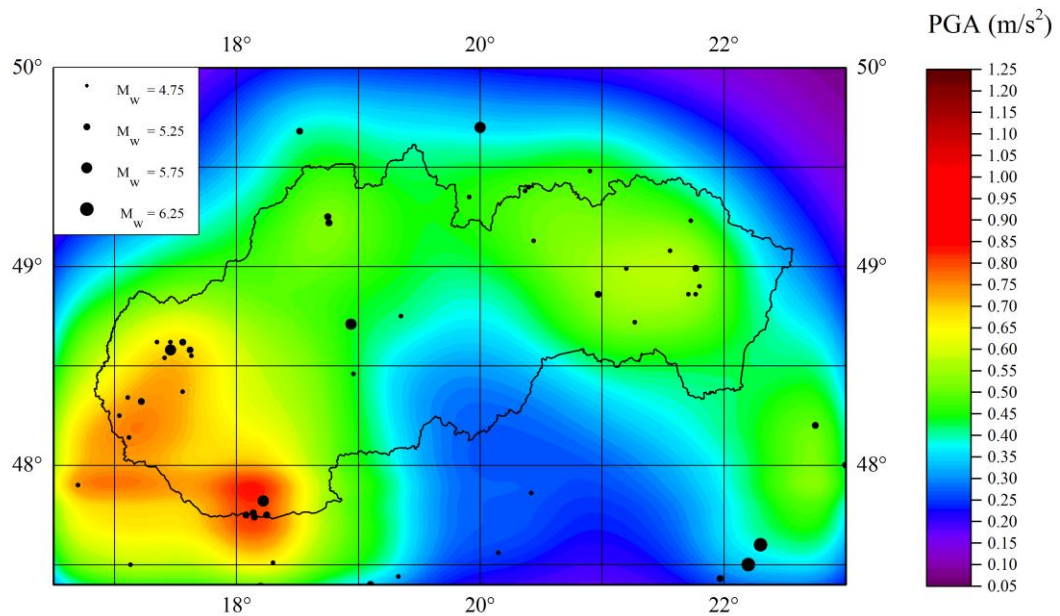


Figure 3.35 – Seismic hazard map for the kernel function K_3 , GMPE Akkar and Bommer (2010), clustered catalogue and effective return periods listed in *Table 3.5*.

As well as for the activity rate maps, hazard values obtained using the kernel function K_2 represent the highest values obtained until now. If we compare these results with the results obtained using the kernel function K_3 , we can see that higher values of PGA in the western and in the eastern part of Slovakia decreased, while lower values in the central part of Slovakia increased. This is due to the shape of the kernel function K_3 . Kernel function K_3 is more widespread and has lower maximum value C_3 . Therefore an event effects its bigger vicinity but a contribution to the hazard in the very place of occurrence is lower.

3.8 Sensitivity study on effective detection periods

In the previous sections sensitivity of the results to the bandwidth function and the kernel function were studied. Other parameter that can affect the resulting hazard values is the effective return period. In this thesis effective return period has been considered correspondent to the completeness period for a given magnitude bin. Until now, the effective return periods listed in *Table 3.5* were used in computations. Determination of the completeness period, however, can sometimes be difficult, especially for higher magnitude bins, since there are very few events. Therefore, in this section different values of the effective return periods, listed in *Table 3.8* were used in hazard computations.

MAGNITUDE BIN	COMPLETENESS TIME INTERVAL	EFFECTIVE RETURN PERIOD
4.50 – 4.99	1810 - 2009	199
5.00 – 5.49	1785 - 2009	224
5.50 – 5.99	1500 - 2009	509
6.00 – 6.49	1500 - 2009	509
6.50 – 6.99	1500 - 2009	509

Table 3.8 – Alternative time completeness of the earthquake catalogue SLOVEC (2011) for magnitudes equal or greater than $M_w = 4.5$ used for effective return period sensitivity study.

3.8.1 Seismic activity rate

Seismic activity rate with modified effective return periods were computed for the clustered catalogue using the kernel function K_1 for the alternatives M/4.5 and S/4.5 and with use of finite kernel functions K_2 and K_3 . Obtained seismic activity rates are shown in *Figure 3.37 – Figure 3.40*.

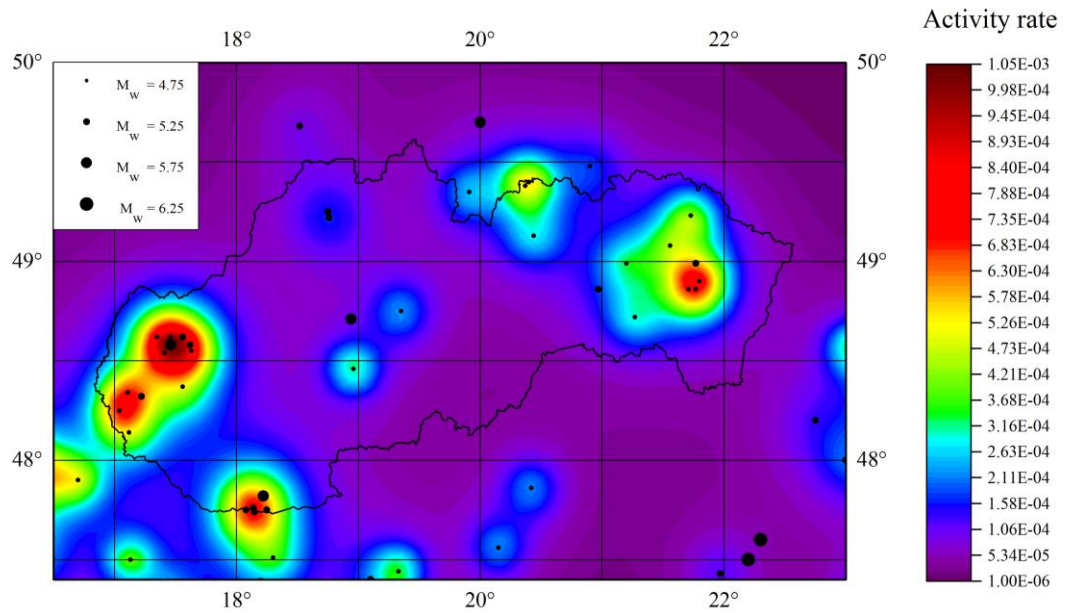


Figure 3.38 – Seismic activity rate for M/4.5, clustered catalogue and alternative effective return periods listed in Table 3.8.

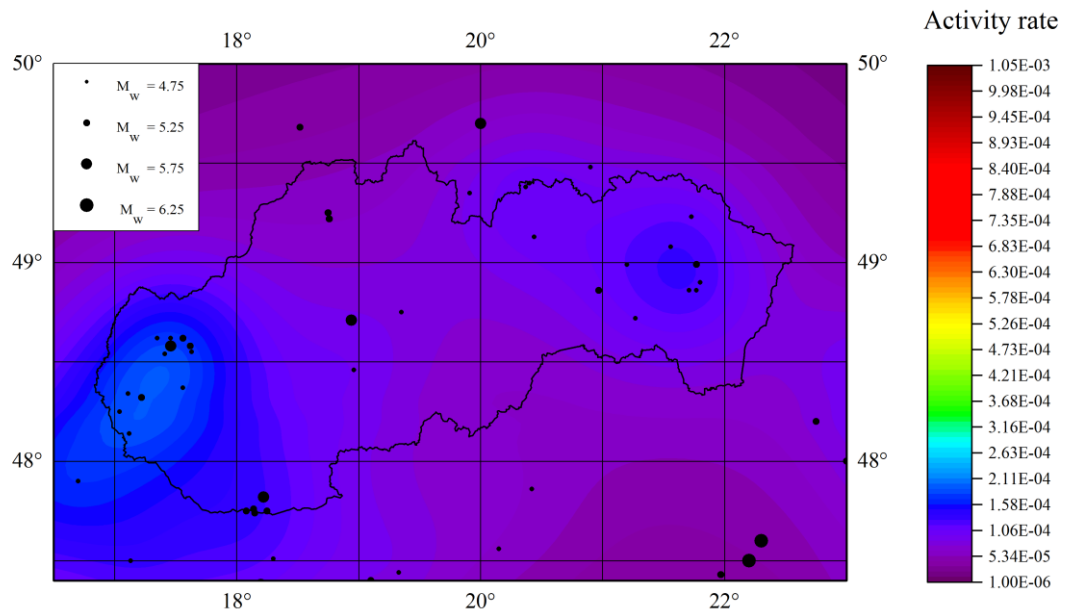


Figure 3.37 – Seismic activity rate for S/4.5, clustered catalogue and alternative effective return periods listed in Table 3.8.

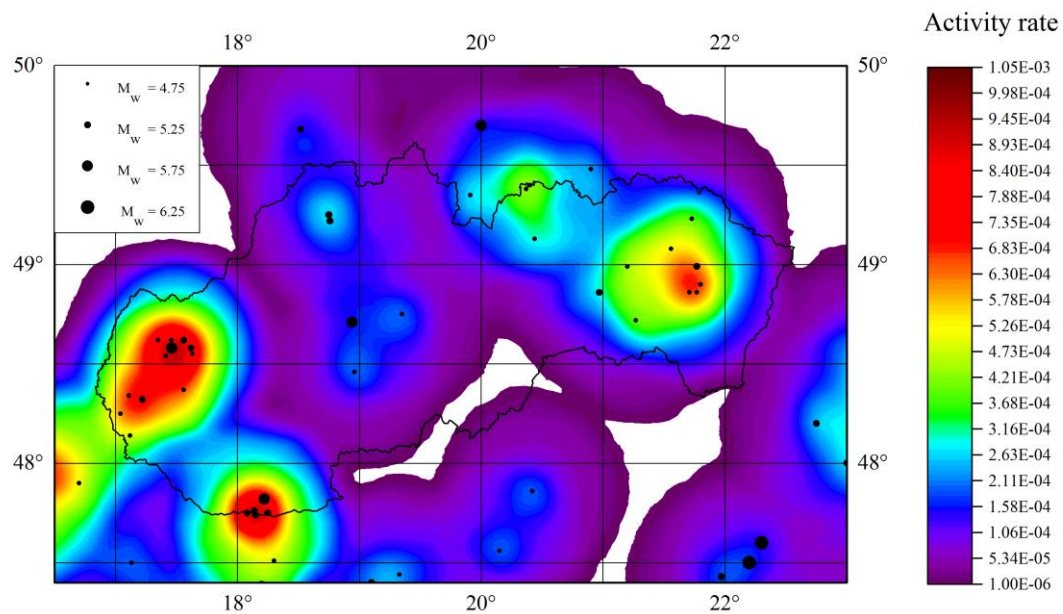


Figure 3.40 – Seismic activity rate for the kernel function K_2 , clustered catalogue and alternative effective return periods listed in Table 3.8.

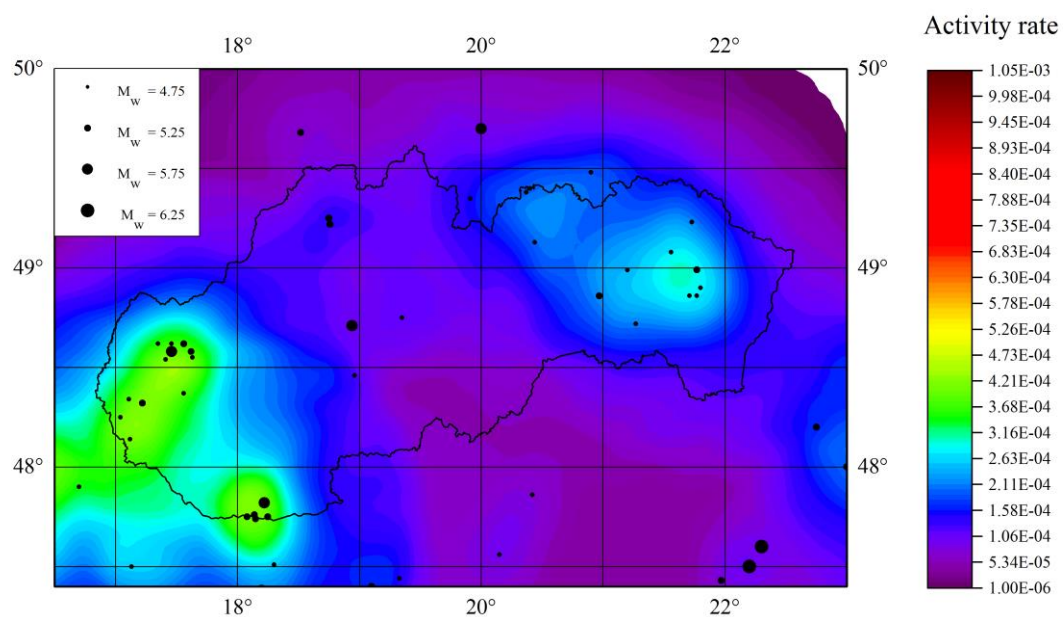
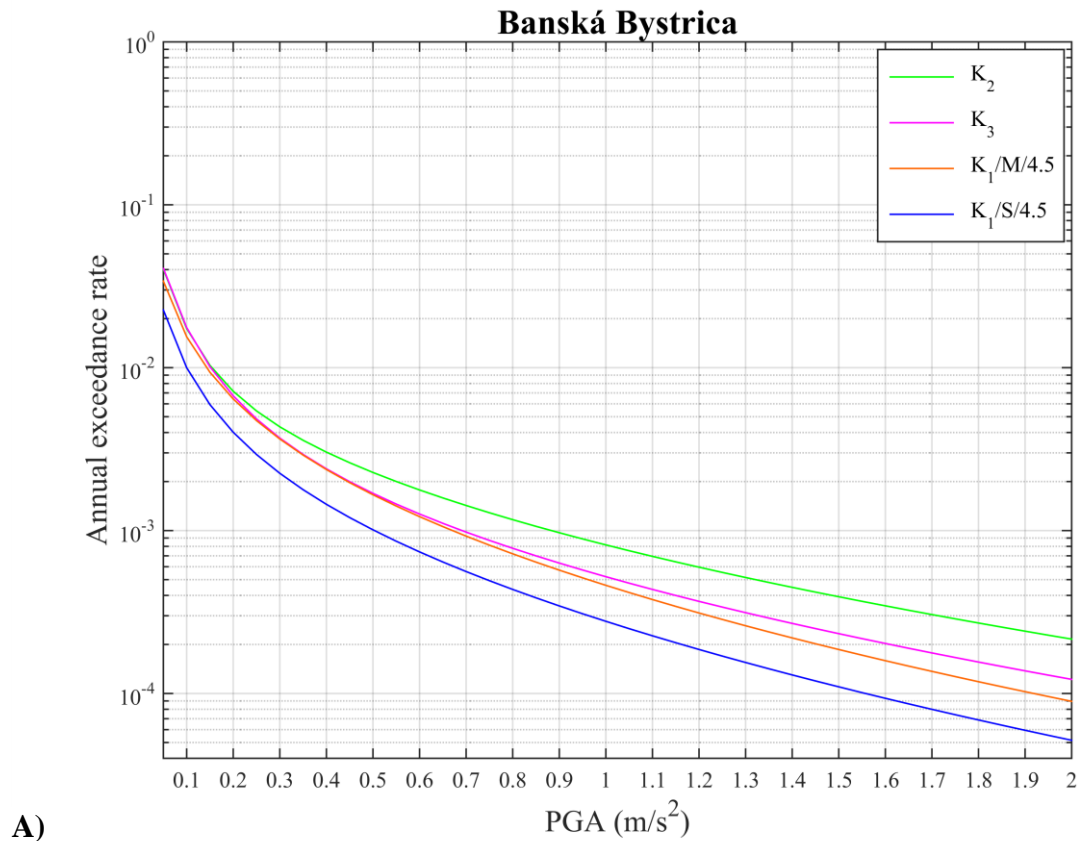


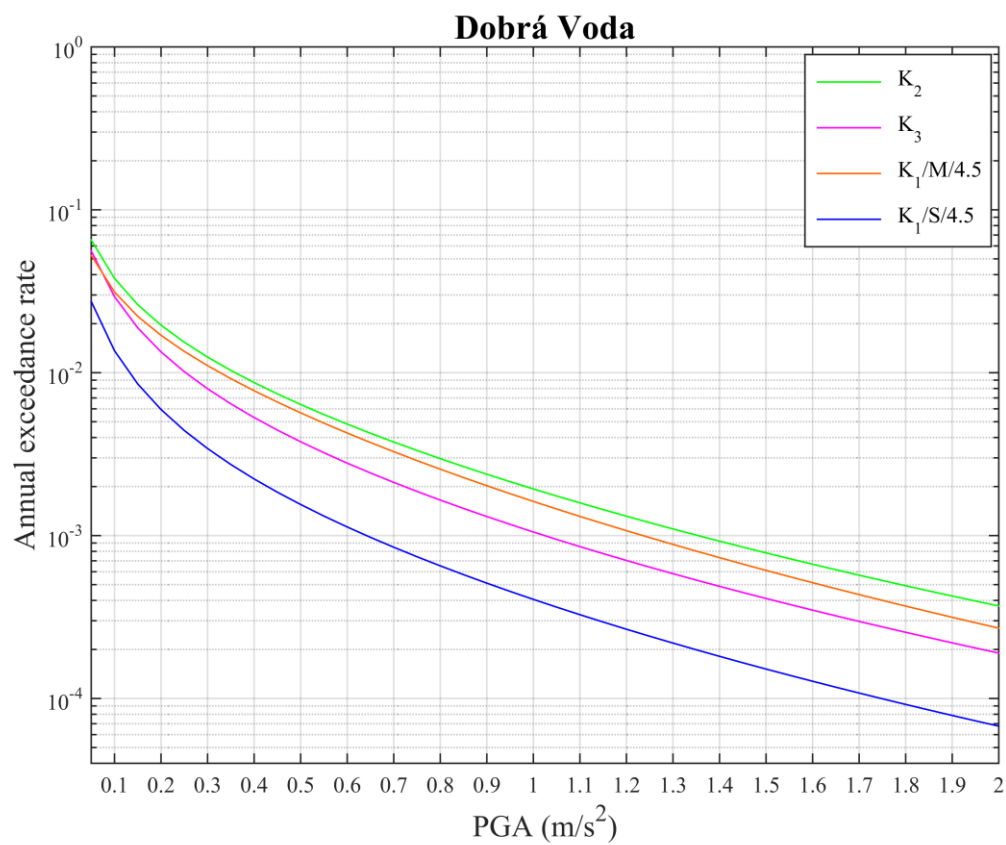
Figure 3.39 – Seismic activity rate for the kernel function K_3 , clustered catalogue and alternative effective return periods listed in Table 3.8.

If we compare these activity rate maps with previously presented results, we can see, that there are no significant changes in the spatial distribution of the activity rate. But if we compare for example *Figure 3.33* with *Figure 3.40* we can see that the values of the activity rate around events with magnitude close to $M_w = 6.25$ located in southeast corner of computational area increased with decreasing effective return period.

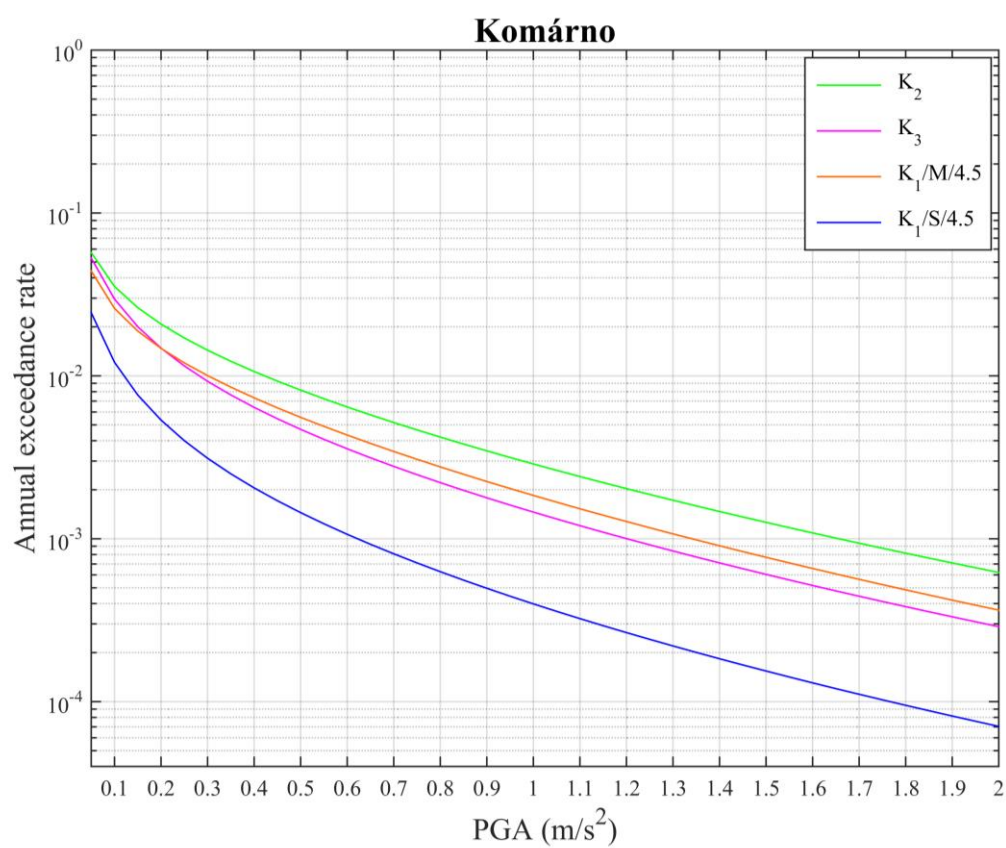
3.8.2 Seismic hazard curves

Obtained seismic hazard curves for four cities listed in *Table 3.7* are shown in *Figure 3.41*. For all four cities, values of the annual exceedance rate are slightly higher, what can be expected, since values of the effective return periods decreased and contributions of individual events were weighted by lower values, but there is no significant difference when compared to seismic hazard curves in *Figure 3.34*.





B)



C)

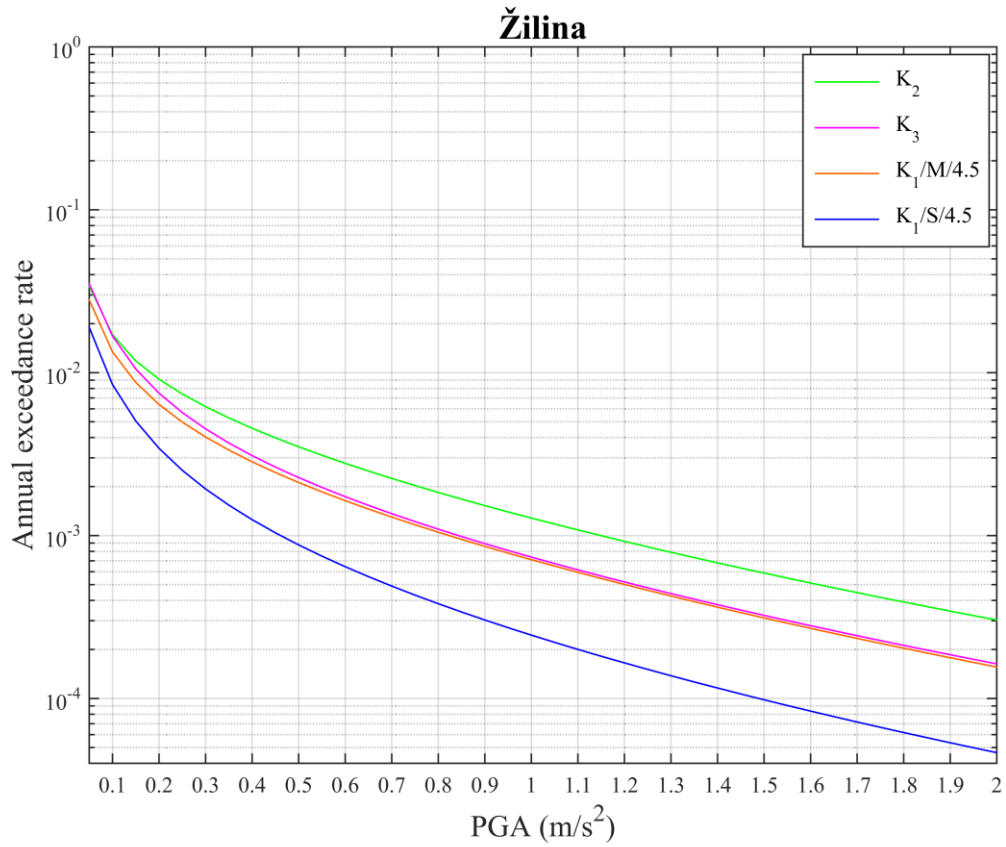


Figure 3.41 A) – D) –Seismic hazard curves for four cities listed in Table 3.7 for different kernel functions, clustered catalogue and alternative effective return periods listed in Table 3.8.

3.8.3 Seismic hazard maps

Decrease of the effective return period lead to overall increase of the hazard values, as can be seen in Figure 3.42 – Figure 3.45. The most significant increase was obtained using the kernel function K_2 and can be seen in southeast corner of computational area the Figure 3.45 when compared to the Figure 3.36.

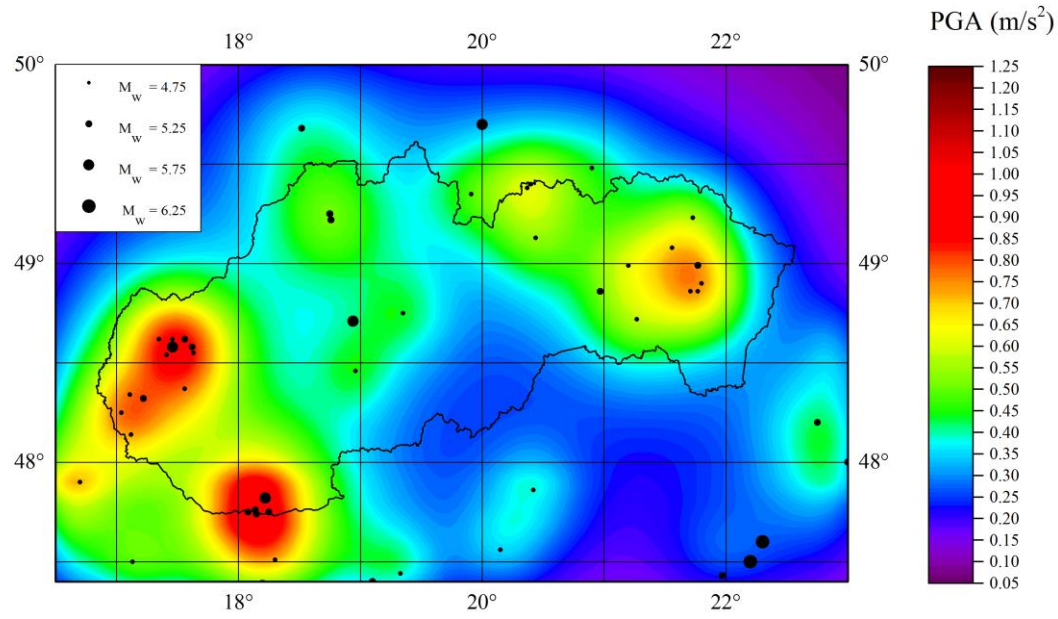


Figure 3.43 – Seismic hazard map for $M/4.5$, GMPE Akkar and Bommer (2010), clustered catalogue and alternative effective return periods listed in Table 3.8.

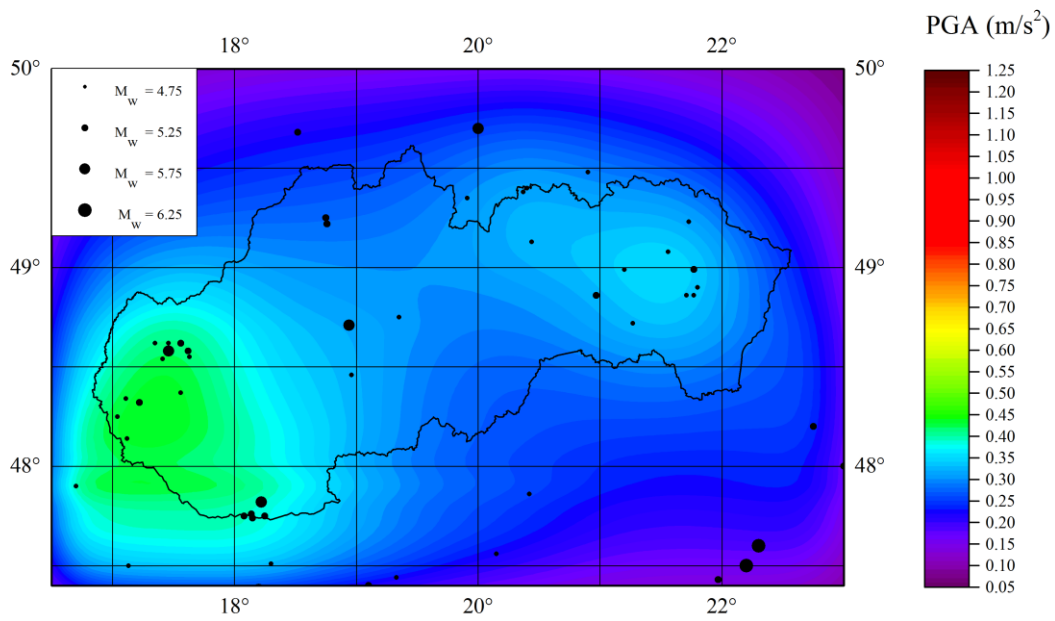


Figure 3.42 – Seismic hazard map for $S/4.5$, GMPE Akkar and Bommer (2010), clustered catalogue and alternative effective return periods listed in Table 3.8.

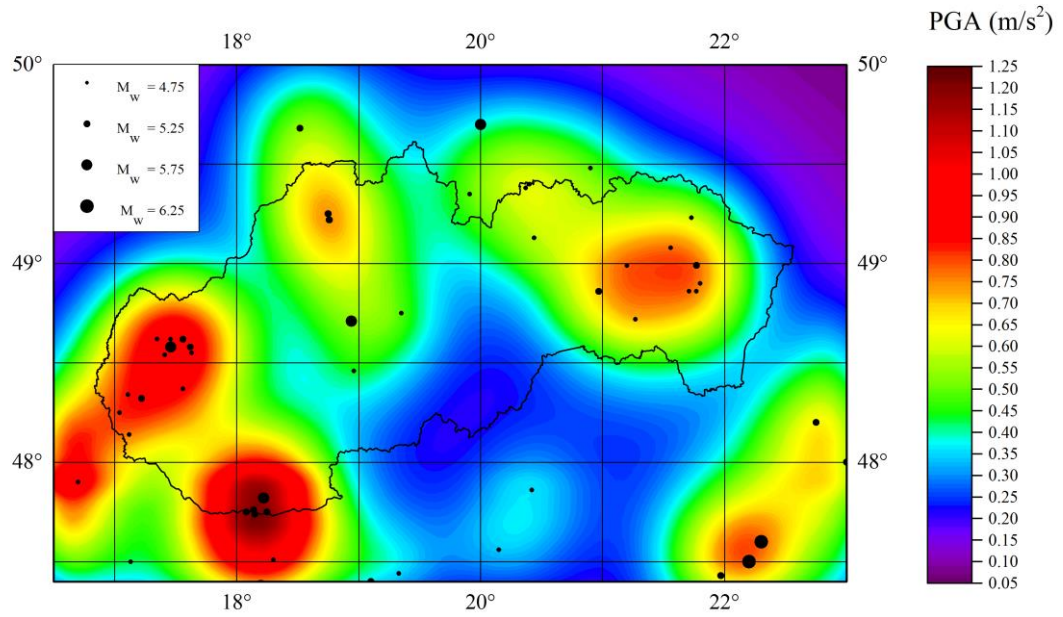


Figure 3.45 – Seismic hazard map for the kernel function K_2 , GMPE Akkar and Bommer (2010) clustered catalogue and alternative effective return periods listed in Table 3.8.

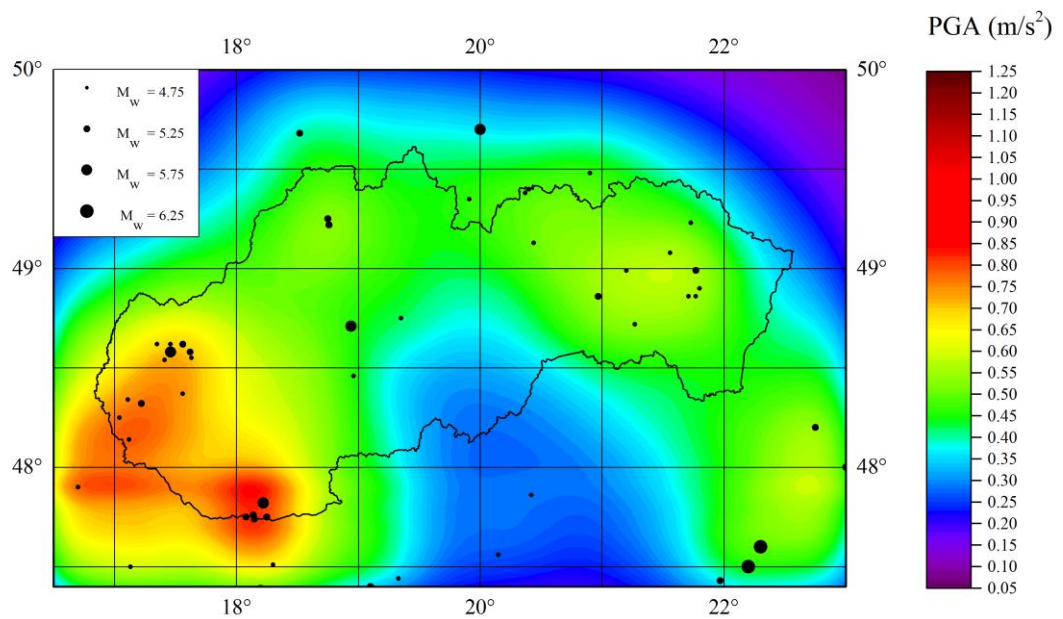


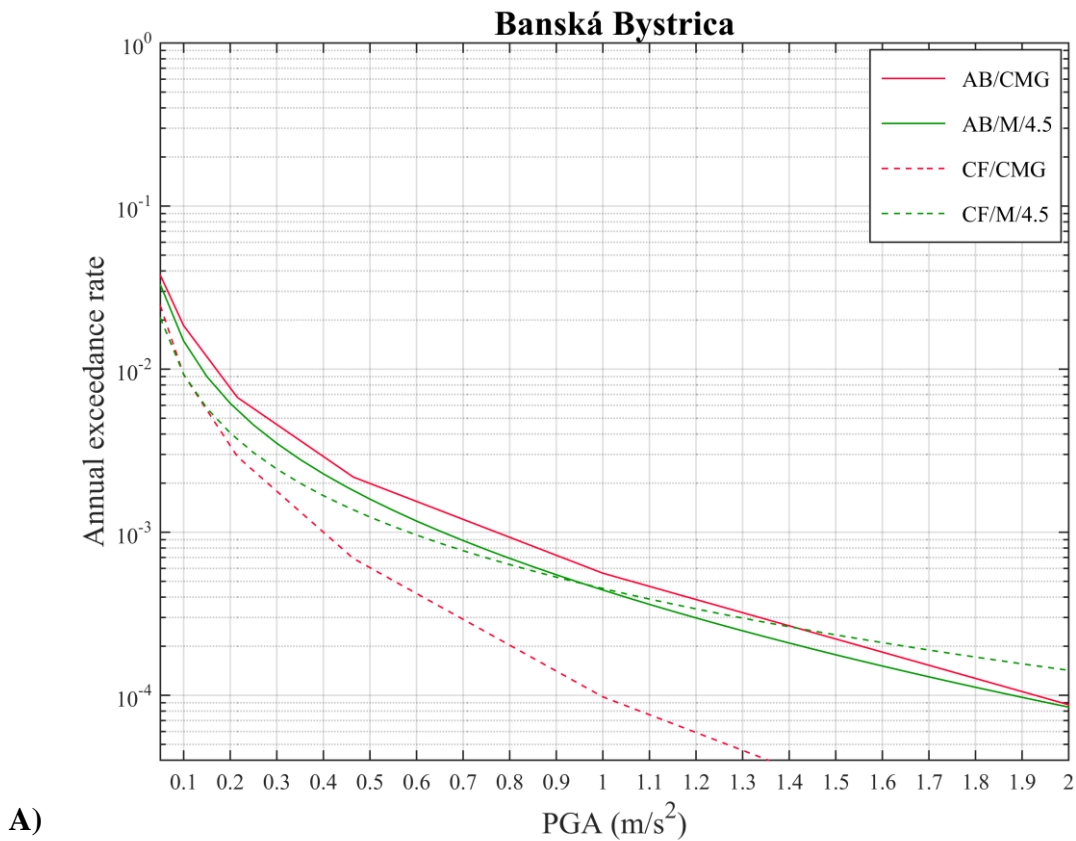
Figure 3.44 – Seismic hazard map for the kernel function K_3 , GMPE Akkar and Bommer (2010) clustered catalogue and alternative effective return periods listed in Table 3.8.

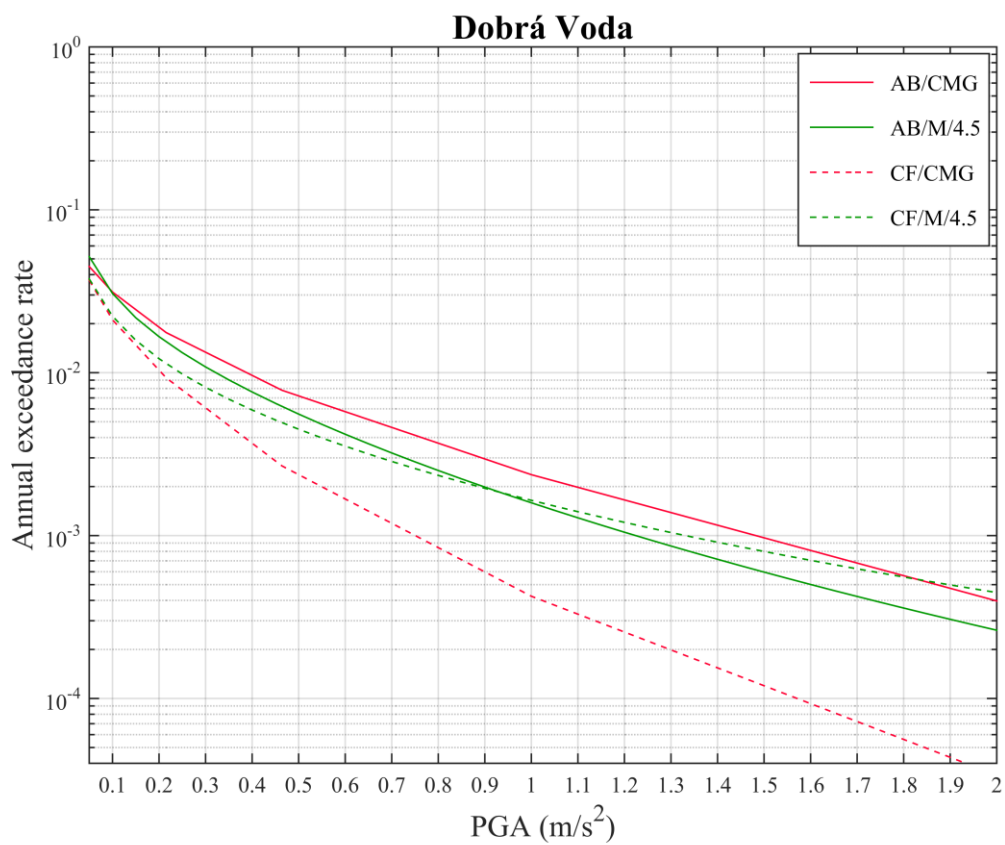
3.9 Comparison with classical Cornell-McGuire approach

In this section, results obtained using classical Cornell-McGuire approach (Kysel 2014) are presented and compared to the results obtained by zoneless approach in this thesis.

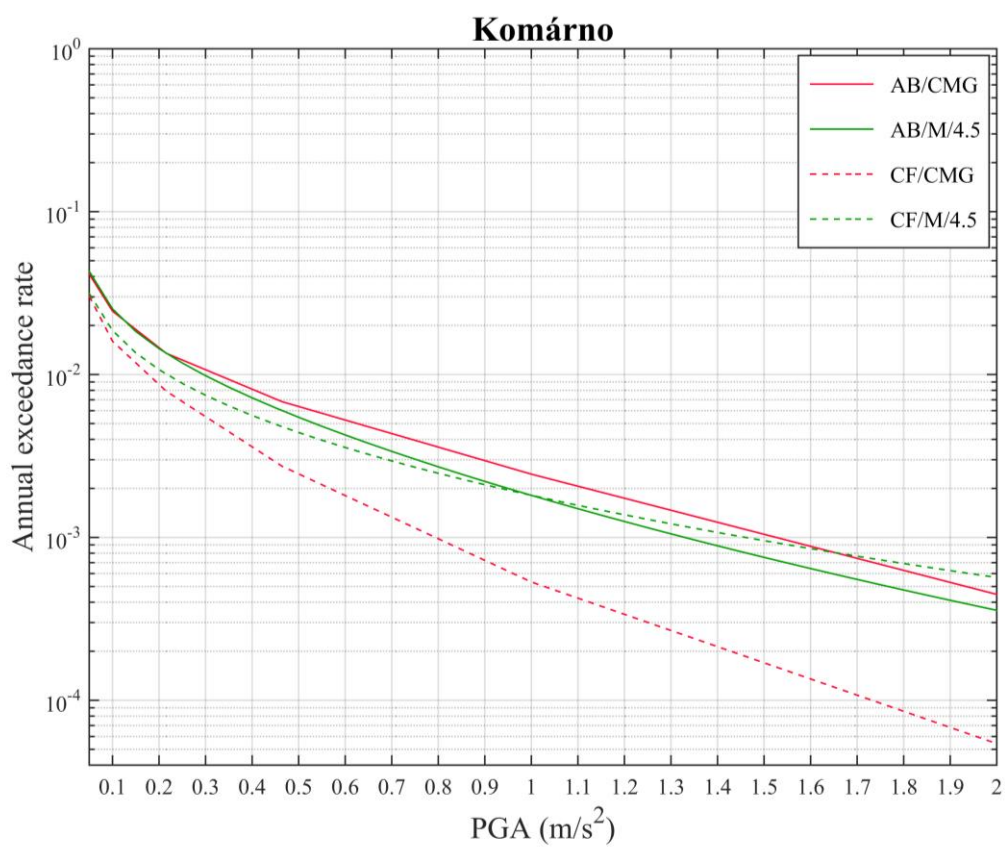
3.9.1 Seismic hazard curves

Seismic hazard curves for four cities listed in *Table 3.7* for both GMPEs are shown in *Figure 3.46*. Since threshold magnitude used for the computation of the bandwidth function parameters and the use of either clustered or declustered catalogue do not influence the results so significantly, only seismic hazard curves obtained using the kernel function K_1 for the alternative M/4.5 are compared to seismic hazard curves obtained from the logic tree computation by Kysel (2014) for both chosen GMPEs.





B)



C)

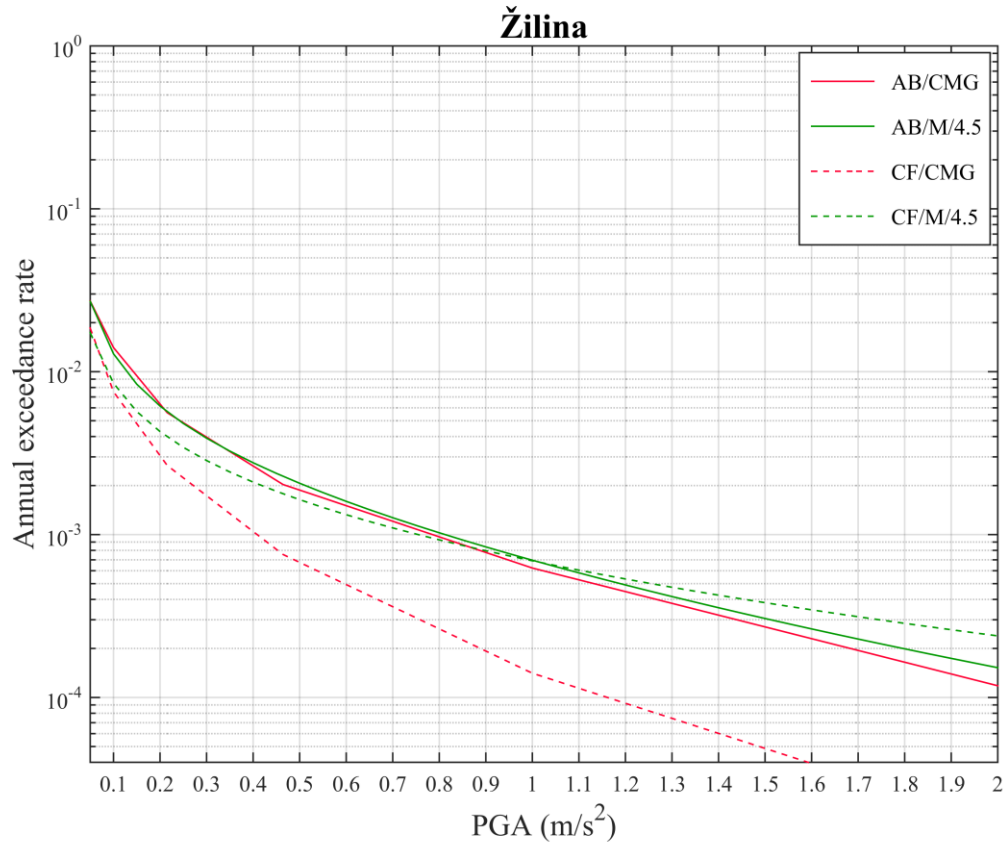


Figure 3.46 – Comparison of the seismic hazard curves for four cities listed in Table 3.7 computed using classical logic tree approach (Kysel 2014) with seismic hazard curves computed using zoneless approach for infinite kernel function K_1 for the alternative M/4.5 and clustered catalogue.

It can be seen, that seismic hazard curves obtained using classical approach and GMPE Akkar and Bommer (2010) yielded comparable results as zoneless approach for both GMPEs. On the other hand, seismic hazard curves obtained using classical approach and Cauzzi and Faccioli (2008) GMPE have lower values for all four cities and we can see how strongly seismic hazard curves in classical approach are affected by the choice of GMPE compared to the zoneless approach.

3.9.2 Seismic hazard maps

Seismic hazard maps computed using classical Cornell-McGuire approach for the logic tree presented in Kysel (2014) for the return period 475yr are shown in Figure 3.48 and Figure 3.47.

It can be seen in both figures, that hazard distribution follows the seismic source zone definition, with lower hazard values at the borders of the zone and higher hazard values in

the middle. As in the case of seismic hazard curves, hazard values obtained using GMPE Cauzzi and Faccioli (2008) are lower for the whole computational area compared to hazard values obtained using GMPE Akkar and Bommer (2010).

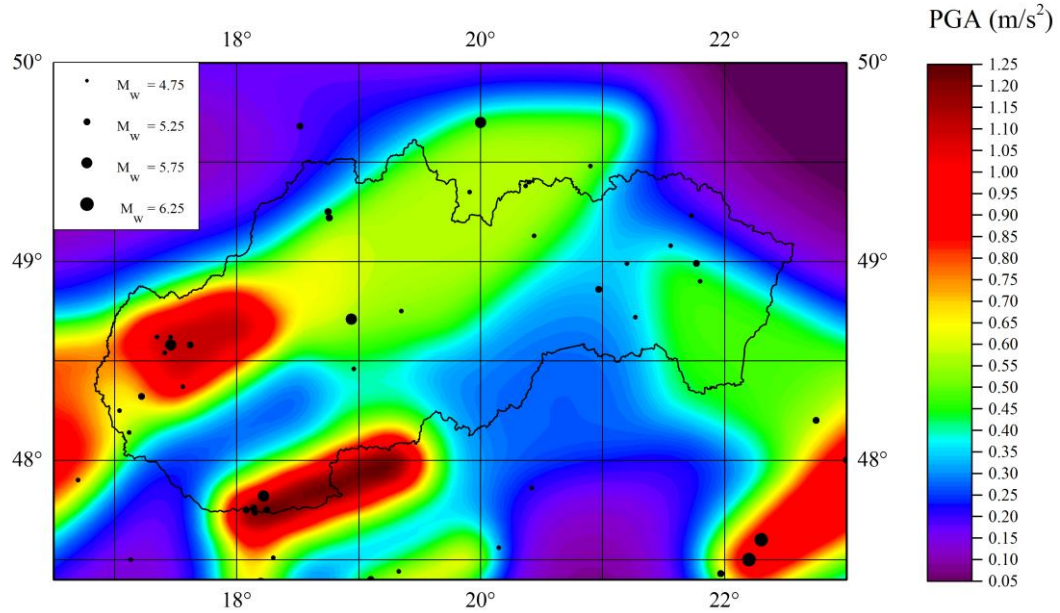


Figure 3.47 – Seismic hazard map obtained using classical Cornell-McGuire approach for the logic tree presented in Kysel (2014) and GMPE Akkar and Bommer (2010).

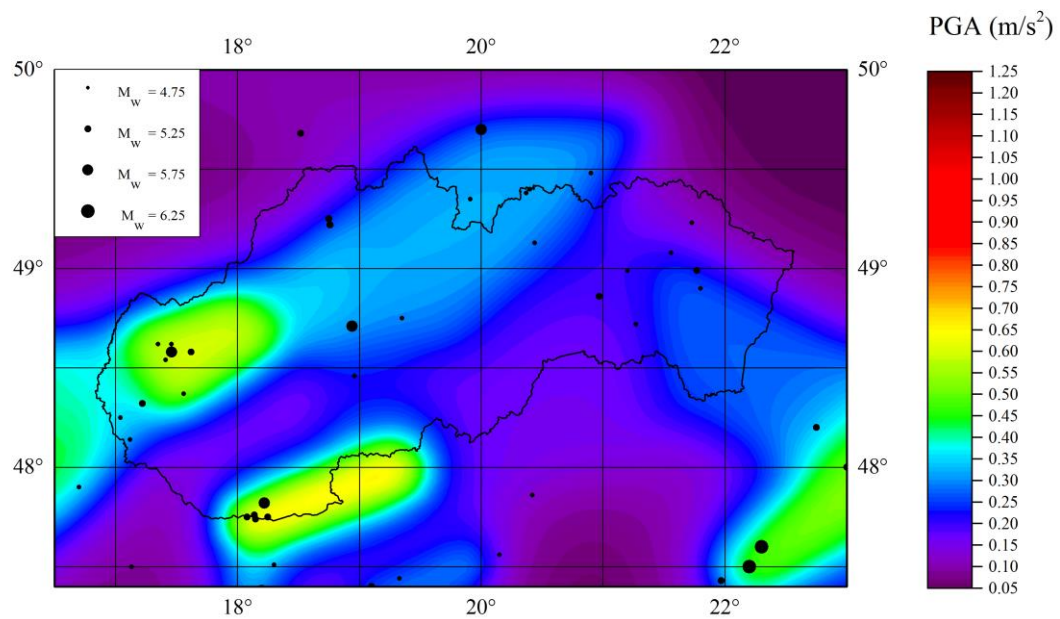


Figure 3.48 – Seismic hazard map obtained using classical Cornell-McGuire approach for the logic tree presented in Kysel (2014) and GMPE Cauzzi and Faccioli (2008).

When compared to seismic hazard maps obtained using zoneless approach, GMPE Akkar and Bommer (2010) yielded higher hazard values in regions with higher seismicity, but this regions also correspond to smaller seismic source zones. The biggest differences can be seen in the southeast corner of computational area – hazard values obtained using classical approach are significantly higher than hazard values obtained by zoneless approach. On the other hand, zoneless approach yielded locally higher hazard values in the Eastern Slovakia, where several medium sized earthquakes occurred in the past.

As we already said before, hazard values obtained using classical Cornell-McGuire approach differ more significantly with respect to chosen GMPE compared to hazard values obtained using zoneless approach. This may be to some extent caused by the fact that depths assigned to each event in the catalogue were not considered in our calculations but were considered in the logic tree computation by Kysel (2014). Since GMPE Akkar and Bommer (2010) is defined for Joyner-Boore distance, inclusion of hypocentral depths would not affect presented hazard values. However, GMPE Cauzzi and Faccioli (2008) is defined for hypocentral distance and inclusion of hypocentral depths may influence the results. The inclusion of hypocentral depths into calculations may be the next step in the analysis of zoneless approach.

CONCLUSION

In this master's thesis, we applied zoneless approach proposed by Woo (1996) for the seismic hazard analysis of the territory of Slovakia. In order to perform the analysis, it was necessary to specify individual input parameters. We used different alternatives of input parameters to test the sensitivity of the results by the one-factor-at-a-time method. Zoneless approach results were also compared to the results from PSHA calculation following classical Cornell-McGuire approach presented in Kysel (2014).

We used SLOVEC (2011) earthquake catalogue and we considered both clustered and declustered variants. Bandwidth function parameters were computed in four different ways – we considered two different threshold magnitudes for the computation of the bandwidth function parameters and for each threshold magnitude, two different bin definitions were used. We used three different kernel functions – one infinite kernel function proposed by Vere-Jones (1992) and two alternatives of finite kernel function proposed by Woo (2001b). Effective return periods which are supposed to be assigned to each event in the catalogue were considered correspondent to the completeness periods for particular magnitude. We considered two different sets of completeness periods. We used two ground motion prediction equations, Akkar and Bommer (2010) and Cauzzi and Faccioli (2008).

For each sensitivity test, seismic activity rate maps, seismic hazard curves for four cities in Slovakia and seismic hazard maps showing peak ground acceleration values for the 475yr return period were obtained. As can be expected, using declustered catalogue overall lower hazard values were obtained but these differences were not significant. Choice of the threshold magnitude used for computation of the bandwidth function parameters also does not influence the results so significantly, but it can be seen that the choice of lower threshold magnitude also yielded lower results. Hazard values obtained using different GMPEs also slightly differ – GMPE Akkar and Bommer (2010) yielded higher hazard values and GMPE Cauzzi and Faccioli (2008) yielded lower hazard values, but these differences are not so significant when compared to differences caused by different bin definitions. Hazard values obtained using bandwidth function parameters for the alternative S/2.5 and S/4.5 are overall lower, with no so significant differences between regions with higher and lower seismicity. Choice of the kernel function has also relevant impact on the results.

Hazard values obtained using classical Cornell-McGuire approach differ significantly with respect to the used GMPE when compared to the zoneless approach. Hazard values obtained using classical approach and GMPE Akkar and Bommer (2010) are higher in regions with higher seismicity, on the other hand, zoneless approach yielded higher hazard values in the Eastern Slovakia, where several medium sized earthquakes occurred in the past.

The results presented in this master's thesis may constitute a starting point for further analysis of zoneless approach (for example for deaggregation studies). Based on the obtained results, we can say that this approach is worth further analysis and in the future may be applied to the seismic hazard analysis of the territory of Slovakia, at least as a part of the logic tree.

References

- Akkar, S., J. J. Bommer 2010. Empirical Equations for the Prediction of PGA, PGV, and Spectral Acceleration in Europe, the Mediterranean Region, and the Middle East. *Seismol. Res. Lett.* 81, 195-206.
- Baker, J.W. 2008. *An Introduction to Probabilistic Seismic Hazard Analysis (PSHA)*. Version 1.3. [Online] Available from: [https://web.stanford.edu/~bakerjw/Publications/Baker_\(2008\)_Intro_to_PSHA_v1_3.pdf](https://web.stanford.edu/~bakerjw/Publications/Baker_(2008)_Intro_to_PSHA_v1_3.pdf) [Accessed 03-03-2016].
- Beauval, C., O. Scotti, F. Bonilla 2006b. The role of seismicity models in probabilistic seismic hazard estimation: comparison of a zoning and a smoothing approach. *Geophys. J. Int.* 165, 584–595.
- Benito, B., M. Navarro, F. Vidal, J. Gaspar-Escribano, M. García-Rodríguez, J. Martínez-Solares 2010. A new seismic hazard assessment in the region of Andalusia (Southern Spain) *Bull. Earthq. Eng.* 98, 739-766.
- Bommer, J., J. Douglas, F. Scherbaum, F. Cotton, H. Bungum, D. Fäh 2010. On the Selection of Ground-Motion Prediction Equations for Seismic Hazard Analysis. *Seismol. Res. Lett.* 81, 783-793.
- Bozzoni, F., M. Corigliano, C. G. Lai, W. Salazar, L. Scandella, E. Zuccolo, J. Latchman, L. Lynch, R. Robertson 2011. Probabilistic Seismic Hazard Assessment at the Eastern Caribbean Islands. *Bull. Seism. Soc. Am.* 101, 2499-2521.
- Cauzzi, C., E. Faccioli 2008. Broadband (0.05 to 20 s) prediction of displacement response spectra based on worldwide digital records. *Journal of Seismology* 12,453-475.
- Corigliano, M., C.G. Lai, L. Scandella, E. Spacone, G. Camata, C. Cantagallo, D. Spallarossa, P. Ghiretti 2014. Probabilistic Seismic Hazard Assessment of the European Extremely Large Telescope (“E-ELT”) Project (Chile). *Proceedings of the 10th National Conference in Earthquake Engineering*. Earthquake Engineering Research Institute, Anchorage.
- Cornell, C. A. 1968. Engineering seismic risk analysis. *Bull. Seism. Soc. Am.* 58, 1583-1606.
- Cornell, C. A., H. Banon, A. F. Shakal 1979. Seismic motion and response prediction alternatives. *Earthquake Eng. Struct. Dyn.* 7, 295-315.

- Cotton, F., F. Scherbaum, J.J. Bommer, H. Bungum 2006. Criteria for selecting and adjusting ground-motion models for specific target applications: Applications to Central Europe and rock sites. *J. Seismol.* 10, 137-156.
- Crespo, M. J., F. Martínez, J. Martí 2014. Seismic hazard of the Iberian Peninsula: evaluation with kernel functions. *Nat. Hazards Earth Syst. Sci.* 14, 1309-1323.
- Esteva, L. 1967. Criterios para la construcción de espectros para diseño sísmico. In: *Proceedings of XII Jornadas Sudamericanas de Ingeniería Estructural y III Simposio Panamericano de Estructuras*, Caracas, 1967. Published later in Boletín del Instituto de Materiales y Modelos Estructurales, Universidad Central de Venezuela, No. 19.
- Frankel, A. 1995. Mapping seismic hazard in the central and eastern United States. *Seismol. Res. Lett.* 66, 8-21.
- Guttenberg, B., C. F. Richter 1944. Frequency of earthquakes in California. *Bull. Seism. Soc. Am.* 34, 185-188.
- Grünthal, G., R. Wahlström, D. Stromeyer 2009. The unified catalogue of earthquakes in central, northern, and northwestern Europe (CENEC) – updated and expanded to the last millennium. *J. Seismol.* 13, 517-541.
- Hók, J., R. Kysel, M. Kováč, P. Moczo, J. Kristek, M. Kristeková, M. Šujan 2016. A seismic source zones model for the seismic hazard assessment of Slovakia. *Geologica Carpathica* (In press).
- IAEA 2010. Seismic Hazards in Site Evaluation for Nuclear Installations. *Specific Safety Guide No. SSG-9*. International Atomic Energy Agency, Vienna.
- Johnson, A. C., K. J. Coppersmith, L. R. Kanter, C. A. Cornell (eds.) 1994. *The Earthquakes of Stable Continental Regions*, Vol. 1: Assessment of Large Earthquake Potential. EPRI, Palo Alto.
- Kijko, A. 2004. Estimation of the maximum earthquake magnitude m_{max} . *Pure Appl. Geophys.* 161, 1-27.
- Kramer, S. L. 1996. *Geotechnical Earthquake Engineering*. Prentice Hall, New Jersey. ISBN 978-0133749434.

- Kysel R. 2014. Seizmické ohrozenie územia Slovenska. Rigorous thesis (in Slovak). Faculty of Mathematics, Physics and Informatics, Comenius University in Bratislava, Slovakia. 106 p.
- Labák, P., A. Bystrická, P. Moczo, L. Rosenberg 1997. Pravdepodobnostný výpočet seizmického ohrozenia pre lokalitu Atómových elektrární Bohunice. Geofyzikálny ústav SAV, Bratislava.
- Labák, P. 1998. Katalóg zemetrasení lokalizovaných na území Slovenska (Verzia 1997). Geofyzikálny ústav SAV, Bratislava.
- Leonard, M. 2010. Earthquake Fault Scaling: Self-Consistent Relating of Rupture Length, Width, Average Displacement, and Moment Release. *Bull. Seism. Soc. Am.* 100, 1971-1988.
- McGuire, R. 1976. Fortran program for seismic risk analysis. *U.S. Geological Survey Open-File Report 67-76*.
- McGuire, R. K. 2004. *Seismic Hazard and Risk Analysis*. Earthquake Engineering Research Institute, Oakland. ISBN 0-943198-01-1.
- McGuire, R. 2008. Probabilistic seismic hazard analysis: Early history. *Earthquake Eng. Struct. Dyn.* 37, 329-338.
- Molina, S. 1998. Sismotectonica y peligrosidad sismica del area de contacto entre Iberia y Africa. *PhD. Thesis*. Universidad de Granada.
- Molina, S., C. D. Lindholm, H. Bungum 2001. Probabilistic seismic hazard analysis: zoning free versus zoning methodology. *Boll. Geof. Teor. Appl.* 42, 19-39.
- Peláez-Montilla, J.A., C. López-Casado 2002. Seismic hazard estimation at the Iberian Peninsula. *Pure Appl. Geophys.* 159, 2699-2713.
- Progseis, 2010. Katalóg zemetrasení zaznamenaných lokálnymi sieťami seizmických staníc v okolí jadrových elektrární Jaslovské Bohunice a Mochovce (Verzia 2009). Progseis, s.r.o., Trnava.
- Ramanna, C. K., G. R. Dodagoudar 2011. Kernel density estimation techniques for seismic hazard analysis of South India. *III ECCOMAS Thematic Conference on Computational Methods in Structural Dynamics and Earthquake Engineering*. Corfu, Greece.

- Ramanna, C. K., G. R. Dodagoudar 2012. Seismic Hazard Analysis Using the Adaptive Kernel Density Estimation Technique for Chennai City. *Pure Appl. Geophys.* 169, 55-69.
- Reiter, L. 1990. *Earthquake hazard analysis. Issues and insights*. Columbia University Press. New York. ISBN 0-231-06534-5.
- Salazar, W., L. Brown, G. Mannette 2013. Probabilistic Seismic Hazard Assessment for Jamaica. *Journal of Civil Engineering and Architecture.* 70, 1118-1140.
- Schenk, V., Z. Schenková, P. Kottnauer, B. Guterch, P. Labák 2000. Earthquake Hazard for the Czech Republic, Poland and Slovakia – Contribution to the ILC/IASPEI Global Seismic Hazard Assessment Program. *Natural Hazards* 21, 331-345.
- Secanell, R., D. Bertil, C. Martin, X. Goula, T. Susagna, M. Tapia, P. Dominique, D. Carbon, J. Fleta 2008. Probabilistic seismic hazard assessment of the Pyrenean region. *J. Seismol.* 12, 323-341.
- Silverman, B.W. 1986. *Density estimation for statistic and data analysis*. Chapman and Hall. London. ISBN 0-412-24620-1.
- SLOVEC 2011. Slovak earthquake catalogue (version 2011). Data file of the Earth Science Institute, Slovak Academy of Sciences, Bratislava, Slovakia.
- Vere-Jones, D. 1992. Statistical methods for the description and display of earthquake catalogues. In: *Statistic in the Environmental and Earth Sciences*, ed. A.T. Walden and P. Guttorp, Arnold, London, and Halsted Press, Toronto. 220-246.
- Wells, D. L., K. J. Coppersmith 1994. New Empirical Relationships among Magnitude, Rupture Length, Rupture Width, Rupture Area, and Surface Displacement. *Bull. Seism. Soc. Am.* 84, 974-1002.
- Woo, G. 1996. Kernel Estimation Methods for Seismic Hazard Area Source Modeling. *Bull. Seism. Soc. Am.* 86, 1-10.
- Woo, G. 2001a. Computer code KERGRID. [Obtained by personal communication]
- Woo, G. 2001b. Kergrid1 – manual of the computer code KERGRID. [Obtained by personal communication]

APPENDIX I – ABSTRACT (ENGLISH)

Probabilistic seismic hazard analysis developed by Allin Cornell and Luis Esteva in the late 60s is based on the seismic source zones definition in which spatially and temporarily homogenous seismic activity is assumed. In regions where the association between seismicity and geology is complex, the definition of the source zones is often difficult and to some extent is a matter of expert judgement. It is also known, that the seismicity is not homogeneous within a source zone, but it is only approximation for computational purposes. To overcome these difficulties alternative approaches to probabilistic seismic hazard analysis have been developed. One example is the zoneless approach proposed by Gordon Woo (1996). In zoneless approach, earthquake catalogue is directly used for probabilistic seismic hazard analysis – earthquake epicentres are spatially smoothed using non-parametrically estimated probability density function called the kernel function. Contributions of individual events to the resulting hazard are inversely weighted by their effective return period. Other parameter that is incorporated in computations is the bandwidth function that is designed to reflect the degree of spatial clustering of the catalogued earthquakes in individual magnitude bins.

In this master's thesis we used zoneless approach to probabilistic seismic hazard analysis of the territory of Slovakia. We tested the sensitivity of the results to the input parameters. Obtained results by zoneless approach were subsequently compared to results obtained by classical Cornell-McGuire methodology (Kysel 2014). The results obtained using classical Cornell-McGuire methodology differs significantly with respect to the chosen ground motion prediction equation, what we did not observe for zoneless approach. For one of used ground motion prediction equations gives Cornell-McGuire approach higher values of the peak ground acceleration especially in areas with high seismic activity. The peak ground acceleration obtained using zoneless approach was higher mainly in Eastern Slovakia, where several medium sized earthquakes were recorded in the past.

Key words: seismic hazard analysis, zoneless approach, kernel function, Slovakia

APPENDIX II – ABSTRACT (GERMAN)

Die Einschätzung der seismischen Gefährdung, die von Allin Cornell und Luis Esteva in den sechziger Jahren des 20. Jahrhunderts vorgestellt wurde, ist auf dem seismischen Quellzonenmodell gegründet. In jeder Quellzone wird eine Gleichverteilung der Seismizität in Zeit und Raum behauptet. In Gebieten, in denen die Bindung zwischen Seismizität und Geologie zu komplex ist, wird der Prozess der Einteilung eines Gebietes in seismische Quellzonen kompliziert und hängt von der Expertensicht ab. Es ist zwar evident, dass die Seismizität in einer Quellzone nicht homogen ist, für die Berechnungsmodelle müssen wir aber die Approximation in Betracht ziehen. Um diese Schwierigkeiten zu überwinden, wurden verschiedene alternative Methoden der Einschätzung der seismischen Gefährdung entwickelt. Ein Beispiel dieser Herangehensweise ist die zonenfreie Methode, die durch Gordon Woo (1996) entwickelt wurde. Diese zonenfreie Methode basiert bei den Auswertungen auf den Erdbeben-Katalogen – die Erdbebenepizentren werden mit einer nicht-parametrisch bestimmten Wahrscheinlichkeitsdichtefunktion (so genannte Kernel-Funktion) geographisch geglättet. Die resultierende seismische Gefährdung ist die Summe der Daten von den Kernel-Funktionen, wobei der Beitrag jedes Ereignisses invers seiner effektiven Wiederholrate gewichtet ist. Ein anderer wichtiger Parameter der Kernel-Funktion ist die Bandweite, deren Wert von der geographischen Distribution der Erdbebenepizentren beeinflusst wird.

Die vorliegende Masterarbeit verfolgt die zonenfreie Methode bei der Analyse der seismischen Gefährdung für das Gebiet der Slowakei. Bei der Analyse der seismischen Gefährdung wurde die Anfälligkeit von Antrittsparametern getestet und die Resultate, die durch die zonenfreie Methode gewonnen werden konnten, wurden mit den durch die klassische Cornell – McGuire gebundene Methode (Kysel 2014) gewonnenen Resultaten verglichen. Die Resultate, die durch Cornell – McGuire zonengebundene Methode erzielt werden, sind stark von dem benutzten Starkbodenbewegungsmodell (GMPE) abhängig, besonders in den Gebieten mit hoher Seismizität. Dieser Zusammenhang konnte bei der Anwendung der zonenfreien Methode nicht beobachtet werden. Um nur ein Beispiel anzuführen, die Spitzenbodenbeschleunigung von der zonenfreien Methode ist höher in den Gebieten mit moderater Seismizität (z.B. in den Gebieten der Ostslowakei), in denen in Vergangenheit mehrere Erdbeben mit mittleren Intensität dokumentiert wurden.

Schlüsselwörter: Analyse der seismischen Gefährdung, zonenfreie Methode, Kernel-Funktion, Slowakei

CURRICULUM VITAE

Personal information

Date of birth: 30.11.1992
Address: Staré Grunty 36, 84104 Bratislava
Mobile: +421 949 746 487
E-mail: b.badova@gmail.com

Education

September 2014	Comenius University in Bratislava and Universität Wien Faculty of Mathematics, Physics and Informatics Field of Study: Joint Master Study Program Physics of the Earth, title: MSc. Expected time of graduation: July 2016
September 2011 – June 2014	Comenius University in Bratislava Faculty of Mathematics, Physics and Informatics Field of Study: Physics, finished with state examination, title: Bc.
September 2007 - May 2011	August Horislav Škultéty Gymnasium in Veľký Krtíš finished with school - leaving examination